ISSN 1949-8470 (online)

World Journal of *Radiology*

World J Radiol 2016 September 28; 8(9): 764-815

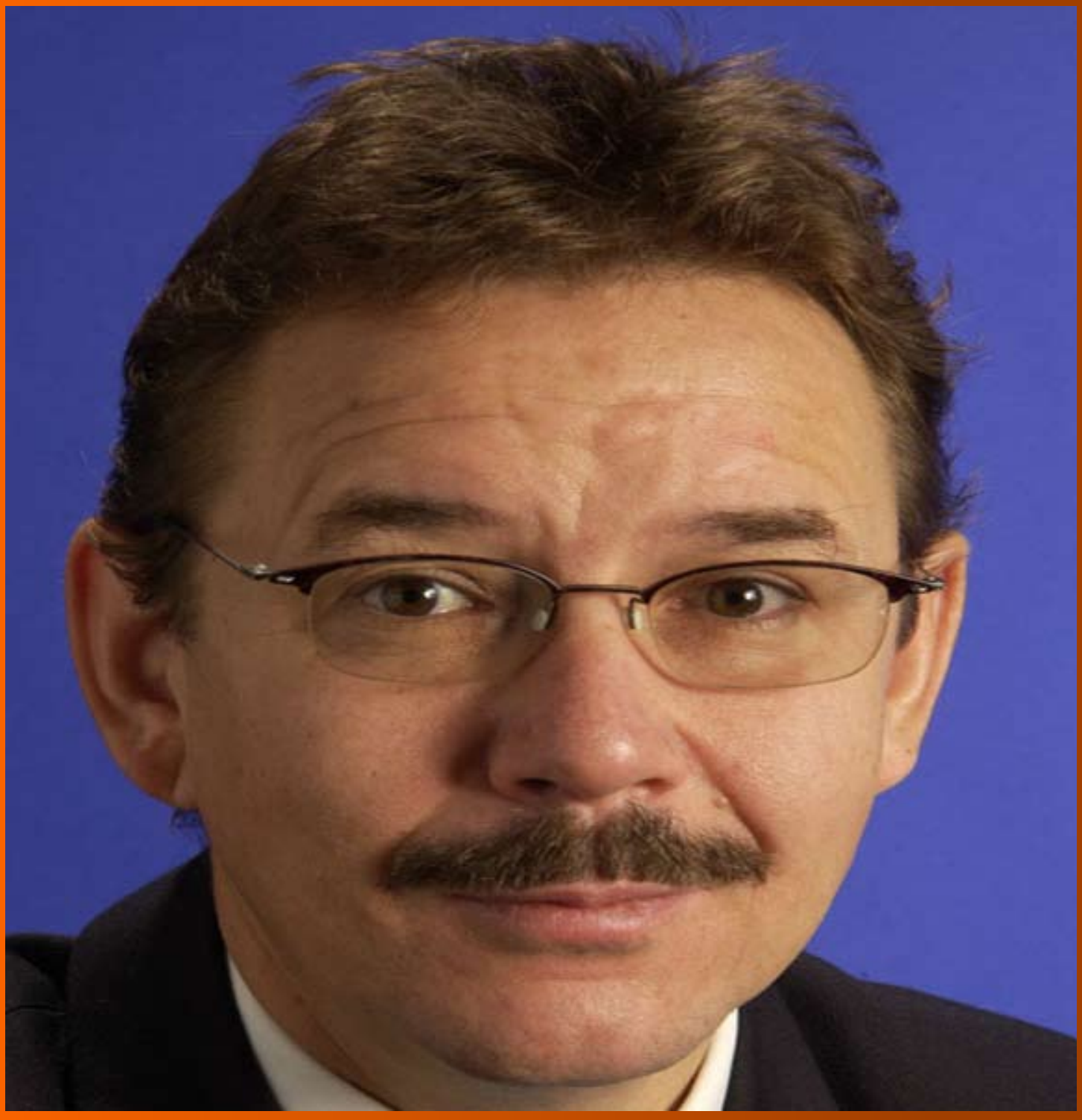

Published by Baishideng Publishing Group Inc

WJR World Journal of Radiology

A peer-reviewed, online, open-access journal of Radiology

Editorial Board

2014-2017

The *World Journal of Radiology* Editorial Board consists of 365 members, representing a team of worldwide experts in radiology. They are from 36 countries, including Afghanistan (1), Argentina (2), Australia (5), Austria (7), Belgium (2), Brazil (8), Canada (6), Chile (1), China (43), Croatia (1), Denmark (4), Egypt (6), France (5), Germany (22), Greece (10), India (12), Iran (6), Ireland (2), Israel (3), Italy (47), Japan (13), Netherlands (1), New Zealand (1), Pakistan (1), Poland (2), Portugal (1), Serbia (1), Singapore (3), Slovakia (1), South Korea (18), Spain (4), Sweden (2), Switzerland (4), Thailand (1), Turkey (26), United Kingdom (11), and United States (82).

Yue-Qi Zhu, *Shanghai*

Croatia

Goran Kusec, Osijek

Denmark

Poul E Andersen, *Odense*
Lars J Petersen, *Aalborg*
Thomas Z Ramsoy, *Frederiksberg*
Morten Ziebell, *Copenhagen*

Egypt

Mohamed F Bazeed, *Mansoura*
Mohamed Abou El-Ghar, *Mansoura*
Reem HA Mohamed, *Cairo*
Mohamed R Nouh, *Alexandria*
Ahmed AKA Razek, *Mansoura*
Ashraf A Zytoon, *Shebin El-Koom*

France

Sabine F Bensamoun, *Compiègne*
Romaric Loffroy, *Dijon*
Stephanie Nougaret, *Montpellier*
Hassane Oudadesse, *Rennes*
Vincent Vinh-Hung, *Fort-de-France*

Germany

Henryk Barthel, *Leipzig*
Peter Bannas, *Hamburg*
Martin Beeres, *Frankfurt*
Ilja F Ciernik, *Dessau*
A Dimitrakopoulou-Strauss, *Heidelberg*
Peter A Fasching, *Erlanegn*
Andreas G Schreyer, *Regensburg*
Philipp Heusch, *Duesseldorf*
Sonja M Kirchhoff, *Munich*
Sebastian Ley, *Munich*
Adel Maataoui, *Frankfurt am Main*
Stephan M Meckel, *Freiburg*
Hans W Muller, *Duesseldorf*
Kay Raum, *Berlin*
Dirk Rades, *Luebeck*
Marc-Ulrich Regier, *Hamburg*
Alexey Surov, *Halle*
Martin Walter, *Magdeburg*
Axel Wetter, *Essen*
Christoph Zilkens, *Düsseldorf*

Greece

Panagiotis Antoniou, *Thessaloniki*
Nikos Efthimiou, *Athens*
Dimitris Karnabatidis, *Patras*
George Latsios, *Athens*
Stylianos Megremis, *Iraklion*
Alexander D Rapidis, *Athens*
Kiki Theodorou, *Larissa*
Ioannis A Tsalafoutas, *Athens*
Evanthia E Tripoliti, *Ioannina*
Athina C Tsili, *Ioannina*

India

Ritesh Agarwal, *Chandigarh*
Chandan J Das, *New Delhi*
Prathamesh V Joshi, *Mumbai*
Naveen Kalra, *Chandigarh*
Chandrasekharan Kesavadas, *Trivandrum*
Jyoti Kumar, *New Delhi*
Atin Kumar, *New Delhi*
Kaushala P Mishra, *Allahabad*
Daya N Sharma, *New Delhi*
Binit Sureka, *New Delhi*
Sanjay Sharma, *New Delhi*
Raja R Yadav, *Allahabad*

Iran

Majid Assadi, *Bushehr*
SeyedReza Najafizadeh, *Tehran*
Mohammad Ali Oghabian, *Tehran*
Amir Reza Radmard, *Tehran*
Ramin Sadeghi, *Mashhad*
Hadi Rokni Yazdi, *Tehran*

Ireland

Tadhg Gleeson, *Wexford*
Frederik JAI Vernimmen, *Cork*

Israel

Dafna Ben Bashat, *Tel Aviv*
Amit Gefen, *Tel Aviv*
Tamar Sella, *Jerusalem*

Italy

Adriano Alippi, *Rome*
Dante Amelio, *Trento*
Michele Anzidei, *Rome*
Filippo F Angileri, *Messinas*
Stefano Arcangeli, *Rome*
Roberto Azzoni, *San Donato milanese*
Tommaso V Bartolotta, *Palermo*
Tommaso Bartalena, *Imola*
Livia Bernardin, *San Bonifacio*
Federico Boschi, *Verona*
Sergio Casciaro, *Lecce*
Emanuele Casciani, *Rome*
Musa M Can, *Napoli*
Alberto Cuocolo, *Napoli*
Michele Ferrara, *Coppito*
Mauro Feola, *Fossano*
Giampiero Francica, *Castel Volturno*
Luigi De Gennaro, *Rome*
Giulio Giovannetti, *Pisa*
Francesca Iacobellis, *Napoli*
Formato Invernizzi, *Monza Brianza*
Francesco Lassandro, *Naples*
Lorenzo Livi, *Florence*
Pier P Mainenti, *Napoli*
Laura Marzetti, *Chieti*
Giuseppe Malinverni, *Crescentino*
Enrica Milanesi, *Turin*
Giovanni Morana, *Treviso*
Lorenzo Monti, *Milan*
Silvia D Morbelli, *Genoa*
Barbara Palumbo, *Perugia*
Cecilia Parazzini, *Milan*
Stefano Pergolizzi, *Messina*
Antonio Pinto, *Naples*
Camillo Porcaro, *Rome*
Carlo C Quattrocchi, *Rome*
Alberto Rebonato, *Perugia*
Giuseppe Rizzo, *Rome*
Roberto De Rosa, *Naples*
Domenico Rubello, *Rovigo*
Andrea Salvati, *Bari*
Sergio Sartori, *Ferrara*
Luca M Sconfienza, *Milano*
Giovanni Storto, *Rionero*
Nicola Sverzellati, *Parma*
Alberto S Tagliafico, *Genova*
Nicola Troisi, *Florence*

Japan

Yasuhiko Hori, *Chiba*
Hidetoshi Ikeda, *Koriyama*
Masahito Kawabori, *Sapporo*
Tamotsu Kamishima, *Sapporo*
Hiro Kiyosue, *Yufu*
Yasunori Minami, *Osaka-sayama*
Yasuhiro Morimoto, *Kitakyushu*
Satoru Murata, *Tokyo*
Shigeki Nagamachi, *Miyazaki*
Hiroshi Onishi, *Yamanashi*
Morio Sato, *Wakayama Shi*
Yoshito Tsushima, *Maebashi*
Masahiro Yanagawa, *Suita*

Netherlands

Willem Jan van Rooij, *Tilburg*

New Zealand

W Howell Round, *Hamilton*

Pakistan

Wazir Muhammad, *Abbottabad*

Poland

Maciej S Baglaj, *Wroclaw*

Piotr Czauderna, *Gdansk*

Portugal

Joao Manuel RS Tavares, *Porto*

Serbia

Olivera Ciraj-Bjelac, *Belgrade*

Singapore

Gopinathan Anil, *Singapore*
Terence KB Teo, *Singapore*
Cher Heng Tan, *Singapore*

Slovakia

Stefan Sivak, *Martin*

South Korea

Ki Seok Choo, *Busan*
Seung Hong Choi, *Seoul*
Dae-Seob Choi, *Jinju*
Hong-Seok Jang, *Seoul*
Yong Jeong, *Daejeon*
Chan Kyo Kim, *Seoul*
Se Hyung Kim, *Seoul*
Joong-Seok Kim, *Seoul*
Sang Eun Kim, *Seongnam*
Sung Joon Kwon, *Seoul*
Jeong Min Lee, *Seoul*
In Sook Lee, *Busan*
Noh Park, *Goyang*
Chang Min Park, *Seoul*
Sung Bin Park, *Seoul*
Deuk Jae Sung, *Seoul*
Choongsoo Shin, *Seoul*
Kwon-Ha Yoon, *Iksan*

Spain

Miguel A De Gregorio, *Zaragoza*
Antonio Luna, *Jaén*
Enrique Marco de Lucas, *Santander*
Fernando Ruiz Santiago, *Granada*

Sweden

Dmitry Grishenkov, *Stockholm*
Tie-Qiang Li, *Stockholm*

Switzerland

Nicolau Beckmann, *Basel*
Christian Boy, *Bern*
Giorgio Treglia, *Bellinzona*

Stephan Ulmer, *Kiel*

Thailand

Sirianong Namwongprom, *Chiang Mai*

Turkey

Kubilay Aydin, *Istanbul*
Ramazan Akdemir, *Sakarya*
Serhat Avcu, *Ankara*
Ayse Aralasmak, *Istanbul*
Oktay Algin, *Ankara*
Nevbahar Akcar, *Meselik*
Bilal Battal, *Ankara*
Zulkif Bozgeyik, *Elazig*
Nazan Ciledag, Aakara
Fuldem Y Donmez, *Ankara*
Gulgun Engin, *Istanbul*
Ahmet Y Goktay, *Izmir*
Oguzhan G Gumustas, *Bursa*
Kaan Gunduz, *Ankara*
Pelin Ozcan Kara, *Mersin*
Kivanc Kamburoglu, *Ankara*
Ozgur Kilickesmez, *Istanbul*
Furuzan Numan, *Istanbul*
Cem Onal, *Adana*
Ozgur Oztekin, *Izmir*
Seda Ozbek (Boruban), *Konya*
Selda Sarikaya, *Zonguldak*
Figen Taser, *Kutahya*
Baran Tokar, *Eskisehir*
Ender Uysal, *Istanbul*
Ensar Yekeler, *Istanbul*

United Kingdom

Indran Davagnanam, *London*
M DC Valdés Hernández, *Edinburgh*
Alan Jackson, *Manchester*
Suneil Jain, *Belfast*
Long R Jiao, *London*
Miltiadis Krokidis, *Cambridge*
Pradesh Kumar, *Liverpool*
Peter D Kuzmich, *Derby*
Georgios Plataniotis, *Brighton*
Vanessa Sluming, *Liverpool*

United States

Garima Agrawal, *Saint Louis*
James R Brasic, *Baltimore*
Rajendra D Badgaiyan, *Buffalo*
Ulas Bagci, *Bethesda*
Anat Biegon, *Stony Brook*
Ramon Casanova, *Winston Salem*
Wenli Cai, *Boston*
Zheng Chang, *Durham*
Corey J Chakarun, *Long Beach*
Kai Chen, *Los Angeles*
Hyun-Soon Chong, *Chicago*
Marco Cura, *Dallas*
Ravi R Desai, *Bensalem*
Delia DeBuc, *Miami*
Carlo N De Cecco, *Charleston*
Timm-Michael L Dickfeld, *Baltimore*
Subba R Digumarthy, *Boston*
Huy M Do, *Stanford*
Todd A Faasse, *Grand Rapids*
Salomao Faintuch, *Boston*
Girish M Fatterpekar, *New York*
Dhakshinamoorthy Ganeshan, *Houston*
Robert J Griffin, *Little Rock*
Andrew J Gunn, *Boston*
Sandeep S Hedgire, *Boston*
Timothy J Hoffman, *Columbia*
Mai-Lan Ho, *San Francisco*
Juebin Huang, *Jackson*
Abid Irshad, *Charleston*
Matilde Inglese, *New York*
El-Sayed H Ibrahim, *Jacksonville*
Paul R Julsrud, *Rochester*
Pamela T Johnson, *Baltimore*
Ming-Hung Kao, *Tempe*
Sunil Krishnan, *Houston*
Richard A Komoroski, *Cincinnati*
Sandi A Kwee, *Honolulu*
King Kim, *Ft. Lauderdale*
Guozheng Liu, *Worcester*
Yiyan Liu, *Newark*
Venkatesh Mani, *New York*
Lian-Sheng Ma, *Pleasanton*
Rachna Madan, *Boston*
Zeyad A Metwalli, *Houston*
Yilong Ma, *Manhasset*
Hui Mao, *Atlanta*
Feroze B Mohamed, *Philadelphia*
Gul Moonis, *Boston*
John L Nosher, *New Brunswick*
Rahmi Oklu, *Boston*
Aytekin Oto, *Chicago*
Bishnuhari Paudyal, *Philadelphia*
Rajul Pandya, *Youngstown*
Chong-Xian Pan, *Sacramento*
Jay J Pillai, *Baltimore*
Neal Prakash, *Duarte*
Reza Rahbar, *Boston*
Ali S Raja, *Boston*
Gustavo J Rodriguez, *El Paso*
David J Sahn, *Portlsand*
Steven Schild, *Scottsdale*
Ali R Sepahdari, *Los Angeles*
Li Shen, *Indianapolis*
JP Sheehan, *Charlottesville*
Atul B Shinagare, *Boston*
Sarabjeet Singh, *Boston*
Charles J Smith, *Columbia*
Kenji Suzuki, *Chicago*
Monvadi Srichai-Parsia, *Washington*
Sree H Tirumani, *Boston*
Hebert A Vargas, *New York*
Sachit Verma, *Philadelphia*
Yoichi Watanabe, *Minneapolis*
Li Wang, *Chapel Hill*
Carol C Wu, *Boston*
Shoujun Xu, *Houston*
Min Yao, *Cleveland*
Xiaofeng Yang, *Atlanta*
Qingbao Yu, *Albuquerque*
Aifeng Zhang, *Chicago*
Chao Zhou, *Bethlehem*
Hongming Zhuang, *Philadelphia*

WJR World Journal of Radiology

Contents

Monthly Volume 8 Number 9 September 28, 2016

REVIEW

MINIREVIEWS

ORIGINAL ARTICLE

Prospective Study

World Journal of Radiology
Volume 8 Number 9 September 28, 2016

Contents

NAME OF JOURNAL
World Journal of Radiology

ISSN
ISSN 1949-8470 (online)

LAUNCH DATE
January 31, 2009

FREQUENCY
Monthly

EDITORIAL OFFICE
Xiu-Xia Song, Director
Fang-Fang Ji, Vice Director
World Journal of Radiology
Baishideng Publishing Group Inc
8226 Regency Drive, Pleasanton, CA 94588, USA
Telephone: +1-925-2238242
Fax: +1-925-2238243
E-mail: editorialoffice@wjgnet.com
Help Desk: http://www.wjgnet.com/esps/helpdesk.aspx
http://www.wjgnet.com

PUBLISHER
Baishideng Publishing Group Inc
8226 Regency Drive,
Pleasanton, CA 94588, USA
Telephone: +1-925-2238242
Fax: +1-925-2238243
E-mail: bpgoffice@wjgnet.com
Help Desk: http://www.wjgnet.com/esps/helpdesk.aspx
http://www.wjgnet.com

PUBLICATION DATE
September 28, 2016

INSTRUCTIONS TO AUTHORS
http://www.wjgnet.com/bpg/gerinfo/204

ONLINE SUBMISSION
http://www.wjgnet.com/esps/

World Journal of Radiology

Submit a Manuscript: http://www.wjgnet.com/esps/
Help Desk: http://www.wjgnet.com/esps/helpdesk.aspx
DOI: 10.4329/wjr.v8.i9.764

World J Radiol 2016 September 28; 8(9): 764-774
ISSN 1949-8470 (online)

REVIEW

Imaging pancreatic islet cells by positron emission tomography

Junfeng Li, Johann Karunananthan, Bradley Pelham, Fouad Kandeel

Junfeng Li, Johann Karunananthan, Bradley Pelham, Fouad Kandeel, Department of Diabetes, Endocrinology and Metabolism, Beckman Research Institute of the City of Hope, Duarte, CA 91010, United States

Author contributions: All authors equally contributed to this paper with conception and design of the study, literature review and analysis, drafting and critical revision and editing, and final approval of the final version.

Supported by The grant from the Larry L. Hillblom Foundation.

Conflict-of-interest statement: No potential conflicts of interest for this article.

Manuscript source: Invited manuscript

Correspondence to: Fouad Kandeel, MD, PhD, Department of Diabetes, Endocrinology and Metabolism, Beckman Research Institute of the City of Hope, 1500 E. Duarte Rd., Duarte, CA 91010, United States. fkandeel@coh.org
Telephone: +1-626-2180224
Fax: +1-626-4719373

Received: December 29, 2015
Peer-review started: January 14, 2016
First decision: February 29, 2016
Revised: July 25, 2016
Accepted: August 6, 2016
Article in press: August 8, 2016
Published online: September 28, 2016

Abstract

It was estimated that every year more than 30000 persons in the United States - approximately 80 people per day - are diagnosed with type 1 diabetes (T1D). T1D is caused by autoimmune destruction of the pancreatic islet (β cells) cells. Islet transplantation has become a promising therapy option for T1D patients, while the lack of suitable tools is difficult to directly evaluate of the viability of the grafted islet over time. Positron emission tomography (PET) as an important non-invasive methodology providing high sensitivity and good resolution, is able to accurate detection of the disturbed biochemical processes and physiological abnormality in living organism. The successful PET imaging of islets would be able to localize the specific site where transplanted islets engraft in the liver, and to quantify the level of islets remain alive and functional over time. This information would be vital to establishing and evaluating the efficiency of pancreatic islet transplantation. Many novel imaging agents have been developed to improve the sensitivity and specificity of PET islet imaging. In this article, we summarize the latest developments in carbon-11, fluorine-18, copper-64, and gallium-68 labeled radioligands for the PET imaging of pancreatic islet cells.

Key words: Diabetes; Pancreatic islet cells; Positron emission tomography; Imaging tracers

Core tip: Positron emission tomography (PET) is an important non-invasive functional imaging modality that is being explored for the purpose of quantifying engrafted pancreatic islet. There are still several issues that must be overcome before PET can be adopted as the gold standard for the accurate, noninvasive, and non-toxic evaluation of native β cells or pancreatic islet mass *in vivo*, which remains a difficultly and highly challenging goal. To complement the previous review published in 2010 by our group, this review summarizes the latest developments in PET tracers (such as carbon-11,

fluorine-18, copper-64 and gallium-68) for the imaging of pancreatic islet cells.

Li J, Karunananthan J, Pelham B, Kandeel F. Imaging pancreatic islet cells by positron emission tomography. *World J Radiol* 2016; 8(9): 764-774 Available from: URL: http://www.wjgnet.com/1949-8470/full/v8/i9/764.htm DOI: http://dx.doi.org/10.4329/wjr.v8.i9.764

INTRODUCTION

Type 1 diabetes (T1D) remains the predominant form of diabetes in childhood. Although disease onset may occur at any time, the peak onset for diagnosis is in the mid-teens[1]. The prevalence of T1D in the United States population under 20 years of age has increased by 30% between 2001 and 2009[2].

Pancreatic islets are comprised of clusters of cells, of which there are five different types: Alpha, beta, delta, gamma, and epsilon cells, all of which produce hormones that are secreted directly into the blood-stream. However, the majority of the pancreatic islet mass is made up of beta cells (65%-80%), which help regulate blood glucose levels *via* their production of insulin. T1D is caused by the autoimmune destruction of the pancreatic beta cells[3], which limits or completely eliminates the production and secretion of insulin. As the result of long-term hyperglycemia, patients with T1D may develop serious micro- and macrovascular complications such as heart disease, stroke, kidney failure, blindness, leg amputations, and premature death[4-6].

Currently, there is no cure for T1D. Experimental treatments are based on strategies that aim to modify the autoimmune processes responsible for beta cell destruction, replace beta cell mass, or both, including stem cell and immunotherapy, as well as the transplantation of islets[7]. Compared to whole-pancreatic transplant, the current standard of care for diabetes, the transplantation of islets are much less invasive[8]. Islet transplantation using the Edmonton protocol can momentarily control blood sugar levels with insulin independence in T1D patients. Currently only one-tenth of patients have successfully upheld insulin independence for five years[9].

Due to the lack of suitable methods for tracking post-transplantation islet loss, detection of grafted islet fate and functionality are restricted to indirect measurement of patient's metabolism or exogenous insulin requirements, which is not always accurate due to vacillations in the metabolic state and insulin secretory capacity of beta cells under various pathophysiologic and physiologic condition[10,11].

A noninvasive methodology monitoring transplanted islets would localize its site in the liver and quantity the viability level of islets and estimate their functionality over time. This information would be crucial to creating and assessing the effectiveness of pancreatic islet transplantation, revealing why some islet transplants are more successful that others, and would lead to new methods for islet grafts to last longer periods of time on a more widespread basis for every T1D patients.

Table 1 Representative beta-cell-specific biomarkers for positron emission tomography imaging of islets

Biomarkers	Probe name	Ref.
Vesicular monoamine transporter (VMAT2)	[^{11}C] (+)-dihydrotetrabenazine	[13,39-41]
	[(+)-^{11}C-DTBZ]	
	^{18}F-FP-(+)-DTBZ	[14,15,42,43]
	^{64}Cu-CB-TE2A-(+)-DTBZ	[44,45]
	^{64}Cu-CB-TE2A-(-)-DTBZ	[44,45]
Glucagon-like peptide-1	^{18}F-TTCO-Cys^{40}-Exendin-4	[23]
	^{18}F-FBEM-Cys^{x}-exendin-4	[26]
	^{68}Ga-DO3AVS-Cys^{40}-Exendin-4	[19,27,56,57]
	^{64}Cu-DO3A-VS-Cys^{40}-Exendin-4	[55]
	^{64}Cu-BaMalSar-Exendin-4	[22]
	^{64}Cu-Mal$_2$Sar-(Exendin-4)$_2$	[22]
	[Lys40(DOTA-^{64}Cu)-NH$_2$]-Exendin-4	[58]
Glucokinase	[^{11}C]AZ12504948	[20]
Somatostatin receptors	^{68}Ga-DOTA-octreotide	[63]

Positron emission tomography (PET) is highly sensitive, noninvasive imaging methodology[12] in biomedical research, which uses the γ-rays associated with positron annihilation events to localize positron-emitting targeted tracers inside an organism. The low interaction of γ-rays in the human body allows physicians to accurately detect signals in patients even if they originate deep below the body surface. Given an appropriate tracer, PET can accurately detect the disturbed biochemical processes and physiological abnormality in living organism. Thus, the development of safe, effective and highly specific PET tracers of pancreatic islets (*i.e.*, primarily β cells) would help us the early diagnosis of β-cell-associated metabolic diseases, as well as the capability of monitoring the therapeutic efficacy of islet transplantation. This information will greatly assist us in developing new techniques for extending the survival of islet grafts on a more widespread basis for every T1D patients.

Many investigators are currently searching for and evaluating beta-cell-specific biomarkers for PET imaging of islets[13-20]. A number of potential candidates have been reported, such as glucagon-like peptide-1 receptor (GLP-1R)[19,21-28], vesicular monoamine transporter (VMAT2)[14,29-32], sulfonylurea receptor (SUR1)[33], glucose transporter 2, glucokinase (GK)[20], reporter gene[34], glycogen, zinc transporters, fluorodithizone[35], and monoclonal antibodies[34]. To complement the previous review published in 2010 by our group[36], this review summarizes the latest developments since 2011 in C-11, F-18, Cu-64, and Ga-68 labeled radioligands targeting these specific biomarkers for PET imaging pancreatic islet cells (Table 1).

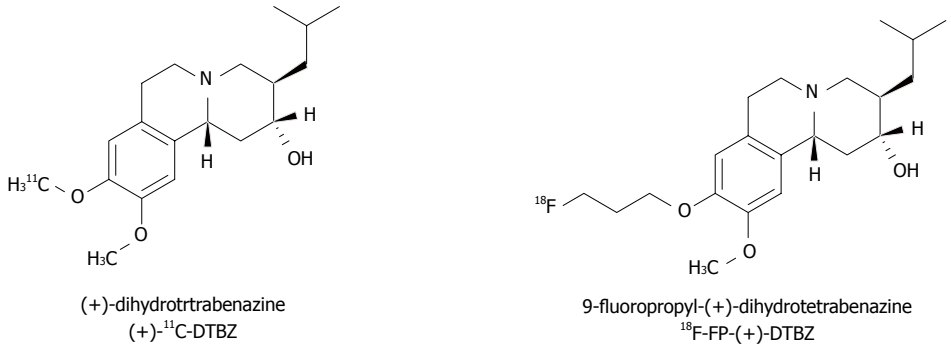

Figure 1 Structures of (+)-^{11}C-DTBZ and ^{18}F-FP-(+)-DTBZ.

^{11}C-, ^{18}F- AND ^{64}Cu-LABELED DTBZ ANALOGUES AS VMAT2 PROBES FOR IMAGING PANCREATIC ISLET CELLS

VMAT2 is mainly responsible for carrying monoamines, such as dopamine, from the neuron into the storage granules. It was demonstrated that VMAT2 mainly distributed in the central nervous system (CNS) and β-cells in the pancreatic islets by histology studies of gene expression[37]. VMAT2 expression is correlative with the insulin levels in monkey and human pancreatic tissue[38]. Therefore, VMAT2 could become a suitable target for trapping â-cell function. [^{11}C] (+)-dihydrotetrabenazine [(+)-^{11}C-DTBZ, Figure 1] as VMAT2 ligand was first synthesized by DaSilva *et al*[39] in 1993, and has been applied for imaging VMAT2 in the pancreas of mice, non-human primate and humans[13,40]. However, recent findings of nonspecific binding of (+)-^{11}C-DTBZ in human pancreas overcasts its clinical applications[41].

Kung *et al*[42] developed a novel DTBZ fluorine-18 probe, ^{18}F-FP-(+)-DTBZ (Figure 1). It has been evaluated of VMAT2 pancreatic binding sites of animals and humans in PET imaging. In the *in vivo* rats biodistribution studies, the probe showed the highest pancreas uptake (5% ID/g at 30 min p.i.). In the blocking study, 78% blockade of pancreas uptake in rats was observed. PET imaging result indicated that F-18 tracer has avid pancreatic uptake in health rats[43].

In healthy and T1D subject studies[14], pancreatic uptake showed the significant difference uptake between control and T1D subjects (Figure 2): (1) pancreas uptake of T1D patients (10.7 ± 2.6) was lower than that of control subjects (17.2 ± 4.0); and (2) there is not different in the kidney cortex uptake (3.01 ± 0.34 *vs* 2.90 ± 0.48).

However, the initial result of ^{18}F-FP-(+) DTBZ-PET in T1D patient, similarly with (+) ^{11}C- DTBZ[41], indicated that it has more VMAT2 value than expected. For this reason, Harris *et al*[15] suggested that tracer non-displaceable binding in T1D and health pancreas are different. In the result indicted that it was distinctly increased approximately two-fold in tissues of diabetic individuals *vs* healthy individuals from fresh frozen cadaveric pancreas. This initial result supports their hypothesis and currently, they are ongoing to focus on directly measurement of V_{ND} in the healthy human and T1D patient pancreas by (R) and (S) enantiomers.

Although ^{11}C- and ^{18}F-labeled DTBZ as VMAT2 PET probes have been performed in the pancreas of animal and human subjects, they would be limited in clinical application due to non-specific issues. Currently, there have only been limited reports using other PET nuclides. Recently, Kumar *et al*[44] reported synthesis of the ^{64}Cu-specific bifunctional chelator scaffold DTBZ analogues: ^{64}Cu-CB-TE2A-(+)-DTBZ (IC_{50} = 16.8 ± 6.9 nmol/L) and ^{64}Cu-CB-TE2A-(-)-DTBZ (IC_{50} = 253.2 ± 107.8 nmol/L). As we knew that, the IC_{50} values of (+)-DTBZ and (-)-DTBZ were 0.97 ± 0.48 nmol/L and 2.2 ± 0.3 μmol/L, respectively[45]. The VMAT2 specific binding affinity of ^{64}Cu-CB-TE2A-(+)-DTBZ was not compromised by their chemical modifications, while that of its (-) counterpart remained low as in ^{11}C- or ^{18}F-labeled (±) DTBZ[44]. Currently, there are no further reports on PET imaging using ^{64}Cu-CB-TE2A-(+)-DTBZ in animal studies.

In conclusion, ^{11}C- and ^{18}F-labeled DTBZ analogues for β cell imaging/pancreatic islet cells imaging have been applied in primates and humans studies; however, nonspecific binding of (+)-^{11}C-DTBZ and ^{18}F-FP-(+)-DTBZ in human pancreas overcasts their clinical applications. The suitable imaging tracer should exhibit selective binding to β-cells along with low non-specific binding to adjacent tissues.

^{18}F-, ^{68}Ga-, AND ^{64}Cu-LABELING EXENDIN ANALOGUES AS GLP-1 PROBES FOR IMAGING PANCREATIC ISLET CELLS

Discovered in the early 1980s[46,47], GLP-1, an incretin peptide secreted by the intestine as a response to nutrient ingestion, plays a significant role in glucose homeostasis. GLP-1 is an endogenous incretin peptide released from the intestine in response to nutrient ingestion and plays a significant role in glucose homeostasis. Although GLP-1R is found in pancreas, brain, heart, kidney, and GI tract[48,49], a recent study revealed that

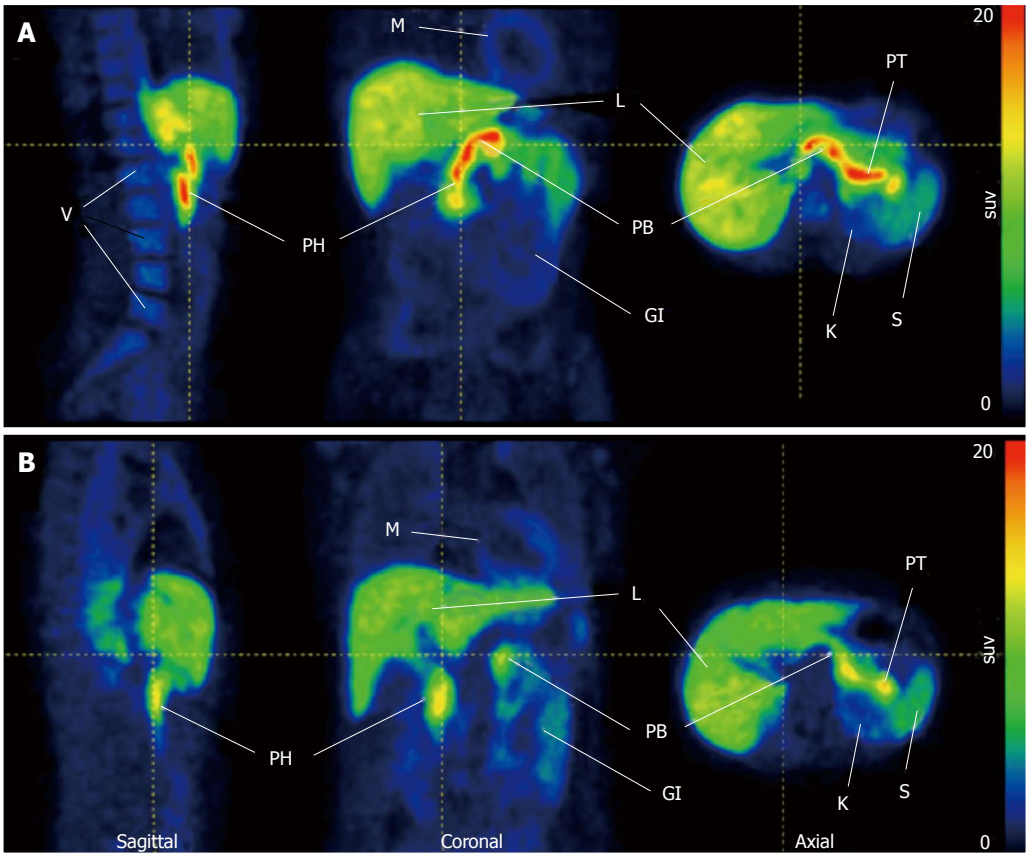

Figure 2 Representative ^{18}F-FP-(+)-DTBZ positron emission tomography images in healthy control subject and type 1 diabetes patient. A: High uptake in healthy pancreas; B: Compare with health control pancreas, lower uptake was observed in T1D patient. Both images PET data summed 0-90 min p.i. Reprinted with permission from Ref.[14]. GI: Gastrointestinal tract; K: Kidney; L: Liver; M: Myocardium; PB: Pancreas body; PH: Pancreas head; PT: Pancreas tail; S: Spleen; V: Vertebrae; T1D: Type 1 diabetes; PET: Positron emission tomography.

GLP-1R is highly expressed in β-cells in the pancreatic islet[50], suggesting that ligands of GLP-1R could be ideal tracers for imaging pancreatic islet. However, native GLP-1 is degraded rapidly (half-life < 2 min) by dipeptidyl peptidase-IV. Thus, dipeptidyl peptidase-IV-resistant agonist or antagonist targeted GLP-1R are suitable for PET imaging tracers[51,52].

In 1992, Eng *et al*[52-54] discovered exendin-4, which currently it is more attractive as a high-affinity probe. Exendin-4 has a 53% similar sequence identity to human GLP-1 and exhibits closely related properties[51]; on the other hand, it is much more stability than GLP-1. Thus exendin-4 has attracted significant attention on developing promising PET tracers for imaging pancreatic islet cells in rodent, primates and human studies since 2011, such as ^{18}F-TTCO-Cys^{40}-exendin-4[23], ^{18}F-FBEM-Cys^{x}-exendin-4 (x = 0 or 40)[26], ^{68}Ga-DO3AVS-Cys^{40}-exendin-4[19,27], and ^{64}Cu-DO3A-VS-Cys^{40}-exendin-4[55] (Figure 3).

We developed a novel fluorine-18 exendin-4 probe: ^{18}F-TTCO-Cys^{40}-exendin-4 (Figure 4)[23] with high radiosynthesis yield (80%) and high radiochemical purity (99%). An insulinoma INS-1 tumor model used in PET images of small animals, the result indicated that ^{18}F-TTCO-Cys^{40}-exendin-4 has high specific bind to GLP-1R (Figure 4A). Additionally, in contrast to the radiometal-labeled exendin-4 analogues, ^{18}F-tracer has a significantly lower uptake in kidney and quicker clearance rate[55].

We also tested the probe in the islet (1000 IEQ) graft in the liver in mice. The data indicated that the mice with transplanted islets (Figure 4D) had significantly higher (P < 0.01) uptake into the liver post injection as compared to the control mice (Figure 4E). To the blocking study, it also demonstrated that the tracer only specific GLP-1R in the liver. Currently, we are undertaking the evaluation of 18F-TTCO-Cys40-exendin-4 in non-human primates.

Recently, Selvaraju *et al*[27] developed a promising gallium-68 probe: ^{68}Ga-DO3AVS-Cys^{40}-exendin-4. Their imaging results in primates indicated the pancreas was easily visualized after injection ^{68}Ga-DO3A-exendin-4 by iv (injection dose, 0.05 μg/kg) (Figure 5). The probe was excreted in the urine and trapped in the kidney cortex (Figure 5, bottom row). No other organs displayed accumulation similarly with the pancreas and kidneys. The intestine, liver, spleen, heart, and lungs were displayed lower uptake.

In the specific study (Figure 5), co-injection of different doses of cold DO3A-exendin-4 (0.05-20 μg/kg)

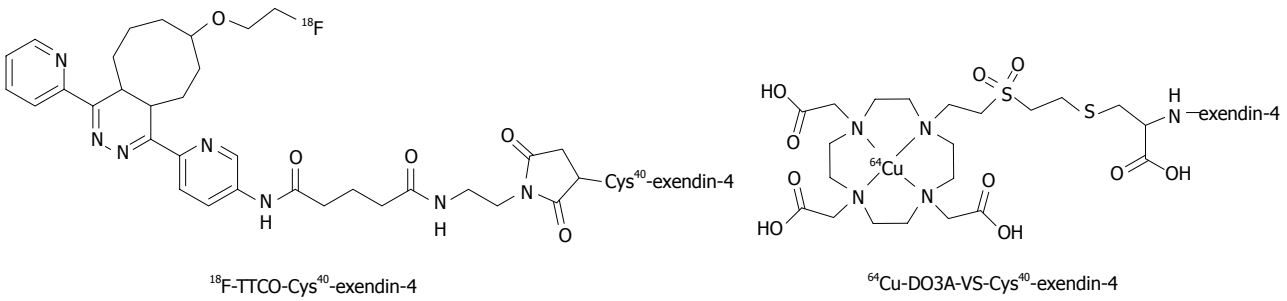

Figure 3 The structures of ^{18}F-TTCO-Cys^{40}-exendin-4 and ^{64}Cu-DO3A-VS-Cys^{40}-exendin-4 as glucagon-like peptide-1 receptor target probes.

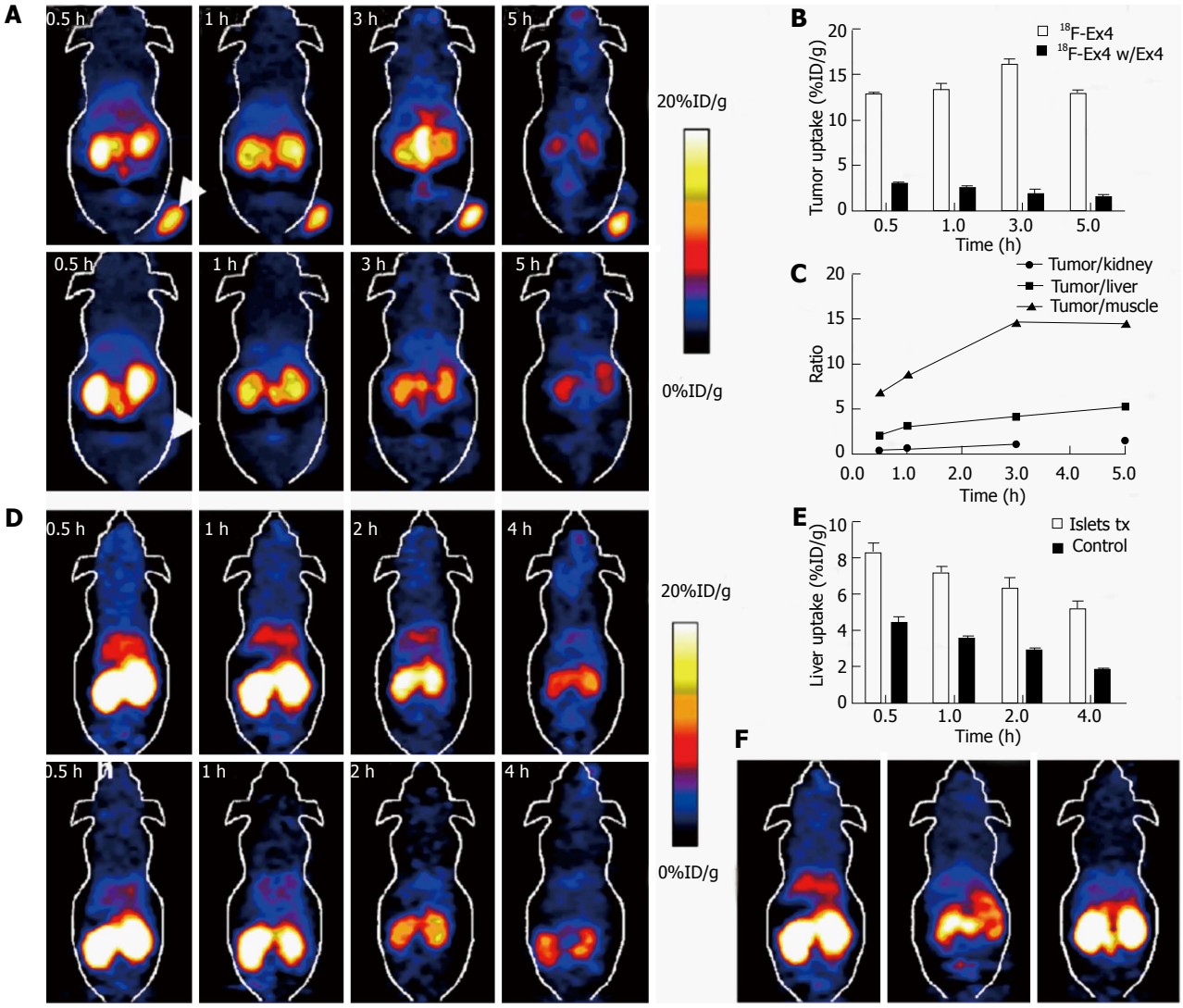

Figure 4 Representative ^{18}F-TTCO-Cys^{40}-exendin-4 positron emission tomography images in NOD/SCID mice. A: Representative microPET images of 18F-TTCOCys40-exendin-4 (top) and blocking (bottom) for NOD/SCID mice with INS-1; B: Tumor uptakes between control and blocking groups; C: Tumor to organs ratios of radiotracer at different time points p.i.; D: Representative microPET images of tracer in NOD/SCID mice transplanted with human islets into liver (top) and control mice (bottom) at different time points p.i.; E: Liver uptake between intraportal islet transplantation and sham control groups; F: MicroPET mages of mice transplanted with human islets (Left: Control; Middle: Blocking and sham control mice at 1 h p.i.). Reprinted with permission from Ref.[23]. PET: Positron emission tomography.

decreased the uptake in the pancreas from 9.2 to 0.8 in SUV curve (0.05-20 μg/kg) at 90 min p.i. The highest pharmacologic dose (20 μg/kg) was almost blocked more than 90% uptake. These imaging and kinetic results indicated that the tracer has specific binding to GLP-1R. The result of progressive competition with exendin-4 exhibited it was dose-dependently inhibited.

Eriksson *et al*[56] evaluated the first patient with pan-

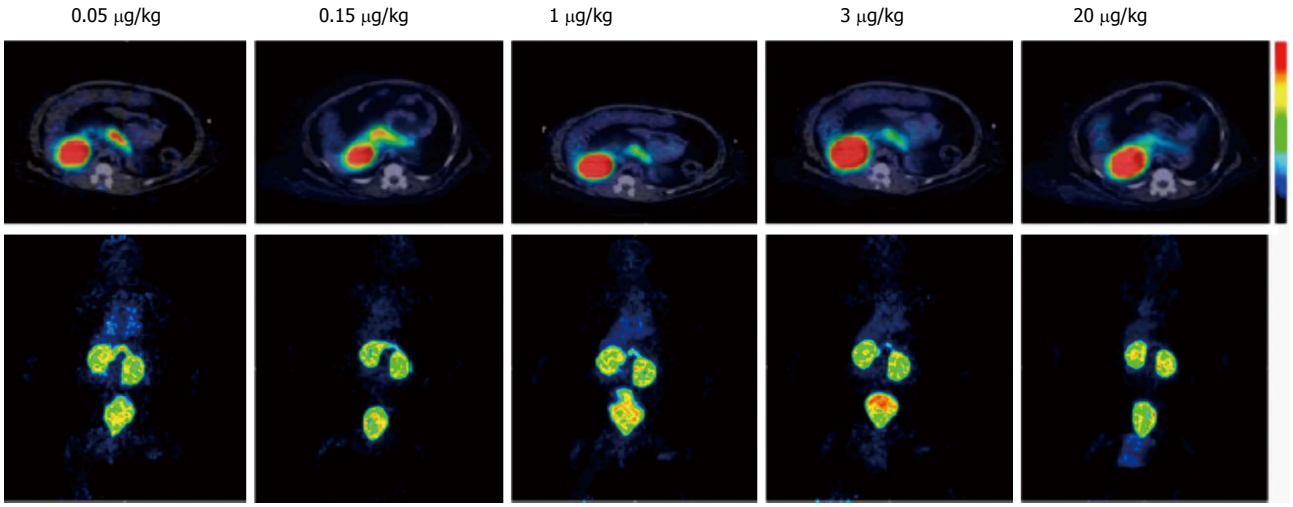

Figure 5 Positron emission tomography/computed tomography images of ^{68}Ga-DO3A-exendin-4 for cynomolgus monkeys. Increasing concentration of unlabeled peptide resulted in competition for glucagon-like peptide-1 receptor in pancreas only. Transaxial images (dynamic sequences 30-90 min, top row) and whole-body maximum-intensity projections (dynamic sequences 90-120 min, bottom row). Reprinted with permission from Ref. [27].

creatic insulinoma using ^{68}Ga-DO3AVS-Cys^{40}-exendin-4. PET/CT imaging of whole-body ^{68}Ga-DO3AVS-Cys^{40}-exendin-4 showed several small GLP-1R-positive lesions in the liver and a lymph node. Neither of the lesions had been conclusively detected by morphological imaging with CT and ultrasound or molecular imaging with [^{11}C]5-HTP or [^{18}F]FDG PET/CT. Native pancreas, containing a large number of cells positive for GLP-1R, exhibited marked uptake of ^{68}Ga-DO3AVS-Cys^{40}-exendin-4. The PET/CT imaging result indicated that ^{68}Ga-exendin-4 probe has more specific binding GLP-1R than other imaging techniques and provided the basis for continued systemic therapy.

Due to the renal excretion of [^{68}Ga]Ga-DO3A-VS-Cys^{40}-exendin-4 and the extensive intracellular retention of radioactivity in the kidney cortex, which remains a concern given the likelihood of repeated imaging studies in humans, Eriksson thus evaluated the dosimetry of [^{68}Ga]Ga-DO3A-VS-Cys^{40}-exendin-4 in rats, pigs, non-human primates and a human[57]: (1) human whole body effective dose: 0.014-0.017 mSv/MBq; (2) The absorbed dose in the kidneys: 0.28-0.65 mGy/MBq; and (3) The maximum yearly administered amounts: 536-455 MBq. More than 200 MBq of this probe can be serviced yearly in clinical, allowing for repeated (2-4 times) scanning.

In addition, several ^{64}Cu-labeled exendin-4 tracers also were reported: (1) [Lys40(DOTA-^{64}Cu)-NH$_2$]-exendin-4[58] showed high binding specificity to rodent β cells by *ex vivo* autoradiography; (2) ^{64}Cu-DO3A-VS-Cys^{40}-exendin-4 (Figure 3)[55], demonstrated the feasibility of *in vivo* PET imaging islets grafted in mouse liver by virtue of a high and specific uptake in INS-1 tumors despite high renal uptake; and (3) ^{64}Cu-BaMalSar-exendin-4 and ^{64}Cu-Mal$_2$Sar-(exendin-4)$_2$[22], indicated persistent and specific uptake in an INS-1 insulinoma model with high renal uptake.

Taken together, these results indicated that Exendin analogues hold great potential for non-invasive imaging of pancreatic islet cells/beta cells.

^{11}C-LABELED TRACER AS GK PROBE FOR IMAGING PANCREATIC ISLET CELL

GK as an enzyme predominantly presents in β cells in the pancreas[59] and in hepatocytes[60], which plays a key role on regulation of glucose homeostasis in blood[20]. GK could be a potentially biomarker for imaging pancreatic islet since it expressed in pancreatic β cells, not in exocrine cells.

Recently, Jahan *et al*[20] reported the synthesis of [^{11}C]AZ12504948 (Figure 6) as a new probe for GK imaging in pancreas and liver. PET/CT imaging in pigs indicated that moderate pancreatic uptake was observed. The hepatic distribution was homogeneous and followed similar kinetics as the pancreas but with higher amplitude 30 min p.i. In the block study, co-injection of cold AZ12504948 with probe reduced radioactivity uptake by 24% in pancreas and by 15% in the liver after 30-60 min p.i. However, due to high uptake in the liver, it was not suitable to quantify the level of islet cells in liver for treatment of T1D by islet transplantation.

PANCREATIC SOMATOSTATIN RECEPTORS (SSTRS) -TARGETED PROBES FOR β-CELL IMAGING

Natural somatostatin as a peptide hormone, distributes in the hypothalamus, adrenals and pancreas, which it is a cyclic tetradecapeptide[61]. In the pancreas, somatostatin is considered an important regulator of insulin and other pancreatic endocrine hormones secretion[62]. In the rodent islets of Langerhans that consist of endocrine

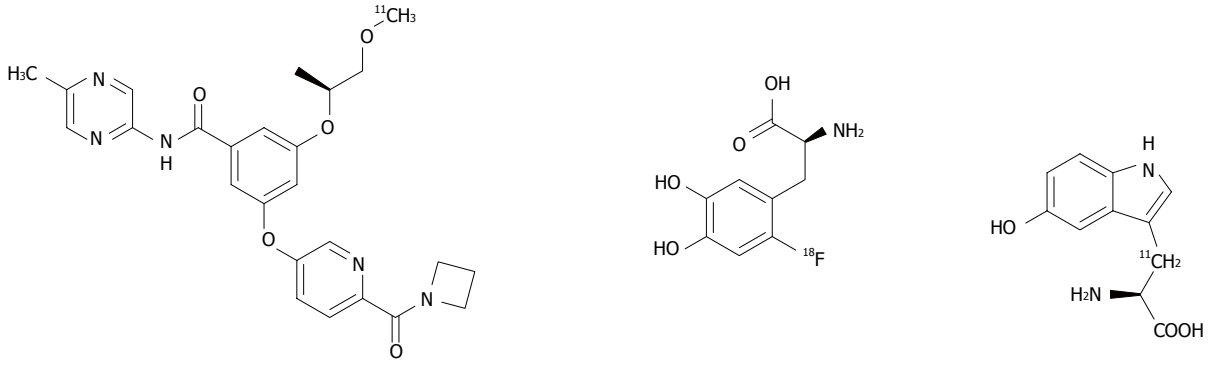

Figure 6 Chemical structures of [^{11}C]AZ12504948, L-3,4-Dihydroxy-6-^{18}F-fluoro-phenylalanine and ^{11}C-5-hydroxy-Ltryptophan. [^{18}F]F-DOPA: L-3,4-Dihydroxy-6-18F-fluoro-phenylalanine; [^{11}C]5-HTP: ^{11}C-5-hydroxy-Ltryptophan.

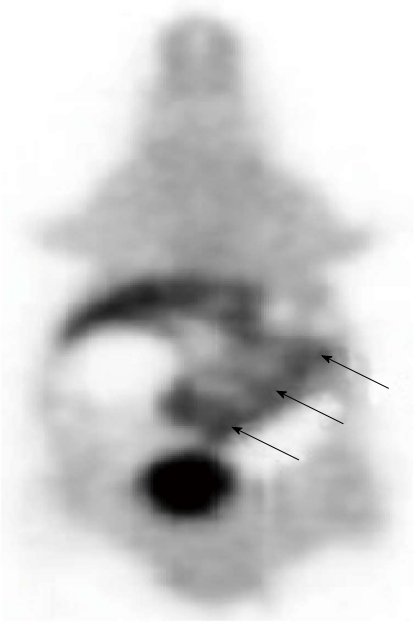

Figure 7 Positron emission tomography imaging of L-3,4-Dihydroxy-6-^{18}F-fluoro-phenylalanine for detection of sites of viable islet cells transplanted in STZ-induced type 1 diabetes nu/nu mouse model. The images shown irregular distribution of radiotracer uptake at the site of the grafted islet cells in the abdominal wall (black arrows). Reprinted with permission from Ref. [16].

cells, the insulin-secreting beta cells are the majority of the cell population and abundantly express SSTRs. Therefore, the expression of SSTRs is considered a potential biomarker for the measurement of beta cells.

Sako *et al*[63] developed a novel gallium-68 analogue: ^{68}Ga-DOTA-octreotide. In normal and diabetic rats studies, high accumulation of ^{68}Ga-tracer was observed in the urinary bladder and kidney. Accumulation of ^{68}Ga-tracer was apparent in the normal pancreas, while weak radioactivity was detected in the liver. The ^{68}Ga-DOTA-octreotide radioactivity in the pancreas showed a rapid increase within 1 min p.i. and then gradually increased and reached 0.99% ± 0.24% ID at the end of the PET scans. In contrast, ^{68}Ga-tracer radioactivity in the liver quickly reached a peak at 15 s p.i. and decreased rapidly thereafter reaching 0.17% ± 0.08% ID at the end of the PET scans. The accumulation of ^{68}Ga-DOTA-octreotide was much higher in the kidney and urinary bladder. Blocking studies indicated that the pancreatic accumulation of ^{68}Ga-tracer was significantly decreased in the unlabeled octreotide-treated group. In the STZ-treated DM model rats, it exhibited lower accumulation in the pancreas than that in normal rats. Thus ^{68}Ga-tracer could be a potential PET tracer for quantifying islet cells.

OTHER PROBES FOR ISLET CELLS IMAGING

L-3,4-Dihydroxy-6-^{18}F-fluoro-phenylalanine

Sweet *et al*[35] discovered the scaffolds of L-Dihydroxyphenylalanine could become β-cell probes for PET imaging. [^{18}F]F-DOPA (Figure 7) was successfully radiosynthesized and its biochemical mechanism was researched. The mechanism of [^{18}F]F-DOPA was changed to ^{18}F-dopamine by decarboxylation in the aromatic amino decarboxylase has been confirmed by blocking study, which resulted in back diffusion of the PET probe from the neuroendocrine cells into extracellular spaces.

In 2014, Eriksson *et al*[16] attempted to use [^{18}F]F-DOPA as the probe for imaging transplanted islet cells. *In vivo* imaging revealed irregular distribution of the transplantation islet mass in the abdominal wall, since the probe was excreted in biliary excretion, which could be potentially effect of graft map (Figure 7).

^{11}C-5-hydroxy-Ltryptophan

5-hydroxy-L-^{11}C-tryptophan ([^{11}C]5-HTP, Figure 6) as biogenic precursor, was first applied for evaluation of rate of serotonin biosynthesis by dopa decarboxylase (DDC) in CNS[64]. High pancreas uptake of the probe in the health human has not previously been systematically investigated.

Recently, Eriksson *et al*[65] reported that *in vitro* binding assay for [^{11}C]5-HTP in endocrine cells, and

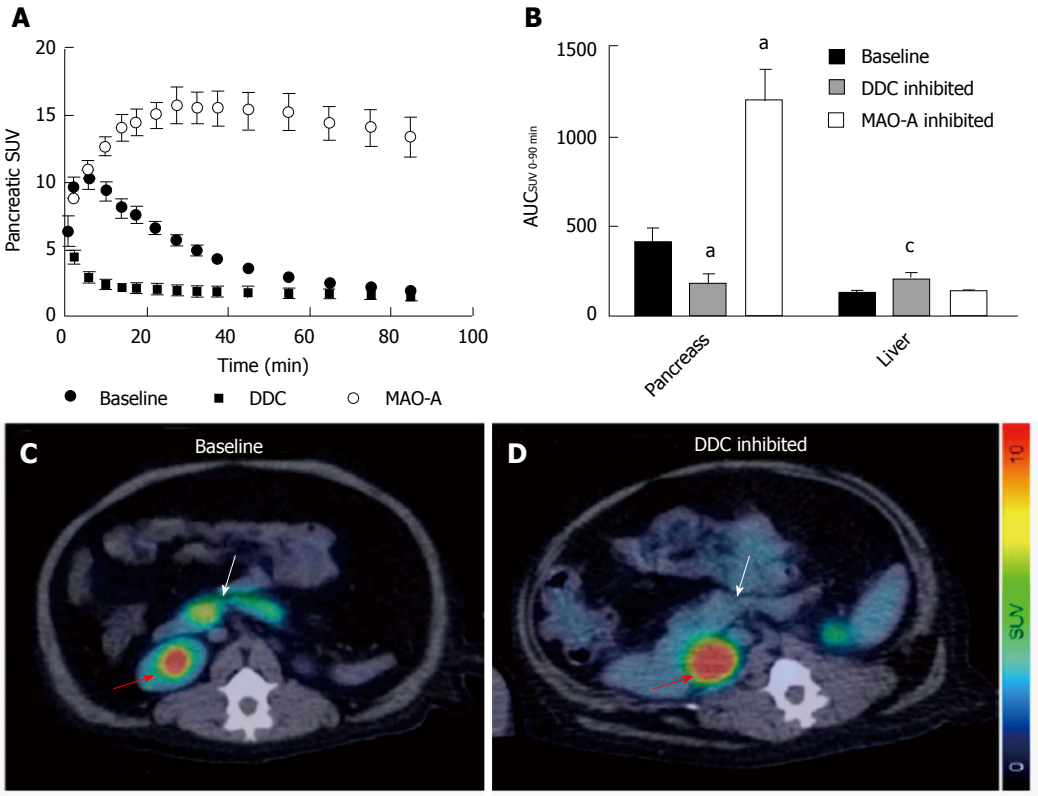

Figure 8 Positron emission tomography/computed tomography imaging of 5-hydroxy-L-^{11}C-tryptophan in non-human primates. A: SUV of [^{11}C]5-HTP uptake in pancreas of nonhuman primate after 0-100 min p.i.; B: Pancreas uptake was significantly decreased by pretreated inhibitors ($^{a}P < 0.05$; $^{c}P < 0.001$); C and D: Abdominal HTP and PET/CT fusion images. Pancreas: White arrow; Kidney pelvis: Red arrow. Reprinted with permission from Ref.[65]. [^{11}C]5-HTTP: 5-hydroxy-L-^{11}C-tryptophan; PET/CT: Positron emission tomography/computed tomography. DDC:Dopa decarboxylase.

exocrine cells. The result showed that only specific binding in insulinoma cell line and human islets, namely endocrine cells. The further studied indicated that the probe targeted serotonin, which was produced by intracellular. In the non-human primate studies, they were pretreated by inhibition of DDC enzyme, which the probe was converted to ^{11}C-serotonin, and inhibition of monoamine oxidase-A (MAO-A), which was responsible for serotonin degradation (Figure 8). In the result indicated that it was distinctly decreased in DDC and increased in MAO-A in primates pancreas. It displayed the similarly result in the rat by inhibition of MAO-A, and uptake was decreased in rodent with induced diabetes. Therefore, [^{11}C]5-HTP as PET probe could be suitable to quantitative the level of the serotonergic system in pancreas.

CONCLUSION

Ideal islet and β cell imaging probes would have a suitable washout and residence time in the subjects, be able to provided high specific binding for PET images with lowest non-specific binding in surrounding tissues without toxic to islets, and without pretreatment of islets before transplanted islet.

Currently, many research investigators are developing and evaluating biomarkers specific for pancreatic islet cells, particularly beta cells. A number of potential candidates for islet cell imaging have been reported, such as VMAT2, GLP-1R, SUR1, and GK. Carbon-11, fluorine-18, gallium-68 and copper-64 labeled PET tracers targeting these biomarkers have been evaluated in rodents, non-human primates, and humans. Among them, some tracers displayed great potential for non-invasive imaging of pancreatic islet cells. For example, ^{18}F-TTCO-Cys^{40}-exendin-4 demonstrated specific binding to GLP-1R and was suitable to quantity the level of islet cells in the rodent; [^{68}Ga]Ga-DO3AVS-Cys^{40}-exendin-4 displayed promising data of PET imaging in human studies and evaluated the dosimetry in rats, pigs, monkey and one patient for transfer into clinic study.

However, the accurate, noninvasive, and safe detection of β-cell mass or grafted islet mass *in vivo* remains a highly and difficultly challenging goal. Developing PET tracers with nontoxic, high specific binding to β-cell in the pancreatic islet is an important objective for future studies.

REFERENCES

1 **Atkinson MA**, Eisenbarth GS, Michels AW. Type 1 diabetes. *Lancet* 2014; **383**: 69-82 [PMID: 23890997 DOI: 10.1016/S0140-6736(13)60591-7]

2 **Dabelea D**, Mayer-Davis EJ, Saydah S, Imperatore G, Linder B, Divers J, Bell R, Badaru A, Talton JW, Crume T, Liese AD, Merchant AT, Lawrence JM, Reynolds K, Dolan L, Liu LL, Hamman RF. Prevalence of type 1 and type 2 diabetes among

children and adolescents from 2001 to 2009. *JAMA* 2014; **311**: 1778-1786 [PMID: 24794371 DOI: 10.1001/jama.2014.3201]

3 **Marathe CS**, Drogemuller CJ, Marathe JA, Loudavaris T, Hawthorne WJ, O'Connell PJ, Radford T, Kay TW, Horowitz M, Coates PT, Torpy DJ. Islet cell transplantation in Australia: screening, remote transplantation, and incretin hormone secretion in insulin independent patients. *Horm Metab Res* 2015; **47**: 16-23 [PMID: 25350521 DOI: 10.1055/s-0034-1389941]

4 **Bluestone JA**, Herold K, Eisenbarth G. Genetics, pathogenesis and clinical interventions in type 1 diabetes. *Nature* 2010; **464**: 1293-1300 [PMID: 20432533 DOI: 10.1038/nature08933]

5 **Harjutsalo V**, Forsblom C, Groop PH. Time trends in mortality in patients with type 1 diabetes: nationwide population based cohort study. *BMJ* 2011; **343**: d5364 [PMID: 21903695 DOI: 10.1136/bmj.d5364]

6 **Kashiwagi A**. General concept and pathophysiological mechanisms of progression of macrovascular complications in diabetes. *Nihon Rinsho* 2010; **68**: 777-787 [PMID: 20446569]

7 **van Belle TL**, Coppieters KT, von Herrath MG. Type 1 diabetes: etiology, immunology, and therapeutic strategies. *Physiol Rev* 2011; **91**: 79-118 [PMID: 21248163 DOI: 10.1152/physrev.00003.2010]

8 **Vrochides D**, Paraskevas S, Papanikolaou V. Transplantation for type 1 diabetes mellitus. Whole organ or islets? *Hippokratia* 2009; **13**: 6-8 [PMID: 19240814]

9 **Langer RM**. Islet transplantation: lessons learned since the Edmonton breakthrough. *Transplant Proc* 2010; **42**: 1421-1424 [PMID: 20620447 DOI: 10.1016/j.transproceed.2010.04.021]

10 **Shapiro AM**, Hao EG, Lakey JR, Yakimets WJ, Churchill TA, Mitlianga PG, Papadopoulos GK, Elliott JF, Rajotte RV, Kneteman NM. Novel approaches toward early diagnosis of islet allograft rejection. *Transplantation* 2001; **71**: 1709-1718 [PMID: 11455247]

11 **Shapiro AM**, Lakey JR, Ryan EA, Korbutt GS, Toth E, Warnock GL, Kneteman NM, Rajotte RV. Islet transplantation in seven patients with type 1 diabetes mellitus using a glucocorticoid-free immunosuppressive regimen. *N Engl J Med* 2000; **343**: 230-238 [PMID: 10911004 DOI: 10.1056/Nejm200007273430401]

12 **Gambhir SS**. Molecular imaging of cancer with positron emission tomography. *Nat Rev Cancer* 2002; **2**: 683-693 [PMID: 12209157 DOI: 10.1038/nrc882]

13 **Souza F**, Freeby M, Hultman K, Simpson N, Herron A, Witkowsky P, Liu E, Maffei A, Harris PE. Current progress in non-invasive imaging of beta cell mass of the endocrine pancreas. *Curr Med Chem* 2006; **13**: 2761-2773 [PMID: 17073627 DOI: 10.2174/092986706778521940]

14 **Normandin MD**, Petersen KF, Ding YS, Lin SF, Naik S, Fowles K, Skovronsky DM, Herold KC, McCarthy TJ, Calle RA, Carson RE, Treadway JL, Cline GW. In vivo imaging of endogenous pancreatic β-cell mass in healthy and type 1 diabetic subjects using 18F-fluoropropyl-dihydrotetrabenazine and PET. *J Nucl Med* 2012; **53**: 908-916 [PMID: 22573821 DOI: 10.2967/jnumed.111.100545]

15 **Harris PE**, Farwell MD, Ichise M. PET quantification of pancreatic VMAT 2 binding using (+) and (-) enantiomers of [^{18}F]FP-DTBZ in baboons. *Nucl Med Biol* 2013; **40**: 60-64 [PMID: 23102539 DOI: 10.1016/j.nucmedbio.2012.09.003]

16 **Eriksson O**, Mintz A, Liu C, Yu M, Naji A, Alavi A. On the use of [18F]DOPA as an imaging biomarker for transplanted islet mass. *Ann Nucl Med* 2014; **28**: 47-52 [PMID: 24166476 DOI: 10.1007/s12149-013-0779-4]

17 **Manandhar B**, Ahn JM. Glucagon-like peptide-1 (GLP-1) analogs: recent advances, new possibilities, and therapeutic implications. *J Med Chem* 2015; **58**: 1020-1037 [PMID: 25349901 DOI: 10.1021/jm500810s]

18 **Karlsson F**, Antonodimitrakis PC, Eriksson O. Systematic screening of imaging biomarkers for the Islets of Langerhans, among clinically available positron emission tomography tracers. *Nucl Med Biol* 2015; **42**: 762-769 [PMID: 26138288 DOI: 10.1016/j.nucmedbio.2015.06.004]

19 **Nalin L**, Selvaraju RK, Velikyan I, Berglund M, Andréasson S, Wikstrand A, Rydén A, Lubberink M, Kandeel F, Nyman G, Korsgren O, Eriksson O, Jensen-Waern M. Positron emission tomography imaging of the glucagon-like peptide-1 receptor in healthy and streptozotocin-induced diabetic pigs. *Eur J Nucl Med Mol Imaging* 2014; **41**: 1800-1810 [PMID: 24643781 DOI: 10.1007/s00259-014-2745-3]

20 **Jahan M**, Johnström P, Nag S, Takano A, Korsgren O, Johansson L, Halldin C, Eriksson O. Synthesis and biological evaluation of [^{11}C]AZ12504948; a novel tracer for imaging of glucokinase in pancreas and liver. *Nucl Med Biol* 2015; **42**: 387-394 [PMID: 25633247 DOI: 10.1016/j.nucmedbio.2014.12.003]

21 **Wang Y**, Lim K, Normandin M, Zhao X, Cline GW, Ding YS. Synthesis and evaluation of [18F]exendin (9-39) as a potential biomarker to measure pancreatic β-cell mass. *Nucl Med Biol* 2012; **39**: 167-176 [PMID: 22033026 DOI: 10.1016/j.nucmedbio.2011.07.011]

22 **Wu Z**, Liu S, Nair I, Omori K, Scott S, Todorov I, Shively JE, Conti PS, Li Z, Kandeel F. (64)Cu labeled sarcophagine exendin-4 for microPET imaging of glucagon like peptide-1 receptor expression. *Theranostics* 2014; **4**: 770-777 [PMID: 24955138 DOI: 10.7150/thno.7759]

23 **Wu Z**, Liu S, Hassink M, Nair I, Park R, Li L, Todorov I, Fox JM, Li Z, Shively JE, Conti PS, Kandeel F. Development and evaluation of 18F-TTCO-Cys40-Exendin-4: a PET probe for imaging transplanted islets. *J Nucl Med* 2013; **54**: 244-251 [PMID: 23297075 DOI: 10.2967/jnumed.112.109694]

24 **Gao H**, Niu G, Yang M, Quan Q, Ma Y, Murage EN, Ahn JM, Kiesewetter DO, Chen X. PET of insulinoma using ^{18}F-FBEM-EM3106B, a new GLP-1 analogue. *Mol Pharm* 2011; **8**: 1775-1782 [PMID: 21800885 DOI: 10.1021/mp200141x]

25 **Kiesewetter DO**, Guo N, Guo J, Gao H, Zhu L, Ma Y, Niu G, Chen X. Evaluation of an [(18)F]AlF-NOTA Analog of Exendin-4 for Imaging of GLP-1 Receptor in Insulinoma. *Theranostics* 2012; **2**: 999-1009 [PMID: 23139727 DOI: 10.7150/thno.5276]

26 **Kiesewetter DO**, Gao H, Ma Y, Niu G, Quan Q, Guo N, Chen X. 18F-radiolabeled analogs of exendin-4 for PET imaging of GLP-1 in insulinoma. *Eur J Nucl Med Mol Imaging* 2012; **39**: 463-473 [PMID: 22170321 DOI: 10.1007/s00259-011-1980-0]

27 **Selvaraju RK**, Velikyan I, Johansson L, Wu Z, Todorov I, Shively J, Kandeel F, Korsgren O, Eriksson O. In vivo imaging of the glucagonlike peptide 1 receptor in the pancreas with 68Ga-labeled DO3A-exendin-4. *J Nucl Med* 2013; **54**: 1458-1463 [PMID: 23761918 DOI: 10.2967/jnumed.112.114066]

28 **Mikkola K**, Yim CB, Fagerholm V, Ishizu T, Elomaa VV, Rajander J, Jurttila J, Saanijoki T, Tolvanen T, Tirri M, Gourni E, Béhé M, Gotthardt M, Reubi JC, Mäcke H, Roivainen A, Solin O, Nuutila P. 64Cu- and 68Ga-labelled [Nle(14),Lys(40)(Ahx-NODAGA)NH2]-exendin-4 for pancreatic beta cell imaging in rats. *Mol Imaging Biol* 2014; **16**: 255-263 [PMID: 24101374 DOI: 10.1007/s11307-013-0691-2]

29 **Jahan M**, Eriksson O, Johnström P, Korsgren O, Sundin A, Johansson L, Halldin C. Decreased defluorination using the novel beta-cell imaging agent [18F]FE-DTBZ-d4 in pigs examined by PET. *EJNMMI Res* 2011; **1**: 33 [PMID: 22214308 DOI: 10.1186/2191-219x-1-33]

30 **Tsao HH**, Skovronsky DM, Lin KJ, Yen TC, Wey SP, Kung MP. Sigma receptor binding of tetrabenazine series tracers targeting VMAT2 in rat pancreas. *Nucl Med Biol* 2011; **38**: 1029-1034 [PMID: 21982574 DOI: 10.1016/j.nucmedbio.2011.03.006]

31 **Singhal T**, Ding YS, Weinzimmer D, Normandin MD, Labaree D, Ropchan J, Nabulsi N, Lin SF, Skaddan MB, Soeller WC, Huang Y, Carson RE, Treadway JL, Cline GW. Pancreatic beta cell mass PET imaging and quantification with [11C]DTBZ and [18F]FP-(+)-DTBZ in rodent models of diabetes. *Mol Imaging Biol* 2011; **13**: 973-984 [PMID: 20824509 DOI: 10.1007/s11307-010-0406-x]

32 **Wimalasena K**. Vesicular monoamine transporters: structure-function, pharmacology, and medicinal chemistry. *Med Res Rev* 2011; **31**: 483-519 [PMID: 20135628 DOI: 10.1002/med.20187]

33 **Matsuda H**, Kimura H, Ogawa Y, Kawashima H, Toyoda K, Mukai E, Fujimoto H, Nakamura H, Hirao K, Ono M, Inagaki N, Saji H. Radiosynthesis and evaluation of [F-18]Mitiglinide derivatives as PET tracers for sulfonylurea receptor in pancreatic islets. *J Labelled Compd Rad* 2011; **54**: S510-S510

34 **Brom M**, Andrałojć K, Oyen WJ, Boerman OC, Gotthardt M. Development of radiotracers for the determination of the beta-cell mass in vivo. *Curr Pharm Des* 2010; **16**: 1561-1567 [PMID: 20146667 DOI: 10.2174/138161210791164126]

35 **Sweet IR**, Cook DL, Lernmark A, Greenbaum CJ, Wallen AR, Marcum ES, Stekhova SA, Krohn KA. Systematic screening of potential beta-cell imaging agents. *Biochem Biophys Res Commun* 2004; **314**: 976-983 [PMID: 14751228 DOI: 10.1016/j.bbrc.2003.12.182]

36 **Wu Z**, Kandeel F. Radionuclide probes for molecular imaging of pancreatic beta-cells. *Adv Drug Deliv Rev* 2010; **62**: 1125-1138 [PMID: 20854861 DOI: 10.1016/j.addr.2010.09.006]

37 **Maffei A**, Liu Z, Witkowski P, Moschella F, Del Pozzo G, Liu E, Herold K, Winchester RJ, Hardy MA, Harris PE. Identification of tissue-restricted transcripts in human islets. *Endocrinology* 2004; **145**: 4513-4521 [PMID: 15231694 DOI: 10.1210/en.2004-0691]

38 **Anlauf M**, Eissele R, Schäfer MK, Eiden LE, Arnold R, Pauser U, Klöppel G, Weihe E. Expression of the two isoforms of the vesicular monoamine transporter (VMAT1 and VMAT2) in the endocrine pancreas and pancreatic endocrine tumors. *J Histochem Cytochem* 2003; **51**: 1027-1040 [PMID: 12871984]

39 **DaSilva JN**, Kilbourn MR, Mangner TJ. Synthesis of a [11C]methoxy derivative of alpha-dihydrotetrabenazine: a radioligand for studying the vesicular monoamine transporter. *Appl Radiat Isot* 1993; **44**: 1487-1489 [PMID: 7903060 DOI: 10.1016/0969-8043(93)90103-H]

40 **Harris PE**, Ferrara C, Barba P, Polito T, Freeby M, Maffei A. VMAT2 gene expression and function as it applies to imaging beta-cell mass. *J Mol Med* (Berl) 2008; **86**: 5-16 [PMID: 17665159 DOI: 10.1007/s00109-007-0242-x]

41 **Goland R**, Freeby M, Parsey R, Saisho Y, Kumar D, Simpson N, Hirsch J, Prince M, Maffei A, Mann JJ, Butler PC, Van Heertum R, Leibel RL, Ichise M, Harris PE. 11C-dihydrotetrabenazine PET of the pancreas in subjects with long-standing type 1 diabetes and in healthy controls. *J Nucl Med* 2009; **50**: 382-389 [PMID: 19223416 DOI: 10.2967/jnumed.108.054866]

42 **Kung MP**, Hou C, Lieberman BP, Oya S, Ponde DE, Blankemeyer E, Skovronsky D, Kilbourn MR, Kung HF. In vivo imaging of beta-cell mass in rats using 18F-FP-(+)-DTBZ: a potential PET ligand for studying diabetes mellitus. *J Nucl Med* 2008; **49**: 1171-1176 [PMID: 18552132 DOI: 10.2967/jnumed.108.051680]

43 **Kung HF**, Lieberman BP, Zhuang ZP, Oya S, Kung MP, Choi SR, Poessl K, Blankemeyer E, Hou C, Skovronsky D, Kilbourn M. In vivo imaging of vesicular monoamine transporter 2 in pancreas using an (18)F epoxide derivative of tetrabenazine. *Nucl Med Biol* 2008; **35**: 825-837 [PMID: 19026944 DOI: 10.1016/j.nucmedbio.2008.08.004]

44 **Kumar A**, Lo ST, Öz OK, Sun X. Derivatization of (±) dihydrotetrabenazine for copper-64 labeling towards long-lived radiotracers for PET imaging of the vesicular monoamine transporter 2. *Bioorg Med Chem Lett* 2014; **24**: 5663-5665 [PMID: 25467156 DOI: 10.1016/j.bmcl.2014.10.070]

45 **Kilbourn M**, Lee L, Vander Borght T, Jewett D, Frey K. Binding of alpha-dihydrotetrabenazine to the vesicular monoamine transporter is stereospecific. *Eur J Pharmacol* 1995; **278**: 249-252 [PMID: 7589162 DOI: 10.1016/0014-2999(95)00162-E]

46 **Bell GI**, Santerre RF, Mullenbach GT. Hamster preproglucagon contains the sequence of glucagon and two related peptides. *Nature* 1983; **302**: 716-718 [PMID: 6835407 DOI: 10.1038/302716a0]

47 **Lund PK**, Goodman RH, Dee PC, Habener JF. Pancreatic preproglucagon cDNA contains two glucagon-related coding sequences arranged in tandem. *Proc Natl Acad Sci USA* 1982; **79**: 345-349 [PMID: 7043459 DOI: 10.1073/pnas.79.2.345]

48 **Campos RV**, Lee YC, Drucker DJ. Divergent tissue-specific and developmental expression of receptors for glucagon and glucagon-like peptide-1 in the mouse. *Endocrinology* 1994; **134**: 2156-2164 [PMID: 8156917]

49 **Bullock BP**, Heller RS, Habener JF. Tissue distribution of messenger ribonucleic acid encoding the rat glucagon-like peptide-1 receptor. *Endocrinology* 1996; **137**: 2968-2978 [PMID: 8770921]

50 **Tornehave D**, Kristensen P, Rømer J, Knudsen LB, Heller RS. Expression of the GLP-1 receptor in mouse, rat, and human pancreas. *J Histochem Cytochem* 2008; **56**: 841-851 [PMID: 18541709 DOI: 10.1369/jhc.2008.951319]

51 **Göke R**, Fehmann HC, Linn T, Schmidt H, Krause M, Eng J, Göke B. Exendin-4 is a high potency agonist and truncated exendin-(9-39)-amide an antagonist at the glucagon-like peptide 1-(7-36)-amide receptor of insulin-secreting beta-cells. *J Biol Chem* 1993; **268**: 19650-19655 [PMID: 8396143]

52 **Eng J**, Kleinman WA, Singh L, Singh G, Raufman JP. Isolation and characterization of exendin-4, an exendin-3 analogue, from Heloderma suspectum venom. Further evidence for an exendin receptor on dispersed acini from guinea pig pancreas. *J Biol Chem* 1992; **267**: 7402-7405 [PMID: 1313797]

53 **Edwards CM**, Stanley SA, Davis R, Brynes AE, Frost GS, Seal LJ, Ghatei MA, Bloom SR. Exendin-4 reduces fasting and postprandial glucose and decreases energy intake in healthy volunteers. *Am J Physiol Endocrinol Metab* 2001; **281**: E155-E161 [PMID: 11404233]

54 **Malhotra R**, Singh L, Eng J, Raufman JP. Exendin-4, a new peptide from Heloderma suspectum venom, potentiates cholecystokinin-induced amylase release from rat pancreatic acini. *Regul Pept* 1992; **41**: 149-156 [PMID: 1279756 DOI: 10.1016/0167-0115(92)90044-U]

55 **Wu Z**, Todorov I, Li L, Bading JR, Li Z, Nair I, Ishiyama K, Colcher D, Conti PE, Fraser SE, Shively JE, Kandeel F. In vivo imaging of transplanted islets with 64Cu-DO3A-VS-Cys40-Exendin-4 by targeting GLP-1 receptor. *Bioconjug Chem* 2011; **22**: 1587-1594 [PMID: 21692471 DOI: 10.1021/bc200132t]

56 **Eriksson O**, Velikyan I, Selvaraju RK, Kandeel F, Johansson L, Antoni G, Eriksson B, Sörensen J, Korsgren O. Detection of metastatic insulinoma by positron emission tomography with [(68)ga]exendin-4-a case report. *J Clin Endocrinol Metab* 2014; **99**: 1519-1524 [PMID: 24512490 DOI: 10.1210/jc.2013-3541]

57 **Selvaraju RK**, Bulenga TN, Espes D, Lubberink M, Sörensen J, Eriksson B, Estrada S, Velikyan I, Eriksson O. Dosimetry of [(68)Ga]Ga-DO3A-VS-Cys(40)-Exendin-4 in rodents, pigs, non-human primates and human - repeated scanning in human is possible. *Am J Nucl Med Mol Imaging* 2015; **5**: 259-269 [PMID: 26069859]

58 **Connolly BM**, Vanko A, McQuade P, Guenther I, Meng X, Rubins D, Waterhouse R, Hargreaves R, Sur C, Hostetler E. Ex vivo imaging of pancreatic beta cells using a radiolabeled GLP-1 receptor agonist. *Mol Imaging Biol* 2012; **14**: 79-87 [PMID: 21394533 DOI: 10.1007/s11307-011-0481-7]

59 **Matschinsky FM**, Ellerman JE. Metabolism of glucose in the islets of Langerhans. *J Biol Chem* 1968; **243**: 2730-2736 [PMID: 4870741]

60 **Walker DG**, Rao S. The role of glucokinase in the phosphorylation of glucose by rat liver. *Biochem J* 1964; **90**: 360-368 [PMID: 5834248]

61 **Roth DJ**, Jansen ED, Powers AC, Wang TG. A novel method of monitoring response to islet transplantation: bioluminescent imaging of an NF-kB transgenic mouse model. *Transplantation* 2006; **81**: 1185-1190 [PMID: 16641606 DOI: 10.1097/01.tp.0000203808.84963.13]

62 **Villalobos C**, Nadal A, Núñez L, Quesada I, Chamero P, Alonso MT, García-Sancho J. Bioluminescence imaging of nuclear calcium oscillations in intact pancreatic islets of Langerhans from the mouse. *Cell Calcium* 2005; **38**: 131-139 [PMID: 16095687 DOI: 10.1016/j.ceca.2005.06.029]

63 **Sako T**, Hasegawa K, Nishimura M, Kanayama Y, Wada Y, Hayashinaka E, Cui Y, Kataoka Y, Senda M, Watanabe Y. Positron emission tomography study on pancreatic somatostatin receptors in normal and diabetic rats with 68Ga-DOTA-octreotide: a potential PET tracer for beta cell mass measurement. *Biochem Biophys Res Commun* 2013; **442**: 79-84 [PMID: 24220338 DOI: 10.1016/j.bbrc.2013.11.001]

64 **Lundquist P**, Blomquist G, Hartvig P, Hagberg GE, Torstenson R, Hammarlund-Udenaes M, Långström B. Validation studies on the 5-hydroxy-L-[beta-11C]-tryptophan/PET method for probing the decarboxylase step in serotonin synthesis. *Synapse* 2006; **59**: 521-531 [PMID: 16565973 DOI: 10.1002/syn.20268]

65 **Eriksson O**, Selvaraju RK, Johansson L, Eriksson JW, Sundin

A, Antoni G, Sörensen J, Eriksson B, Korsgren O. Quantitative imaging of serotonergic biosynthesis and degradation in the endocrine pancreas. *J Nucl Med* 2014; **55**: 460-465 [PMID: 24525204 DOI: 10.2967/jnumed.113.125187]

P- Reviewer: Gao BL, Gumustas OG **S- Editor**: Gong XM
L- Editor: A **E- Editor**: Wu HL

World Journal of Radiology

Submit a Manuscript: http://www.wjgnet.com/esps/
Help Desk: http://www.wjgnet.com/esps/helpdesk.aspx
DOI: 10.4329/wjr.v8.i9.775

World J Radiol 2016 September 28; 8(9): 775-784
ISSN 1949-8470 (online)

REVIEW

Thoracic ultrasound: An adjunctive and valuable imaging tool in emergency, resource-limited settings and for a sustainable monitoring of patients

Francesca M Trovato, Daniela Catalano, Guglielmo M Trovato

Francesca M Trovato, Accident and Emergency Department, Ospedale Civile, 97010 Ragusa, Italy

Francesca M Trovato, Daniela Catalano, Guglielmo M Trovato, Department of Clinical and Experimental Medicine, University of Catania, 95124 Catania, Italy

Daniela Catalano, Postgraduate School of Clinical Echography, AOU Policlinico of the University of Catania, 95100 Catania, Italy

Guglielmo M Trovato, Clinical Research and Innovation Project Planning Unit, AOU Policlinico of the University of Catania, 95100 Catania, Italy

Author contributions: The paper was written by the authors stated.

Conflict-of-interest statement: No conflict of interest is declared in this invited manuscript.

Manuscript source: Invited manuscript

Correspondence to: Guglielmo M Trovato, MD, Clinical Research and Innovation Project Planning Unit, AOU Policlinico of the University of Catania, via Santa Sofia 78, 95100 Catania, Italy. guglielmotrovato@unict.it
Telephone: +39-095-3781533

Received: April 28, 2016
Peer-review started: May 3, 2016
First decision: June 17, 2016
Revised: July 14, 2016
Accepted: July 29, 2016
Article in press: August 1, 2016
Published online: September 28, 2016

Abstract

Imaging workup of patients referred for elective assessment of chest disease requires an articulated approach: Imaging is asked for achieving timely diagnosis. The concurrent or subsequent use of thoracic ultrasound (TUS) with conventional (chest X-rays-) and more advanced imaging procedures (computed tomography and magnetic resonance imaging) implies advantages, limitations and actual problems. Indeed, despite TUS may provide useful imaging of pleura, lung and heart disease, emergency scenarios are currently the most warranted field of application of TUS: Pleural effusion, pneumothorax, lung consolidation. This stems from its role in limited resources subsets; actually, ultrasound is an excellent risk reducing tool, which acts by: (1) increasing diagnostic certainty; (2) shortening time to definitive therapy; and (3) decreasing problems from blind procedures that carry an inherent level of complications. In addition, paediatric and newborn disease are particularly suitable for TUS investigation, aimed at the detection of congenital or acquired chest disease avoiding, limiting or postponing radiological exposure. TUS improves the effectiveness of elective medical practice, in resource-limited settings, in small point of care facilities and particularly in poorer countries. Quality and information provided by the procedure are increased avoiding whenever possible artefacts that can prevent or mislead the achievement of the correct diagnosis. Reliable monitoring of patients is possible, taking into consideration that appropriate expertise, knowledge, skills, training, and even adequate equipment's suitability are not always and everywhere affordable or accessible. TUS is complementary imaging

procedure for the radiologist and an excellent basic diagnostic tool suitable to be shared with pneumologists, cardiologists and emergency physicians.

Key words: Thoracic ultrasound; Pneumonia; Pleural effusion; Pneumothorax; Clinical risk management; Overdiagnosis; Wastebasket diagnosis

Core tip: Thoracic ultrasound (TUS), with some technical limitations, may provide useful imaging of pleura, lung and heart disease. The field of application of TUS are pleural effusion, pneumothorax, and lung consolidation. Paediatric and newborn disease are suitable for TUS investigation aimed at the detection of congenital or acquired chest disease avoiding or limiting radiological exposure. TUS improves the effectiveness of medical practice in resource-limited settings, in small point-of-care facilities, in hostile environment and in poorer countries. Monitoring of patients is possible, depending on disease and context, not asking to the procedure more than it can give.

Trovato FM, Catalano D, Trovato GM. Thoracic ultrasound: An adjunctive and valuable imaging tool in emergency, resource-limited settings and for a sustainable monitoring of patients. *World J Radiol* 2016; 8(9): 775-784 Available from: URL: http://www.wjgnet.com/1949-8470/full/v8/i9/775.htm DOI: http://dx.doi.org/10.4329/wjr.v8.i9.775

FOREWORD

The history of imaging in medicine is an adventurous and generous history of high impact ideas, of courage and ingenious translation. This story originates from Marie Curie and her family, especially her daughter, Irene, a Nobel laureate too[1]. They, at the beginning and during the First World War, on 1914, developed and worked inside the mobile field hospitals that Marie Curie had established, training radiographers and technicians and convincing the surgeons to trust in the new technology: It was estimated that over one million wounded men were X-rayed in her units throughout the War[1]. It may be now easy to ignore, but this history, here briefly summarized, can help us to understand the root and the link between genius, emergency, limited resources and quality of training in a field which is the daily work of most physicians working with chest imaging.

OVERVIEW

The recall above reported is needed, even writing of ultrasound, since depicts a detailed model of practice and application of a sustainable innovative diagnostic and of another extremely useful tool in resource-limited settings and in hostile and dangerous situations. It also represents an organizational paradigm supported by ethical reasons. Despite Marie Curie and other heroic pioneers of radiology suffered from long-term radiation damage, the concept of maximum security for that time was highly respected. If claims of clinical risk management criteria, so often warranted nowadays, are not inspired to ethically, medically and scientifically proven aims and evidence, a botched management may ultimately damage doctors and patients, as well as society and population within an organizational machine scarcely productive if not harmful.

Emergency or elective assessment of chest disease requires often an articulated clinical approach to chest imaging, addressed also to the diagnosis of co-morbidities. Clinicians are often facing complex conditions, due to uncertainty or severity of the clinical presentation or to the hurry in which they are called to operate[2-4].

Indeed, despite elective thoracic ultrasound (TUS) may provide useful imaging of pleura, lung and heart disease, emergency scenarios are its current most developed field of application for detecting unsuspected, or for confirming physical signs of, pleural effusion, pneumothorax, and lung consolidation[5-7]. Paediatric and newborn disease are particularly suitable for TUS investigation aimed at the detection of congenital or acquired chest disease avoiding, limiting or post-poning radiological exposure[8,9]. TUS can improve the effectiveness of elective and emergency medical practice in resource-limited settings, in small point of care facilities and particularly in poorer countries[10]. Ultrasound is an excellent risk-reducing tool, which acts by: (1) increasing diagnostic certainty; (2) shortening time to definitive therapy; and (3) decreasing risks from blind procedures that carry an inherent level of complications[11-15]. Actually, the help of skilled ultrasound approaches in emergency or elective medicine is a pivotal component for preventing overdiagnosis and wastebasket diagnosis, apart avoiding as much as possible the risk of missing or erroneous diagnosis. Overdiagnosis, is the diagnosis of "disease" that will never cause symptoms, distress, or death during a patient's lifetime, or that are not the real determinant of a clinical presentation. Wastebasket diagnosis, is a vague, or even completely fake, medical label given for essentially non-medical reasons, such as to reassure the patient by providing an official-sounding label, to make the provider look effective, or to obtain approval for treatment; wastebasket diagnosis often and likely represents a heterogeneous group of disease and conditions[16]. The diagnostic refinements that can quickly provide a timely and expert patient's assessment by ultrasound are, in our experience, a significant corner-stone fostering precision, clarity and quality in any medical approach.

An important step toward the management of risk is insuring that physicians are properly trained and cre-dentialed according to national guidelines such as those

set by ACEP[15]. Proper quality assurance and improvement programs should be in place to identify and correct substandard practice, due to some variability of information of the published reports. Lastly, the standard of care for emergency ultrasound is the performance and interpretation of ultrasound by a physician certified in other specialties or in different settings: In these conditions credentials should have different goals, scope of practice, documentation requirements, and consequently should not be comparable to emergency medicine[12].

CLINICAL RISK ANALYSIS

The most relevant field of possible application of TUS is the diagnosis of lung consolidation, which is also one of the most critical diagnostic field of radiology. TUS may become a reliable tool capable of diagnosing pneumonia with high accuracy. Nonetheless, in the meanwhile, it is still a complementary source of information more than a promising attractive alternative to chest radiography and thoracic computed tomography (CT) scan: Most published studies, aimed at the definitions of the usefulness of lung ultrasound as a lone procedure for the diagnosis of pneumonia, are seemingly limited by methodological biases. Actually, as excellently summarized in a recent metanalysis[17], the most reputed studies on this topic, were "conducted to identify the usefulness of lung ultrasound for the diagnosis of pneumonia, but with inconsistent and inconclusive results"[17]. Nonetheless, the same accurate metanalysis reports the results in 1080 subjects from a selected group of nine studies and concludes that "lung ultrasound is a capable of diagnosing pneumonia with high accuracy and is a promising attractive alternative to chest radiography and thoracic CT scan", with a "97% sensitivity and a 94% specificity". In this regard, several matter of concern persists: There are many part of the lung which are blinded to the ultrasound imaging since, due to skeletal barrier no more than 70% of lung is realistically explorable by TUS[14]. The other not minor concern is that lung consolidation due to any cause - pneumonia or cancer - is not discriminated by ultrasound, also using more advanced ultrasound techniques, such as transient elastography[18]. In both cases the need of a radiological approach, after the preliminary diagnosis of consolidation and mainly if the clinical and/or the ultrasound picture persists, is evident, and the claimed high sensitivity and specificity may need some mitigation[14].

"Risk management in radiology is primarily developed and fostered to help safeguard patients, working personnel and the entire organisation. Protection of the organisation is largely grasped in terms of finance management. Potential drawbacks are linked to unreliable results that could damage its reputation"[19]. This is a particularly sensitive topic, since, apart the scientific foundation of some well conducted clinical trial, the reference to a diffuse "good practice" for TUS diagnosis could still be a slippery slope. "The essence of risk management is to survey all potential reasons for an inaccurate report in advance so that procedures can be put in place to prevent them"[20]. There are still relevant variations in imaging tests accuracy, due to technical reasons of the procedure itself or to inconclusive results and reports due to organization or individual professional limitations; therefore, even the analysis of associated risks has lacked uniformity in the cost-utility literature[21-26].

The central themes of the relevance of TUS in the cost-benefit analysis are the difficult appreciation of the times, ways, quality and consequences which are related to a systematic use of the procedure in emergency and the topics related to contexts, in elective, specialized, intensive or primary care, and in other areas yet.

Frequent and relevant applications, by which TUS may affect beneficially modulating the diagnostic and therapeutic pathways, are summarized in Table 1.

Also in these cases, the integration with more advanced radiological procedure is mandatory. This is true in emergency TUS, in which field the topic of unexpected clues is more frequently reported, but it is equally true in elective TUS, performed by radiologists or by internists-pneumologists.

EMERGENCY: OPPORTUNITIES AND RELIABILITY

Emergency ultrasound is a standard emergency medicine procedure and is included in any definitions of the practice of emergency medicine[15,16]. Since several years, also TUS is a component of this framework, which should be articulated within the specificity of the subsets in regards to risk management and to the clinical scenario, differently demanding according to affordability and policies[14,27-29].

The most relevant and relatively recent application of TUS in emergency is the quick detection of pneumothorax, by the significantly wide disappearance of the pleural line sliding[30-32]; this is a preliminary clinical diagnosis. It is precious in conditions of extreme facility shortage, where urgent intervention may be required and no timely confirm is available[33,34]. Nonetheless, TUS diagnosis of pneumothorax usually requires an urgent confirm, by CXR or CT, better to be available before any intervention procedure[35].

There is a widespread indication to TUS, and notably using the information derived by a great number of artefact, for the diagnosis of acute heart failure[36]. Actually, for this purpose, the detection of a great number of B-lines by TUS is not an imaging technique, but a bulk indication of chest-pulmonary pathology. These artefacts, preventing the view of details of the underlying condition, provide a generic information: Patients with congestive heart failure, COPD, pulmonary fibrosis and many other conditions, including the normal lung and

Table 1 Thoracic ultrasound - main indications

The physical examination by a non-radiologist MD can be usefully completed by a thorough and fast chest exploration. The aims are
To clarify symptoms already known (dyspnea, chest pain, fever, cough) or detected signs, such as rales, crackles or dullness
To detect unexpected chest abnormalities such as pleural effusion or lung consolidation in subjects with few or no evident respiratory symptom
Information and clues derived by TUS may focus better to further diagnostic definition, by radiology or by other procedures, avoiding time-wasting and even detrimental choices
The detection of pneumothorax by TUS is a quite simple and direct diagnosis of a not rare condition (see below), which should be usefully addressed to radiology, often including CT, for confirm. TUS has the great merit of making possible this direct pathway avoiding or postponing the more usual steps of chest pain work-up: Cardiological and laboratory investigations and preventive pharmacological drugs
In addition, the detection of subpleural infiltrates after a blunt thoracic trauma, apparently relatively uneventful, can address to a subsequent better focused diagnostic workup
Signs and symptoms initially addressing to different organs or body areas
Upper abdominal pain, easily attributable to gallbladder
Lumbar-flank pain, usually attributable to kidneys or spine, should prompt also to a TUS examination, since, with or without fever, the detection of pleural effusion or of downward areas of lung consolidation may address, as not infrequently happens, to a different diagnosis

TUS: Thoracic ultrasound; MD: Medical doctors; CT: Computerized tomography.

the empty chest cavity in lung resection patients, may present numerous and diffuse B-lines (ring-down)[37,38]. Moreover, it is unpractical the semi-quantitative use of this criterion for monitoring congestion in intensive care[39-42]. These limitations are well summarized in several reviews and commentaries[43,44]. Also the observation of the increase of the B-lines with ageing, in subjects without specific heart or chest disease[45,46], is a further argument against any great expectation from this criterion. The use of a criterion with so relevant limitations is not neutral, since it averts from the use of more suitable criteria, such as echocardiography or radiology, or TUS itself, more adequately performed[47-52]. Despite it was claimed that TUS is a basic application in intensive care units and that can become a useful daily tool in these subsets, such application is not generally used and, actually and quite unexpectedly, after so many years, is still under assessment and evaluation. Reasonably, as smartly and not only polemically commented by an outstanding radiologist, "lung ultrasound in the intensive care unit is an idea that may be too good to be true"[53]. Actually, limitations of the procedure should be taken in account even more in subsets which may increase the source of errors and even the accessibility of the structures to ultrasound imaging[14]. Similarly, ultrasound diagnosis of pulmonary embolization does not fulfil definite criteria, and a great caution is needed and further efforts are warranted - CT - for reaching a conclusive diagnosis[54].

NEWBORN AND SMALL CHILDREN

The use of chest ultrasound in paediatrics is probably the most important, while still the less developed. The most relevant studies were often pioneered in children, since there is a greater easiness for the procedure, much alike the investigation by ultrasound (US) of abdomen in newborns, where so much is visible by ultrasound, with the obvious advantage of not using ionizing radiations[55,56]. The search for lung diffuse or lobar consolidation was and is the most relevant field of practice, and can allow the avoidance of radiological investigations[57-59]. Moreover, also the detection of congenital abnormalities[60] and the investigation for the more frequent conditions, first of all pleural effusion, is a great opportunity for the paediatrician and for the radiologist, addressing appropriately to more in-depth investigations by radiological procedures, if needed[61,62]. Despite it was claimed that most chest radiological investigation are useless for the diagnosis of pneumonia in children, in our view there is a persistent need of CXR in several cases, particularly in immune-compromised patients[63-66]. The advantage of a systematic screening in paediatric units for an early diagnosis of ventilator-associated pneumonia may become one of the most relevant indication for the dissemination of the procedure[67,68], even with the persisting limitations of the reliability of this tool[14,18,69]. Developing Countries too often have very limited resources for imaging facilities, particularly for the care of low-income population. Wasting and even lethal chest disease are still epidemic in many Regions, and the use of TUS is found precious in tuberculosis[70-74]. Patterns of sub-pleural granularity are described in patients with pulmonary miliary tuberculosis diagnosed by chest radiography, in acquired immunodeficiency syndrome[75-81], as a complementary tool for any type of chest involvements, and in parasitic disease[82], particularly in cystic and alveolar echinococcosis, frequent in endemic areas, both in adults and in children.

OCCUPATIONAL AND SPORT MEDICINE, MILITARY AND MOBILE RESCUE SUPPORT

This is a field of a possible rewarding use of TUS, which is nonetheless still quite neglected. Of the occupational disease that may benefit from an early detection of pleural-lung abnormalities, the most relevant are the asbestos-associated disease, in which an early thickening of the pleural line, above 3 mm, is a clue that can advise for scheduling more timely, if not urgent, CT investigations[14]. Actually, this sign was found useful

because associated with pulmonary fibrosis in systemic sclerosis[83,84]; moreover, the detection of nodes in asbestos exposed patients can be managed safely by US guided fine needle aspirate biopsy[85].

TUS in sport medicine, where there is a great use of musculoskeletal US procedures, is still limited, even if the feature of the procedure make it suitable for the early onsite diagnosis of pneumothorax and lung contusions, of pleural effusion and of lung consolidation, all conditions that are more ominous in a subject performing competitive sport activities[86].

Military rescue support is an important sector of application and of experimental development of TUS, due to the frequent occurrence of traumatic or infectious chest disease in war scenarios[87-94]. Its use is warranted in many mobile facilities, including helicopters[33,95-100], even if an integrated use with other procedures, mainly cardiological, deserves a greater level of precision[101].

ASSESSMENT AND MANAGEMENT OF COMPREHENSIVE ELECTIVE WORKUPS

Since from its beginning, more than 50 years ago, TUS was developed in association with echocardiography[102-106]. There where and there are limitations related to artefacts, to the type of transducers, to the setting of the equipments[107] and only recently a greater care is devoted in the investigation of the more suitable probes[108]. Considering the mostly debated area of the monitoring of congestion in heart failure patients, the use of pleural effusion as a reference remains still the most objective clue, if present[109-114]. Nonetheless, this area of application is quite far from the tasks of the radiologist, and closer to the job of the cardiologist.

Monitoring is possible in several disease and context, with different degrees of reliability related to specific disease (the procedure is highly suitable for the diagnosis of pleural effusion, fairly suitable for the diagnosis of lung consolidation - superficial pneumonitis or cancer-, and pneumothorax). It is warranted not asking to the procedure more than it can give, because available expertise, knowledge, skills and training, but also the equipment's suitability, are not always affordable or accessible; the risk of misunderstanding and of interpreting misleading artefacts that may impair quality and information of the procedure must be limited as much as possible[115-117]. The use of TUS for guided chest procedure was and is mainly devoted to pleura and other chest cavities drainage by needle insertion[118-120]. Equally important are the procedures aimed at a precision nodule biopsy[121-124] or to other diagnostic and therapeutic procedures related to diaphragm neuro-muscular disease[125].

CHEST RADIOLOGY AND ULTRASOUND: WHAT, WHO, WHERE, WHEN, WHY

Topics of trans-TUS are displayed in several handbooks[126,127], which are also available as e-books. The question of the possible use of TUS as a screening tool is the same question of lung CT[128,129] as a screening tool for lung cancer: Population and individuals at risk should be screened, but the use of TUS as a tool useful for addressing earlier more in depth CT controls is a matter of active current investigation[83,116].

The professionals performing TUS must be optimally trained[130]. In our view, and experience, teaching clinical ultrasound along the 3rd year curriculum of the School of Medicine is the optimal choice, beginning as earlier as possible, provided that adequately skilled teachers are available[131-135]; physical examination skills and ultrasound proficiency between trained and untrained medical students improve together[136-139]. Differently, it is quite questionable that very brief periods of training in TUS[140,141] could provide sufficient knowledge and skills, unless they are articulated within a comprehensive US diagnostic and teaching curriculum[142,143]. This is a very important issue since the relevance of a widespread expertise among medical doctors is of pivotal relevance for a sustainable and reliable approach to the diagnosis and management of youngsters with pneumonia[61], an advancement that is a valuable medical breakthrough in children and limited resources subsets[144]. Quoting Thomas Huxley, the biologist, we should say: "Economy does not lie in sparing money, but in spending it wisely". It is exactly what a wise and expert dissemination of knowledge, skills and machine focused to TUS may achieve, if no unrealistic claim will be placed in the procedure, leading to skipping, when needed, *i.e.*, often, the step of conventional or advanced radiology.

CONCLUSION

The field of application of TUS are pleural effusion, pneumothorax, and lung consolidation, both in emergency and in elective subsets. Paediatric and newborn disease are greatly suitable for TUS investigation aimed at the detection of congenital or acquired chest disease avoiding or limiting radiological exposure. This is a still neglected area of application, and its dissemination must be warranted and supported. In any field of application, TUS improves the effectiveness of medical practice in resource-limited settings, in small point-of-care facilities, in hostile environment and in poorer countries. This is true for all the ultrasound diagnostic applications, and the specific knowledge and skills must be adequately propagated, providing advantages for limiting or more appropriately referring patients in any hospital facility[144,145].

REFERENCES

1 **Blair JS**. Marie Curie's other role. *J R Army Med Corps* 2005; **151**: 117-118 [PMID: 16097116 DOI: 10.1136/jramc-151-02-11]
2 **Joyner CR**, Miller LD, Dudrick SJ, Eskin DJ, Bloom P. Reflected ultrasound in the study of diseases of the chest. *Trans Am Clin Climatol Assoc* 1967; **78**: 28-37 [PMID: 6029333]
3 **Rosenberg HK**. The complementary roles of ultrasound and plain

film radiography in differentiating pediatric chest abnormalities. *Radiographics* 1986; **6**: 427-445 [PMID: 3317545 DOI: 10.1148/radiographics.6.3.3317545]
4 **Alessi V**, Bianco S, Bianco BP, Capizzi C, Ganci G, Marotta R, Traina G. The diagnostic potentials of echography in thoracic pathology. *Radiol Med* 1990; **79**: 438-452 [PMID: 2193321]
5 **Sartori S**, Tombesi P. Emerging roles for transthoracic ultrasonography in pleuropulmonary pathology. *World J Radiol* 2010; **2**: 83-90 [PMID: 21160921 DOI: 10.4329/wjr.v2.i2.83]
6 **Sartori S**, Tombesi P. Emerging roles for transthoracic ultrasonography in pulmonary diseases. *World J Radiol* 2010; **2**: 203-214 [PMID: 21160632 DOI: 10.4329/wjr.v2.i6.203]
7 **Sartori S**, Postorivo S, Vece FD, Ermili F, Tassinari D, Tombesi P. Contrast-enhanced ultrasonography in peripheral lung consolidations: What's its actual role? *World J Radiol* 2013; **5**: 372-380 [PMID: 24179632 DOI: 10.4329/wjr.v5.i10.372]
8 **May DA**, Barth RA, Yeager S, Nussbaum-Blask A, Bulas DI. Perinatal and postnatal chest sonography. *Radiol Clin North Am* 1993; **31**: 499-516 [PMID: 8497587]
9 **Giron J**, Sans N, Fajadet P, Baunin C, Sénac JP. [Thoracic ultrasound]. *Rev Pneumol Clin* 2000; **56**: 103-113 [PMID: 10810196]
10 **Chavez MA**, Naithani N, Gilman RH, Tielsch JM, Khatry S, Ellington LE, Miranda JJ, Gurung G, Rodriguez S, Checkley W. Agreement Between the World Health Organization Algorithm and Lung Consolidation Identified Using Point-of-Care Ultrasound for the Diagnosis of Childhood Pneumonia by General Practitioners. *Lung* 2015; **193**: 531-538 [PMID: 25921013 DOI: 10.1007/s00408-015-9730-x]
11 **Beckh S**, Bölcskei PL, Lessnau KD. Real-time chest ultrasonography: a comprehensive review for the pulmonologist. *Chest* 2002; **122**: 1759-1773 [PMID: 12426282 DOI: 10.1378/chest.122.5.1759]
12 **Dietrich CF**, Hirche TO, Schreiber D, Wagner TO. Sonographie von pleura und lunge. *Ultraschall Med* 2003; **24**: 303-311 [PMID: 14562208 DOI: 10.1055/s-2003-42912]
13 **Diacon AH**, Theron J, Bolliger CT. Transthoracic ultrasound for the pulmonologist. *Curr Opin Pulm Med* 2005; **11**: 307-312 [PMID: 15928497 DOI: 10.1097/01.mcp.0000166591.03042.1f]
14 **Sperandeo M**, Rotondo A, Guglielmi G, Catalano D, Feragalli B, Trovato GM. Transthoracic ultrasound in the assessment of pleural and pulmonary diseases: use and limitations. *Radiol Med* 2014; **119**: 729-740 [PMID: 24496592 DOI: 10.1007/s11547-014-0385-0]
15 **American College of Emergency Physicians**. Emergency ultrasound guidelines. *Ann Emerg Med* 2009; **53**: 550-570 [PMID: 19303521 DOI: 10.1016/j.annemergmed.2008.12.013]
16 **Freeman HJ**. Refractory celiac disease and sprue-like intestinal disease. *World J Gastroenterol* 2008; **14**: 828-830 [PMID: 18240339 DOI: 10.3748/wjg.14.828]
17 **Hu QJ**, Shen YC, Jia LQ, Guo SJ, Long HY, Pang CS, Yang T, Wen FQ. Diagnostic performance of lung ultrasound in the diagnosis of pneumonia: a bivariate meta-analysis. *Int J Clin Exp Med* 2014; **7**: 115-121 [PMID: 24482696]
18 **Sperandeo M**, Trovato FM, Dimitri L, Catalano D, Simeone A, Martines GF, Piscitelli AP, Trovato GM. Lung transthoracic ultrasound elastography imaging and guided biopsies of subpleural cancer: a preliminary report. *Acta Radiol* 2015; **56**: 798-805 [PMID: 24951615 DOI: 10.1177/0284185114538424]
19 **The European Society of Radiology**. Risk management in Radiology in Europe [updated 2004 Nov]. Available from: URL: https://www.myesr.org/html/img/pool/ESR_2006_IV_Riskmanagement_Web.pdf
20 **Craciun H**, Mankad K, Lynch J. Risk management in radiology departments. *World J Radiol* 2015; **7**: 134-138 [PMID: 26120383 DOI: 10.4329/wjr.v7.i6.134]
21 **Otero HJ**, Rybicki FJ, Greenberg D, Neumann PJ. Twenty years of cost-effectiveness analysis in medical imaging: are we improving? *Radiology* 2008; **249**: 917-925 [PMID: 19011188 DOI: 10.1148/radiol.2493080237]
22 **Otero HJ**, Rybicki FJ, Greenberg D, Mitsouras D, Mendoza JA, Neumann PJ. Cost-effective diagnostic cardiovascular imaging: when does it provide good value for the money? *Int J Cardiovasc Imaging* 2010; **26**: 605-612 [PMID: 20446040 DOI: 10.1007/s10554-010-9634-z]
23 **Fang C**, Otero HJ, Greenberg D, Neumann PJ. Cost-utility analyses of diagnostic laboratory tests: a systematic review. *Value Health* 2011; **14**: 1010-1018 [PMID: 22152169 DOI: 10.1016/j.jval.2011.05.044]
24 **Otero HJ**, Fang CH, Sekar M, Ward RJ, Neumann PJ. Accuracy, risk and the intrinsic value of diagnostic imaging: a review of the cost-utility literature. *Acad Radiol* 2012; **19**: 599-606 [PMID: 22342653 DOI: 10.1016/j.acra.2012.01.011]
25 **Cannavale A**, Santoni M, Passariello R, Arbarello P. Risk management in radiology. *Radiol Manage* 2013; **35**: 14-19; quiz 20-21 [PMID: 24303642]
26 **Wüstner A**, Gehmacher O, Hämmerle S, Schenkenbach C, Häfele H, Mathis G. Ultrasound diagnosis in blunt thoracic trauma. *Ultraschall Med* 2005; **26**: 285-290 [PMID: 16123922]
27 **Trovato GM**. Sustainable medical research by effective and comprehensive medical skills: overcoming the frontiers by predictive, preventive and personalized medicine. *EPMA J* 2014; **5**: 14 [PMID: 25250099 DOI: 10.1186/1878-5085-5-14]
28 **Golubnitschaja O**, Costigliola V. EPMA summit 2014 under the auspices of the presidency of Italy in the EU: professional statements. *EPMA J* 2015; **6**: 4 [PMID: 25878761 DOI: 10.1186/s13167-015-0026-2]
29 **Lemke HU**, Golubnitschaja O. Towards personal health care with model-guided medicine: long-term PPPM-related strategies and realisation opportunities within 'Horizon 2020'. *EPMA J* 2014; **5**: 8 [PMID: 24883142 DOI: 10.1186/1878-5085-5-8]
30 **Sartori S**, Tombesi P, Trevisani L, Nielsen I, Tassinari D, Abbasciano V. Accuracy of transthoracic sonography in detection of pneumothorax after sonographically guided lung biopsy: prospective comparison with chest radiography. *AJR Am J Roentgenol* 2007; **188**: 37-41 [PMID: 17179343]
31 **Wernecke K**, Galanski M, Peters PE, Hansen J. Pneumothorax: evaluation by ultrasound--preliminary results. *J Thorac Imaging* 1987; **2**: 76-78 [PMID: 3298684]
32 **Targhetta R**, Bourgeois JM, Balmes P. Echography of pneumothorax. *Rev Mal Respir* 1990; **7**: 575-579 [PMID: 2270346]
33 **Press GM**, Miller SK, Hassan IA, Alade KH, Camp E, Junco DD, Holcomb JB. Prospective evaluation of prehospital trauma ultrasound during aeromedical transport. *J Emerg Med* 2014; **47**: 638-645 [PMID: 25281177 DOI: 10.1016/j.jemermed.2014.07.056]
34 **Trovato G**, Sperandeo M. A picture is worth a thousand words: the need for CT for assessment of size and distribution of pneumothorax. *Intensive Care Med* 2014; **40**: 1614-1615 [PMID: 25209129 DOI: 10.1007/s00134-014-3461-y]
35 **Trovato G**, Sperandeo M. Lung Ultrasound in Pneumothorax: The Continuing Need for Radiology. *J Emerg Med* 2016; **51**: 189-191 [PMID: 27317611 DOI: 10.1016/j.jemermed.2015.01.045]
36 **Cardinale L**, Priola AM, Moretti F, Volpicelli G. Effectiveness of chest radiography, lung ultrasound and thoracic computed tomography in the diagnosis of congestive heart failure. *World J Radiol* 2014; **6**: 230-237 [PMID: 24976926 DOI: 10.4329/wjr.v6.i6.230]
37 **Trovato GM**, Sperandeo M. Sounds, ultrasounds, and artifacts: which clinical role for lung imaging? *Am J Respir Crit Care Med* 2013; **187**: 780-781 [PMID: 23540884]
38 **Trovato GM**, Rollo VC, Martines GF, Catalano D, Trovato FM, Sperandeo M. Thoracic ultrasound in the differential diagnosis of severe dyspnea: a reappraisal. *Int J Cardiol* 2013; **167**: 1081-1083 [PMID: 23167999 DOI: 10.1016/j.ijcard.2012.10.057]
39 **Trovato GM**, Catalano D, Martines GF, Sperandeo M. Is it time to measure lung water by ultrasound? *Intensive Care Med* 2013; **39**: 1662 [PMID: 23740276]
40 **Trovato GM**, Sperandeo M. Objectively Measuring the Ghost in the Machine: B-Lines as Uncertain Measures on Which to Base Clinical Assessment. *JACC Cardiovasc Imaging* 2015; **8**: 1470 [PMID: 26699116 DOI: 10.1016/j.jcmg.2014.12.035]

41 **Trovato GM**, Sperandeo M. The resistible rise of B-line lung ultrasound artefacts. *Respiration* 2015; **89**: 175-176 [PMID: 25592165 DOI: 10.1159/000369037]

42 **Sperandeo M**, Trovato GM, Catalano D. Quantifying B-lines on lung sonography: insufficient evidence as an objective, constructive, and educational tool. *J Ultrasound Med* 2014; **33**: 362-365 [PMID: 24449744 DOI: 10.7863/ultra.33.2.362]

43 **Al Deeb M**, Barbic S, Featherstone R, Dankoff J, Barbic D. Point-of-care ultrasonography for the diagnosis of acute cardiogenic pulmonary edema in patients presenting with acute dyspnea: a systematic review and meta-analysis. *Acad Emerg Med* 2014; **21**: 843-852 [PMID: 25176151 DOI: 10.1111/acem.12435]

44 **Trovato GM**, Sperandeo M, Catalano D. Ultrasound diagnosis of acute pulmonary edema: the oblivion of a great future behind us. *Acad Emerg Med* 2015; **22**: 244-245 [PMID: 25640171]

45 **Ciccarese F**, Chiesa AM, Feletti F, Vizioli L, Pasquali M, Forti P, Zoli M, Zompatori M. The Senile Lung as a Possible Source of Pitfalls on Chest Ultrasonography and Computed Tomography. *Respiration* 2015; **90**: 56-62 [PMID: 26044398 DOI: 10.1159/000430994]

46 **Rea G**, Trovato GM. A Farewell to B-Lines: Ageing and Disappearance of Ultrasound Artifacts as a Diagnostic Tool. *Respiration* 2015; **90**: 522 [PMID: 26440116 DOI: 10.1159/000441010]

47 **Katz JF**, Yucel EK. Point-of-care ultrasonography. *N Engl J Med* 2011; **364**: 2075-2076; author reply 2076 [PMID: 21612494 DOI: 10.1056/NEJMc1103704#SA1]

48 **Trovato GM**, Catalano D, Sperandeo M. Assessment of lung ultrasound artifacts (B-lines): incremental contribution to echocardiography in heart failure? *JACC Cardiovasc Imaging* 2014; **7**: 635 [PMID: 24925334 DOI: 10.1016/j.jcmg.2013.11.013]

49 **Catalano D**, Trovato GM, Sperandeo M. Acute heart failure diagnosis by ultrasound: new achievements and persisting limitations. *Am J Emerg Med* 2014; **32**: 384-385 [PMID: 24462395 DOI: 10.1016/j.ajem.2013.12.026]

50 **Trovato GM**, Sperandeo M. Pulmonary ultrasonography: staying within the lines prevents us finding something better on the other side. *Chest* 2015; **147**: e236-e237 [PMID: 26033146 DOI: 10.1378/chest.14-3118]

51 **Trovato GM**, Catalano D, Sperandeo M. M-mode: a valuable tool in cardiology, is not yet ready to use in pneumology. *Respiration* 2014; **88**: 518 [PMID: 25402592 DOI: 10.1159/000367813]

52 **Trovato GM**, Catalano D, Sperandeo M. Echocardiographic and lung ultrasound characteristics in ambulatory patients with dyspnea or prior heart failure. *Echocardiography* 2014; **31**: 406-407 [PMID: 24606228 DOI: 10.1111/echo.12518]

53 **Katz JF**, Bezreh JS, Yucel EK. Lung ultrasound in the intensive care unit: an idea that may be too good to be true. *Intensive Care Med* 2015; **41**: 379-380 [PMID: 25510302 DOI: 10.1007/s00134-014-3606-z]

54 **Maggi M**, Catalano D, Sperandeo M, Trovato G. Comprehensive clinical evidence for pulmonary embolism diagnosis and workup. *Chest* 2014; **145**: 1173-1174 [PMID: 24798850 DOI: 10.1378/chest.13-2792]

55 **Haller JO**, Schneider M, Kassner EG, Friedman AP, Waldroup LD. Sonographic evaluation of the chest in infants and children. *AJR Am J Roentgenol* 1980; **134**: 1019-1027 [PMID: 6768240]

56 **Haran Jogeesvaran K**, Owens CM. Chronic diseases of lung parenchyma in children: the role of imaging. *Pediatr Radiol* 2010; **40**: 850-858 [PMID: 20432003 DOI: 10.1007/s00247-010-1615-9]

57 **Tomà P**, Owens CM. Chest ultrasound in children: critical appraisal. *Pediatr Radiol* 2013; **43**: 1427-1434; quiz 1425-1326 [PMID: 24141909 DOI: 10.1007/s00247-013-2756-4]

58 **Toma P**. Lung ultrasound characteristics of community-acquired pneumonia. *Pediatr Pulmonol* 2013; **48**: 1041-1042 [PMID: 23255323 DOI: 10.1002/ppul.22744]

59 **Toma P**. Lung ultrasound in bronchiolitis. *Eur J Pediatr* 2013; **172**: 713 [PMID: 23328963 DOI: 10.1007/s00431-013-1941-7]

60 **Tomà P**, Rizzo F, Stagnaro N, Magnano G, Granata C. Multislice CT in congenital bronchopulmonary malformations in children. *Radiol Med* 2011; **116**: 133-151 [PMID: 20852957 DOI: 10.1007/s11547-010-0582-4]

61 **Jones BP**, Tay ET, Elikashvili I, Sanders JE, Paul AZ, Nelson BP, Spina LA, Tsung JW. Feasibility and Safety of Substituting Lung Ultrasonography for Chest Radiography When Diagnosing Pneumonia in Children: A Randomized Controlled Trial. *Chest* 2016; **150**: 131-138 [PMID: 26923626 DOI: 10.1016/j.chest.2016.02.643]

62 **Escourrou G**, De Luca D. Lung ultrasound decreased radiation exposure in preterm infants in a neonatal intensive care unit. *Acta Paediatr* 2016; **105**: e237-e239 [PMID: 26880491 DOI: 10.1111/apa.13369]

63 **Pereda MA**, Chavez MA, Hooper-Miele CC, Gilman RH, Steinhoff MC, Ellington LE, Gross M, Price C, Tielsch JM, Checkley W. Lung ultrasound for the diagnosis of pneumonia in children: a meta-analysis. *Pediatrics* 2015; **135**: 714-722 [PMID: 25780071 DOI: 10.1542/peds.2014-2833]

64 **Sperandeo M**, Carnevale V, Muscarella S, Sperandeo G, Varriale A, Filabozzi P, Piattelli ML, D'Alessandro V, Copetti M, Pellegrini F, Dimitri L, Vendemiale G. Clinical application of transthoracic ultrasonography in inpatients with pneumonia. *Eur J Clin Invest* 2011; **41**: 1-7 [PMID: 20731700 DOI: 10.1111/j.1365-2362.2010.02367.x]

65 **Catalano D**, Trovato G, Sperandeo M, Sacco MC. Lung ultrasound in pediatric pneumonia. The persistent need of chest X-rays. *Pediatr Pulmonol* 2014; **49**: 617-618 [PMID: 24178894 DOI: 10.1002/ppul.22941]

66 **Mongodi S**, Via G, Girard M, Rouquette I, Misset B, Braschi A, Mojoli F, Bouhemad B. Lung Ultrasound for Early Diagnosis of Ventilator-Associated Pneumonia. *Chest* 2016; **149**: 969-980 [PMID: 26836896 DOI: 10.1016/j.chest.2015.12.012]

67 **Liccardo B**, Martone F, Trambaiolo P, Severino S, Cibinel GA, D'Andrea A. Incremental value of thoracic ultrasound in intensive care units: Indications, uses, and applications. *World J Radiol* 2016; **8**: 460-471 [PMID: 27247712 DOI: 10.4329/wjr.v8.i5.460]

68 **Sperandeo M**, Filabozzi P, Carnevale V. Ultrasound Diagnosis of Ventilator-Associated Pneumonia: A Not-So-Easy Issue. *Chest* 2016; **149**: 1350-1351 [PMID: 27157222 DOI: 10.1016/j.chest.2016.02.684]

69 **Sperandeo M**, Filabozzi P, Varriale A, Carnevale V, Piattelli ML, Sperandeo G, Brunetti E, Decuzzi M. Role of thoracic ultrasound in the assessment of pleural and pulmonary diseases. *J Ultrasound* 2008; **11**: 39-46 [PMID: 23396553 DOI: 10.1016/j.jus.2008.02.001]

70 **Hunter L**, Bélard S, Janssen S, van Hoving DJ, Heller T. Miliary tuberculosis: sonographic pattern in chest ultrasound. *Infection* 2016; **44**: 243-246 [PMID: 26661658 DOI: 10.1007/s15010-015-0865-8]

71 **Giordani MT**, Giaretta R, Scolarin C, Stefani MP, Pellizzari C, Tamarozzi F, Brunetti E. Ultrasound and infections on the Tibetan Plateau(). *J Ultrasound* 2012; **15**: 83-92 [PMID: 23396850 DOI: 10.1016/j.jus.2012.02.009]

72 **Stolz LA**, Muruganandan KM, Bisanzo MC, Sebikali MJ, Dreifuss BA, Hammerstedt HS, Nelson SW, Nayabale I, Adhikari S, Shah SP. Point-of-care ultrasound education for non-physician clinicians in a resource-limited emergency department. *Trop Med Int Health* 2015; **20**: 1067-1072 [PMID: 25808431 DOI: 10.1111/tmi.12511]

73 **Ramos-Rincón JM**, Cuadros-González J, Malmierca-Corral E, de Górgolas-Hernández M. Medical diagnosis in resource-poor tropical countries. *Rev Clin Esp* 2015; **215**: 43-49 [PMID: 25012088 DOI: 10.1016/j.rce.2014.05.002]

74 **Heuvelings CC**, Bélard S, Janssen S, Wallrauch C, Grobusch MP, Brunetti E, Giordani MT, Heller T. Chest ultrasonography in patients with HIV: a case series and review of the literature. *Infection* 2016; **44**: 1-10 [PMID: 25972115 DOI: 10.1007/s15010-015-0780-z]

75 **Bélard S**, Tamarozzi F, Bustinduy AL, Wallrauch C, Grobusch MP, Kuhn W, Brunetti E, Joekes E, Heller T. Point-of-Care Ultrasound Assessment of Tropical Infectious Diseases--A Review of Applications and Perspectives. *Am J Trop Med Hyg* 2016; **94**: 8-21 [PMID: 26416111 DOI: 10.4269/ajtmh.15-0421]

76 **Brunetti E**, Heller T, Richter J, Kaminstein D, Youkee D, Giordani MT, Goblirsch S, Tamarozzi F. Application of Ultrasonography in the Diagnosis of Infectious Diseases in Resource-Limited Settings. *Curr Infect Dis Rep* 2016; **18**: 6 [PMID: 26781324 DOI: 10.1007/s11908-015-0512-7]

77 **Heller T**, Wallrauch C, Brunetti E, Giordani MT. Changes of FASH ultrasound findings in TB-HIV patients during anti-tuberculosis treatment. *Int J Tuberc Lung Dis* 2014; **18**: 837-839 [PMID: 24902561 DOI: 10.5588/ijtld.13.0029]

78 **Janssen S**, Basso F, Giordani MT, Brunetti E, Grobusch MP, Heller T. Sonographic findings in the diagnosis of HIV-associated tuberculosis: image quality and inter-observer agreement in FASH vs. remote-FASH ultrasound. *J Telemed Telecare* 2013; **19**: 491-493 [PMID: 24222660 DOI: 10.1177/1357633X13512072]

79 **Giordani MT**, Brunetti E, Binazzi R, Benedetti P, Stecca C, Goblirsch S, Heller T. Extrapulmonary mycobacterial infections in a cohort of HIV-positive patients: ultrasound experience from Vicenza, Italy. *Infection* 2013; **41**: 409-414 [PMID: 23001543 DOI: 10.1007/s15010-012-0336-4]

80 **Heller T**, Goblirsch S, Bahlas S, Ahmed M, Giordani MT, Wallrauch C, Brunetti E. Diagnostic value of FASH ultrasound and chest X-ray in HIV-co-infected patients with abdominal tuberculosis. *Int J Tuberc Lung Dis* 2013; **17**: 342-344 [PMID: 23321507 DOI: 10.5588/ijtld.12.0679]

81 **Heller T**, Wallrauch C, Goblirsch S, Brunetti E. Focused assessment with sonography for HIV-associated tuberculosis (FASH): a short protocol and a pictorial review. *Crit Ultrasound J* 2012; **4**: 21 [PMID: 23171481 DOI: 10.1186/2036-7902-4-21]

82 **Li T**, Chen X, Zhen R, Qiu J, Qiu D, Xiao N, Ito A, Wang H, Giraudoux P, Sako Y, Nakao M, Craig PS. Widespread co-endemicity of human cystic and alveolar echinococcosis on the eastern Tibetan Plateau, northwest Sichuan/southeast Qinghai, China. *Acta Trop* 2010; **113**: 248-256 [PMID: 19941830 DOI: 10.1016/j.actatropica.2009.11.006]

83 **Sperandeo M**, De Cata A, Molinaro F, Trovato FM, Catalano D, Simeone A, Varriale A, Martines GF, Trovato G. Ultrasound signs of pulmonary fibrosis in systemic sclerosis as timely indicators for chest computed tomography. *Scand J Rheumatol* 2015; **44**: 389-398 [PMID: 26099251 DOI: 10.3109/03009742.2015.1011228]

84 **Marchbank ND**, Wilson AG, Joseph AE. Ultrasound features of folded lung. *Clin Radiol* 1996; **51**: 433-437 [PMID: 8654011 DOI: 10.1016/S0009-9260(96)80165-6]

85 **Sperandeo M**, Dimitri L, Pirri C, Trovato FM, Catalano D, Trovato GM. Advantages of thoracic ultrasound-guided fine-needle aspiration biopsy in lung cancer and mesothelioma. *Chest* 2014; **146**: e178-e179 [PMID: 25367494 DOI: 10.1378/chest.14-1557]

86 **Jacobson JA**. Ultrasound in sports medicine. *Radiol Clin North Am* 2002; **40**: 363-386 [PMID: 12118829 DOI: 10.1016/S0033-8389(02)00005-2]

87 **Rozanski TA**, Edmondson JM, Jones SB. Ultrasonography in a forward-deployed military hospital. *Mil Med* 2005; **170**: 99-102 [PMID: 15782826]

88 **Hile DC**, Morgan AR, Laselle BT, Bothwell JD. Is point-of-care ultrasound accurate and useful in the hands of military medical technicians? A review of the literature. *Mil Med* 2012; **177**: 983-987 [PMID: 22934381]

89 **Madill JJ**. In-flight thoracic ultrasound detection of pneumothorax in combat. *J Emerg Med* 2010; **39**: 194-197 [PMID: 19880267 DOI: 10.1016/j.jemermed.2009.08.026]

90 **de Kerangal X**, Tourtier JP, Cotez-Gacia S, Grand B, Borne M. FAST and undertriage. *Langenbecks Arch Surg* 2010; **395**: 595-596 [PMID: 20512351 DOI: 10.1007/s00423-010-0624-3]

91 **Ward DI**. Prehospital point-of-care ultrasound use by the military. *Emerg Med Australas* 2007; **19**: 282 [PMID: 17564699]

92 **Melanson SW**, McCarthy J, Stromski CJ, Kostenbader J, Heller M. Aeromedical trauma sonography by flight crews with a miniature ultrasound unit. *Prehosp Emerg Care* 2001; **5**: 399-402 [PMID: 11642593]

93 **Otsuka H**, Sato T, Morita S, Nakagawa Y, Inokuchi S. A Case of Blunt Traumatic Cardiac Tamponade Successfully Treated by Out-of-hospital Pericardial Drainage in a "Doctor-helicopter" Ambulance Staffed by Skilled Emergency Physicians. *Tokai J Exp Clin Med* 2016; **41**: 1-3 [PMID: 27050887]

94 **O'Dochartaigh D**, Douma M. Prehospital ultrasound of the abdomen and thorax changes trauma patient management: A systematic review. *Injury* 2015; **46**: 2093-2102 [PMID: 26264879 DOI: 10.1016/j.injury.2015.07.007]

95 **Burns BJ**, Aguirrebarrena G. Occult traumatic loculated tension pneumothorax--a sonographic diagnostic dilemma. *Prehosp Emerg Care* 2013; **17**: 92-94 [PMID: 22920267 DOI: 10.3109/10903127.2012.710720]

96 **Darocha T**, Gałązkowski R, Sobczyk D, Żyła Z, Drwiła R. Point-of-care ultrasonography during rescue operations on board a Polish Medical Air Rescue helicopter. *J Ultrason* 2014; **14**: 414-420 [PMID: 26674604 DOI: 10.15557/JoU.2014.0043]

97 **Roline CE**, Heegaard WG, Moore JC, Joing SA, Hildebrandt DA, Biros MH, Caroon LV, Plummer DW, Reardon RF. Feasibility of bedside thoracic ultrasound in the helicopter emergency medical services setting. *Air Med J* 2013; **32**: 153-157 [PMID: 23632224 DOI: 10.1016/j.amj.2012.10.013]

98 **Ketelaars R**, Hoogerwerf N, Scheffer GJ. Prehospital chest ultrasound by a dutch helicopter emergency medical service. *J Emerg Med* 2013; **44**: 811-817 [PMID: 23332805 DOI: 10.1016/j.jemermed.2012.07.085]

99 **Hasler RM**, Kehl C, Exadaktylos AK, Albrecht R, Dubler S, Greif R, Urwyler N. Accuracy of prehospital diagnosis and triage of a Swiss helicopter emergency medical service. *J Trauma Acute Care Surg* 2012; **73**: 709-715 [PMID: 22929499 DOI: 10.1097/TA.0b013e31825c14b7]

100 **Hoyer HX**, Vogl S, Schiemann U, Haug A, Stolpe E, Michalski T. Prehospital ultrasound in emergency medicine: incidence, feasibility, indications and diagnoses. *Eur J Emerg Med* 2010; **17**: 254-259 [PMID: 20164777 DOI: 10.1097/MEJ.0b013e328336ae9e]

101 **Bataille B**, Riu B, Ferre F, Moussot PE, Mari A, Brunel E, Ruiz J, Mora M, Fourcade O, Genestal M, Silva S. Integrated use of bedside lung ultrasound and echocardiography in acute respiratory failure: a prospective observational study in ICU. *Chest* 2014; **146**: 1586-1593 [PMID: 25144893 DOI: 10.1378/chest.14-0681]

102 **Joyner CR**. Echocardiography. *Circulation* 1972; **46**: 835-838 [PMID: 5081138 DOI: 10.1161/01.CIR.46.5.835]

103 **Joyner CR**. Echocardiography. *Am Heart J* 1975; **90**: 413-419 [PMID: 126014 DOI: 10.1016/0002-8703(75)90419-6]

104 **Joyner CR**. Ultrasonic diagnosis of pulmonary embolism--the second time around. *Int J Cardiol* 1984; **6**: 116-120 [PMID: 6746133 DOI: 10.1016/0167-5273(84)90258-4]

105 **Kelbel C**, Börner N, Schadmand S, Klose KJ, Weilemann LS, Meyer J, Thelen M. Diagnosis of pleural effusions and atelectases: sonography and radiology compared. *Rofo* 1991; **154**: 159-163 [PMID: 1847539 DOI: 10.1055/s-2008-1033105]

106 **Fournier D**. [Thoracic ultrasound]. *Schweiz Med Wochenschr* 1997; **127**: 1734-1742 [PMID: 9446192]

107 **Trovato GM**, Catalano D, Sperandeo M, Graziano P. Artifacts, Noise and Interference: Much Ado about Ultrasound. *Respiration* 2015; **90**: 85 [PMID: 25824977 DOI: 10.1159/000375316]

108 **Tasci O**, Hatipoglu ON, Cagli B, Ermis V. Sonography of the chest using linear-array versus sector transducers: Correlation with auscultation, chest radiography, and computed tomography. *J Clin Ultrasound* 2016; **44**: 383-389 [PMID: 26863904 DOI: 10.1002/jcu.22331]

109 **Kataoka H**, Takada S. The role of thoracic ultrasonography for evaluation of patients with decompensated chronic heart failure. *J Am Coll Cardiol* 2000; **35**: 1638-1646 [PMID: 10807471]

110 **Kataoka H**. Pericardial and pleural effusions in decompensated chronic heart failure. *Am Heart J* 2000; **139**: 918-923 [PMID: 10783228]

111 **Kataoka H**. Utility of thoracic sonography for follow-up examination of chronic heart failure patients with previous decompensation. *Clin Cardiol* 2007; **30**: 336-341 [PMID:

17674378]
112 **Kataoka H**. Ultrasound pleural effusion sign as a useful marker for identifying heart failure worsening in established heart failure patients during follow-up. *Congest Heart Fail* 2012; **18**: 272-277 [PMID: 22994441 DOI: 10.1111/j.1751-7133.2012.00285.x]
113 **Oylumlu M**, Davutoglu V, Sucu M, Ercan S, Ozer O, Yuce M. Prognostic role of echocardiographic and hematologic parameters in heart failure patients complicated with incidental pleural effusion diagnosed during echocardiographic evaluation. *Int J Cardiovasc Imaging* 2014; **30**: 907-910 [PMID: 24710708 DOI: 10.1007/s10554-014-0421-0]
114 **Kataoka H**, Madias JE. Effects of heart failure status on electrocardiogram precordial leads and their value for monitoring body fluid changes in heart failure patients. *Int J Cardiol* 2011; **152**: 113-115 [PMID: 21802157 DOI: 10.1016/j.ijcard.2011.07.030]
115 **Trovato GM**, Sperandeo M, Catalano D. Optimization of thoracic US guidance for lung nodule biopsy. *Radiology* 2014; **270**: 308 [PMID: 24354382 DOI: 10.1148/radiol.13131527]
116 **Trovato G**, Sperandeo M, Catalano D. Letter to the editor: Mostbeck G. Elastography everywhere--now even the lungs! Ultraschall in Med. 2014; 35: 5-8. *Ultraschall Med* 2014; **35**: 371; discussion 371-372 [PMID: 25127226 DOI: 10.1055/s-0034-1366523]
117 **Sperandeo M**, Dimitri L, Trovato FM, Simeone A, Catalano D, Pirri C, Trovato G. Thoracic Ultra Sound (TUS) integrated approach for FNAB-US guided diagnosis and for monitoring environmental exposed subjects at risk of malignant pleural mesothelioma (MPM) and lung cancer (LC). Overview and preliminary report of TUS monitoring and screening approach. *FASEB J* 2014; **28** Suppl: LB498
118 **Ravin CE**. Thoracocentesis of loculated pleural effusions using grey scale ultrasonic guidance. *Chest* 1977; **71**: 666-668 [PMID: 852349]
119 **Dede D**, Akmangit I, Yildirim ZN, Sanverdi E, Sayin B. Ultrasonography and fluoroscopy-guided insertion of chest ports. *Eur J Surg Oncol* 2008; **34**: 1340-1343 [PMID: 18191364 DOI: 10.1016/j.ejso.2007.12.001]
120 **Fitch MT**, Nicks BA, Pariyadath M, McGinnis HD, Manthey DE. Videos in clinical medicine. Emergency pericardiocentesis. *N Engl J Med* 2012; **366**: e17 [PMID: 22435385 DOI: 10.1056/NEJMvcm0907841]
121 **Trevisani L**, Sartori S, Putinati S, Abbasciano V, Cervi PM. Needle aspiration biopsy and ultrasonic guidance. *Chest* 1994; **106**: 650 [PMID: 7774373]
122 **Sartori S**, Nielsen I, Trevisani L, Tombesi P, Ceccotti P, Abbasciano V. Contrast-enhanced sonography as guidance for transthoracic biopsy of a peripheral lung lesion with large necrotic areas. *J Ultrasound Med* 2004; **23**: 133-136 [PMID: 14756362]
123 **Tombesi P**, Nielsen I, Tassinari D, Trevisani L, Abbasciano V, Sartori S. Transthoracic ultrasonography-guided core needle biopsy of pleural-based lung lesions: prospective randomized comparison between a Tru-cut-type needle and a modified Menghini-type needle. *Ultraschall Med* 2009; **30**: 390-395 [PMID: 19544230 DOI: 10.1055/s-0028-1109442]
124 **Di Vece F**, Tombesi P, Ermili F, Sartori S. Contrast-enhanced ultrasound (CEUS) and CEUS-guided biopsy in the diagnosis of lung abscess in a patient with achalasia: Case report. *Interv Med Appl Sci* 2013; **5**: 31-33 [PMID: 24265886 DOI: 10.1556/IMAS.5.2013.1.6]
125 **Boon AJ**, Sekiguchi H, Harper CJ, Strommen JA, Ghahfarokhi LS, Watson JC, Sorenson EJ. Sensitivity and specificity of diagnostic ultrasound in the diagnosis of phrenic neuropathy. *Neurology* 2014; **83**: 1264-1270 [PMID: 25165390 DOI: 10.1212/WNL.0000000000000841]
126 **Bolliger CT**, Herth FJF, Mayo, PH Miyazawa T. Clinical Chest Ultrasound. Eds. Progress in Respiratory Research, Vol. 37. Karger: Basel, 2009
127 **Sperandeo M**, Trovato G. Ecografia Toracica. Diagnosi e tecniche interventistiche. Milan: EDRA, 2015
128 **Trovato GM**, Sperandeo M, Catalano D. Computed tomography screening for lung cancer. *Ann Intern Med* 2013; **159**: 155 [PMID: 23856687 DOI: 10.7326/0003-4819-159-2-201307160-00016]
129 **van Beek EJ**, Mirsadraee S, Murchison JT. Lung cancer screening: Computed tomography or chest radiographs? *World J Radiol* 2015; **7**: 189-193 [PMID: 26339461 DOI: 10.4329/wjr.v7.i8.189]
130 **Keddis MT**, Cullen MW, Reed DA, Halvorsen AJ, McDonald FS, Takahashi PY, Bhagra A. Effectiveness of an ultrasound training module for internal medicine residents. *BMC Med Educ* 2011; **11**: 75 [PMID: 21955400 DOI: 10.1186/1472-6920-11-75]
131 **Fodor D**, Badea R, Poanta L, Dumitrascu DL, Buzoianu AD, Mircea PA. The use of ultrasonography in learning clinical examination - a pilot study involving third year medical students. *Med Ultrason* 2012; **14**: 177-181 [PMID: 22957320]
132 **Fox JC**, Schlang JR, Maldonado G, Lotfipour S, Clayman RV. Proactive medicine: the "UCI 30," an ultrasound-based clinical initiative from the University of California, Irvine. *Acad Med* 2014; **89**: 984-989 [PMID: 24826849 DOI: 10.1097/ACM.0000000000000292]
133 **Trovato GM**, Catalano D, Sperandeo M. Top or Flop: The Need to Improve Knowledge and Skills Achieved by Ultrasound Medical Curricula. *Acad Med* 2015; **90**: 839-840 [PMID: 26414050 DOI: 10.1097/ACM.0000000000000745]
134 **Chiem AT**, Soucy Z, Dinh VA, Chilstrom M, Gharahbaghian L, Shah V, Medak A, Nagdev A, Jang T, Stark E, Hussain A, Lobo V, Pera A, Fox JC. Integration of Ultrasound in Undergraduate Medical Education at the California Medical Schools: A Discussion of Common Challenges and Strategies From the UMeCali Experience. *J Ultrasound Med* 2016; **35**: 221-233 [PMID: 26764278 DOI: 10.7863/ultra.15.05006]
135 **Dinh VA**, Fu JY, Lu S, Chiem A, Fox JC, Blaivas M. Integration of Ultrasound in Medical Education at United States Medical Schools: A National Survey of Directors' Experiences. *J Ultrasound Med* 2016; **35**: 413-419 [PMID: 26782166 DOI: 10.7863/ultra.15.05073]
136 **Dinh VA**, Dukes WS, Prigge J, Avila M. Ultrasound Integration in Undergraduate Medical Education: Comparison of Ultrasound Proficiency Between Trained and Untrained Medical Students. *J Ultrasound Med* 2015; **34**: 1819-1824 [PMID: 26333569 DOI: 10.7863/ultra.14.12045]
137 **Palma JK**. Successful strategies for integrating bedside ultrasound into undergraduate medical education. *Mil Med* 2015; **180**: 153-157 [PMID: 25850144 DOI: 10.7205/MILMED-D-14-00573]
138 **Dinh VA**, Frederick J, Bartos R, Shankel TM, Werner L. Effects of ultrasound implementation on physical examination learning and teaching during the first year of medical education. *J Ultrasound Med* 2015; **34**: 43-50 [PMID: 25542938 DOI: 10.7863/ultra.34.1.43]
139 **Dinh VA**, Lakoff D, Hess J, Bahner DP, Hoppmann R, Blaivas M, Pellerito JS, Abuhamad A, Khandelwal S. Medical Student Core Clinical Ultrasound Milestones: A Consensus Among Directors in the United States. *J Ultrasound Med* 2016; **35**: 421-434 [PMID: 26782162 DOI: 10.7863/ultra.15.07080]
140 **Dinh VA**, Giri PC, Rathinavel I, Nguyen E, Hecht D, Dorotta I, Nguyen HB, Chrissian AA. Impact of a 2-Day Critical Care Ultrasound Course during Fellowship Training: A Pilot Study. *Crit Care Res Pract* 2015; **2015**: 675041 [PMID: 26346694 DOI: 10.1155/2015/675041]
141 **Chiem AT**, Chan CH, Ander DS, Kobylivker AN, Manson WC. Comparison of expert and novice sonographers' performance in focused lung ultrasonography in dyspnea (FLUID) to diagnose patients with acute heart failure syndrome. *Acad Emerg Med* 2015; **22**: 564-573 [PMID: 25903470 DOI: 10.1111/acem.12651]
142 **Moy RJ**, Chapman AL, Bapusamy A. The effectiveness of an informal teaching programme for junior doctors identifying pleural effusions using ultrasound at the bedside. *J R Army Med Corps* 2010; **156**: 233-235 [PMID: 21275356]
143 **Trovato FM**, Musumeci G. Lung ultrasound: the need of an adequate training for the next generation of internists. *Neth J Med* 2015; **73**: 305 [PMID: 26228202]
144 **Catalano D**, Trovato FM, Pirri C, Trovato GM. Outpatient diagnosis and therapeutic units linked with ED referrals: a sustainable

quality-centered approach. *Am J Emerg Med* 2013; **31**: 1612 [PMID: 24070979 DOI: 10.1016/j.ajem.2013.07.008]
145 **Trovato FM**, Catalano D. Diagnosis of Pneumonia by Lung Ultrasound in Children and Limited Resources Subsets: A Valuable Medical Breakthrough. *Chest* 2016; **150**: 258-260 [PMID: 27396790 DOI: 10.1016/j.chest.2016.04.032]

P- Reviewer: Murdaca G, Porfyridis I, Sartori S **S- Editor**: Ji FF
L- Editor: A **E- Editor**: Wu HL

World Journal of Radiology

Submit a Manuscript: http://www.wjgnet.com/esps/
Help Desk: http://www.wjgnet.com/esps/helpdesk.aspx
DOI: 10.4329/wjr.v8.i9.785

World J Radiol 2016 September 28; 8(9): 785-798
ISSN 1949-8470 (online)

REVIEW

Diffusion weighted imaging: Technique and applications

Vinit Baliyan, Chandan J Das, Raju Sharma, Arun Kumar Gupta

Vinit Baliyan, Chandan J Das, Raju Sharma, Arun Kumar Gupta, Department of Radiology, All India Institute of Medical Sciences, New Delhi 110029, India

Author contributions: Baliyan V wrote the paper; Das CJ has designed and concepted the article; Sharma R and Gupta AK perfomed literarure search and manuscript reviewing.

Conflict-of-interest statement: Authors declare no conflict of interests for this article.

Manuscript source: Invited manuscript

Correspondence to: Chandan J Das, MD, Department of Radiology, All India Institute of Medical Sciences, Ansari Nagar, New Delhi 110029, India. docchandan17@gmail.com
Telephone: +91-11-26593628
Fax: +91-11-26588663

Received: February 29, 2016
Peer-review started: March 9, 2016
First decision: May 13, 2016
Revised: July 24, 2016
Accepted: August 11, 2016
Article in press: August 15, 2016
Published online: September 28, 2016

Abstract

Diffusion weighted imaging (DWI) is a method of signal contrast generation based on the differences in Brownian motion. DWI is a method to evaluate the molecular function and micro-architecture of the human body. DWI signal contrast can be quantified by apparent diffusion coefficient maps and it acts as a tool for treatment response evaluation and assessment of disease progression. Ability to detect and quantify the anisotropy of diffusion leads to a new paradigm called diffusion tensor imaging (DTI). DTI is a tool for assessment of the organs with highly organised fibre structure. DWI forms an integral part of modern state-of-art magnetic resonance imaging and is indispensable in neuroimaging and oncology. DWI is a field that has been undergoing rapid technical evolution and its applications are increasing every day. This review article provides insights in to the evolution of DWI as a new imaging paradigm and provides a summary of current role of DWI in various disease processes.

Key words: Diffusion weighted imaging; Diffusion tensor imaging; Onco-imaging; Neuro-imaging

Core tip: Diffusion weighted imaging has revolutionised the magnetic resonance imaging. There is wide use of this technique in neuroimaging, body imaging as well as in oncoimaging. This article reviews the current role of diffusion weighted imaging in medical imaging and highlights the current challenges and limitations to this technique.

Baliyan V, Das CJ, Sharma R, Gupta AK. Diffusion weighted imaging: Technique and applications. *World J Radiol* 2016; 8(9): 785-798 Available from: URL: http://www.wjgnet.com/1949-8470/full/v8/i9/785.htm DOI: http://dx.doi.org/10.4329/wjr.v8.i9.785

INTRODUCTION

Approximately 60%-70% of the human body is composed of water. Diffusion is the random Brownian motion of the molecules driven by thermal energy. In a perfectly homogenous medium diffusion is random and isotropic; *i.e.*, equal probability in all directions. But in a complex environment of human body, water is divided

between cells and extracellular compartments. Water molecules in extracellular environments experience relatively free diffusion while intracellular molecules show relatively "restricted diffusion". Different tissues of the human body have a characteristic cellular architecture and proportions of intra and extracellular compartments; and hence have characteristic diffusion properties. The relative proportion of the water distribution between these compartments is affected by the pathologic processes. For example in high grade malignancies and acutely infarcted tissues, intracellular proportion is increased, so the diffusion becomes relatively more restricted. Diffusion weighted imaging provides qualitative and quantitative information about the diffusion properties. It adds a new dimension to the magnetic resonance imaging (MRI) examinations by adding functional information to the largely anatomical information gathered by the conventional sequences. Water diffusion is anisotropic in brain white matter, because axon membranes limit molecular movement perpendicular to the fibers. Diffusion tensor imaging (DTI) exploits this property to produce micro-architectural detail of white matter tracts and provides information about white matter integrity.

Technical evolution of diffusion weighted imaging

The goal of all imaging procedures is generation of an image contrast with a good spatial resolution. Initial evolution of diagnostic imaging focussed on tissue density function for signal contrast generation. In 1970s, the work of Lauterbur PC, Mansfield P and Ernst R, modern clinical MRI came into the field of medicine[1]. MRI provided an excellent contrast resolution not only from tissue (proton) density, but also from tissue relaxation properties. After initial focus on T1 and T2 relaxation properties researchers explored other methods to generate contrast exploiting other properties of water molecules. Diffusion weighted imaging (DWI) was a result of such efforts by researchers like Stejskal, Tanner and Le Bihan[2].

In 1984, before MRI contrast became available, Denis Le Bihan, tried to differentiate liver tumors from angiomas. He hypothesized that a molecular diffusion measurement would result in low values for solid tumors, because of restriction of molecular movement. Based on the pioneering work of Stejskal and Tanner in the 1960s, he thought that diffusion encoding could be accomplished using specific magnetic gradient pulses. It was a challenging task to integrate the diffusion encoding gradients in to the conventional sequences and initial experience in the liver with a 0.5T scanner was very disappointing. Firstly diffusion MRI was a very slow method and it was very sensitive to motion artifacts due to respiration[2].

It was not until the availability of Echo-Planar Imaging (EPI) in the early 1990s, that DWI could become a reality in the field of clinical imaging[2,3]. EPI based diffusion sequences were fast and solved the problems of motion artifacts. Early work by Moseley *et al*[4] and Warach *et al*[5] established DWI as a cornerstone for early detection of acute stroke.

In a DWI sequence diffusion sensitization gradients are applied on either side of the 180° refocusing pulse. The parameter "*b* value" decides the diffusion weighting and is expressed in s/mm^2. It is proportional to the square of the amplitude and duration of the gradient applied. Diffusion is qualitatively evaluated on trace images and quantitatively by the parameter called apparent diffusion coefficient (ADC). Tissues with restricted diffusion are bright on the trace image and hypointense on the ADC map.

DTI evolution

Moseley *et al*[4] observed that white matter contrast on diffusion images changes according to the spatial direction of the diffusion encoding gradients. Douek *et al*[6] suggested that this was due to the fact that water diffusion in white matter fibres was faster in the direction of the fibers and slower perpendicular to them, *i.e.,* anisotropic. The initial attempts were not very impressive, because diffusion measurements were done only along two directions. With the use of a tensor formalism by Basser *et al*[7] and development of 3D representation algorithms for fibre bundle depiction modern DTI came into existence. Initial clinical applications of DTI were limited to the central nervous system. Imaging artefacts and the small calibre of peripheral nerves hampered its use in the peripheral nervous system. However recent advances in MRI technology have extended its application to the peripheral nervous system[8].

CLINICAL APPLICATIONS OF DWI

Acute brain ischemia

Ever since its inception acute brain ischemia has been the most successful application of DWI (Figure 1). Diffusion MRI today is the imaging modality of choice for stroke patients[9]. The use of DWI in combination with perfusion MRI, which outlines salvageable areas of ischemia and MR angiography, provides a useful guide for stroke management. The *b*-values up-to 1000 are used for standard neuroimaging application. Despite the historical success the interpretation of the molecular basis behind the diffusion restriction has been poorly understood. The relationship of diffusion restriction with the severity of the ischemia and the clinical outcome remains unresolved[10].

Brain tumors

ADC values have been shown to be decreased in highly cellular tumors such as CNS lymphoma, medulloblastoma, and high-grade glioma. Lower ADC values have been reported to be associated with higher-grades and poorer prognosis. Quantitative ADC measurements have also been helpful in prediction of therapeutic response. It is especially useful in detecting pseudo-response and pseudo-progression. Pseudo-response is a phenomenon seen after anti-angiogenic therapy where

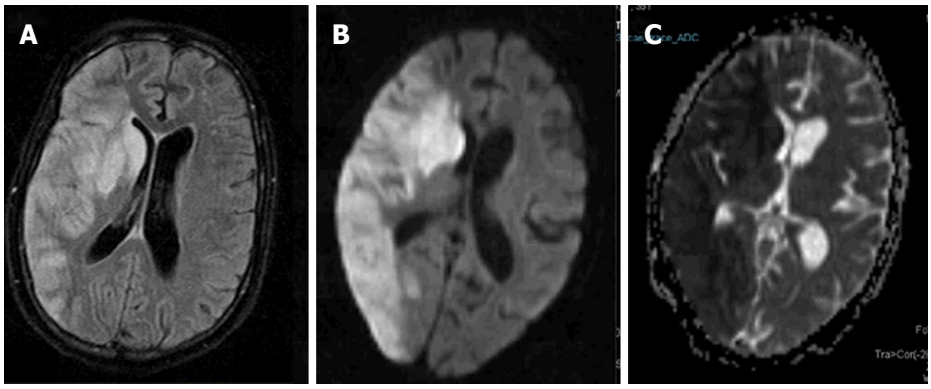

Figure 1 Acute infarct. Axial FLAIR image (A) shows geographic hyperintensity involving right parieto-occipital region and basal ganglia. Diffusion weighted imaging shows restricted diffusion with high signal on b1000 image (B) and low signal intensity on apparent diffusion coefficient map (C).

tumor doesn't enhance despite the intact viability or actual progression. DWI may be useful to demonstrate persistent or progressive tumor despite the lack of contrast enhancement. Pseudo-progression is seen in the setting of edema associated with the inflammatory response rather than progression of the true tumor. ADC values have been reported to be have an accuracy of up-to 80% in resolving the two entities[11]. DTI is helpful for intraoperative navigational purposes in order to avoid injuring the corticospinal tracts[12].

White matter diseases

The exquisite sensitivity of DW MRI to microstructural changes enables us to detect the abnormalities much before changes on conventional images. In white matter, any change in tissue orientation patterns inside the MRI voxel results in a change in the degree of anisotropy and there is growing evidence in literature to support this assumption. Clinical studies carried on patients with white matter diseases have shown the sensitivity of DTI to detect abnormalities at an early stage and to demonstrate the microstructural abnormalities in various white matter diseases. Examples include multiple sclerosis, Alzheimer disease, leukoencephalopathies, Wallerian degeneration, Cerebral Autosomal Dominant Arteriopathy with Subcortical Infarcts and Leukoencephalopathy and HIV-1 encephalopathy[13-18].

Anisotropy measurements may highlight more subtle anomalies in the organization of white matter tracks otherwise not visible on anatomical imaging. This property extends the potential of DTI in detecting more subtle changes, *e.g.,* functional disorders that do not necessarily have an anatomical basis. The potential is enormous and covers cognitive impairment, schizophrenia, dyslexia and various other psychiatric disorders[10].

Pediatric brain development and aging

Brain's microstructure is not static, white matter tracts mature during early life and then degenerate with aging. Effects of aging on white matter organization have been studied[19,20]. DTI has a potential in the evaluation pediatric population. The degree of diffusion anisotropy in white matter increases during the myelination process and hence water diffusion properties of white matter in the brain change dramatically during development. Diffusion metrics are isotropic in the adult brain cortex but there is a short time window of anisotropy. This transient anisotropy effect probably reflects the cellular migration and organization process within the cortical layers[10]. DTI can be used to monitor the myelination process during the different phases of development in fetuses, infants and childhood[20,21]. Similarly DTI can also be used to characterize white matter disorders and grey matter migration disorders in children[22,23].

Oncological applications

Diffusion-weighted imaging has got immense potential in the field of onco-imaging. It is easy to implement and adds very little time to a standard MR examination. Malignant lesions have lower ADC values compared to surrounding normal tissue, edema and benign tumors in brain, head and neck malignancies, prostate and liver cancer[24]. Malignant tumors differ in their cellularity and biologic aggressiveness, which can be quantified in terms of ADC values[24,25]. Whole-body DWI, *i.e.,* diffusion weighted whole body imaging with background suppression (DWIBS) is performed using a STIR EPI sequence with a high *b* value for background suppression. Imaging is performed at multiple stations and then post-processed to form a composite image of the whole body. The images are displayed as maximum intensity projections with a reversed gray scale[26]. Signals from majority of normal tissue are suppressed with some exceptions such as the prostate, spleen, ovaries, testes, spinal cord and endometrium. Areas showing restricted diffusion such as highly cellular lymph nodes are strikingly highlighted. Small foci of tumors within the abdomen or peritoneum may also get highlighted by using this technique[26,27]. Recent applications of DWI in oncology include evaluation of response to chemoradiotherapy. Increase in ADC value can be detected before the size of the tumor decreases[28,29].

Head and neck malignancies

DW-MRI has been applied in head and neck neoplasms (Figure 2). There is a significant difference in ADC

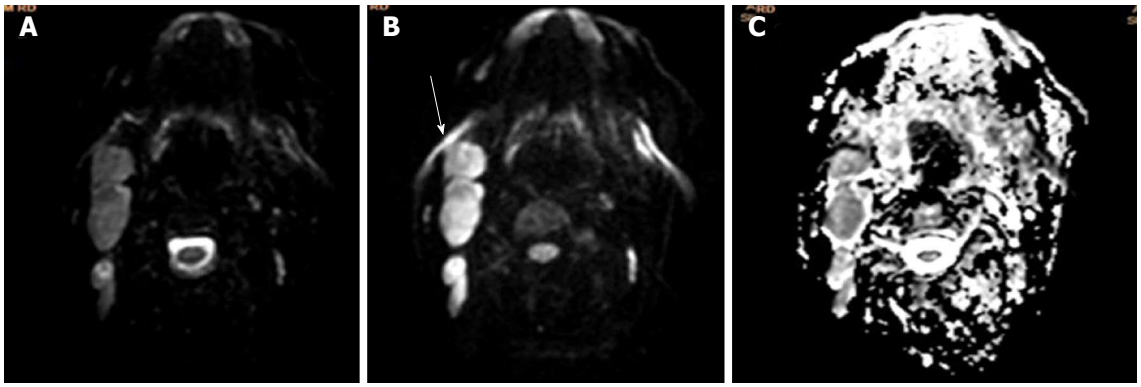

Figure 2 Non-hodgkin's lymphoma. Axial b0 (A), b1000 (B) and apparent diffusion coefficient map are showing multiple enlarged neck nodes. Nodes are showing slightly hyperintense signal on b0 images and retaining their signal on b1000 image with low signal on corresponding ADC (C). ADC: Apparent diffusion coefficient.

values of carcinomas, lymphomas, benign salivary gland tumors and benign cysts. Wang *et al*[30] reported that ADC less than 1.22 × 10^{-3} mm^2/s has 86% predictive accuracy for malignancy with 84% sensitivity and 91% specificity. DWI helps in the differentiation of benign from malignant tumors, lymphoma from squamous cell cancer, and benign from metastatic lymphadenopathy. It also helps in differentiation of necrotic tumors from abscesses and selection of appropriate site for biopsy. ADC value of necrosis is especially helpful in discriminating metastasis from lymphadenitis. Kato *et al*[31] reported significantly lower ADC value in suppurative lymphadenitis (0.89 ± 0.21) than in malignancies (1.46 ± 0.46). In another study Zhang *et al*[32] reported additional value of ADC measurements in necrotic and solid portions. ADC calculations are also useful in monitoring the patient after chemo-radiotherapy and differentiation of recurrent tumors from post-treatment changes[28,29,33,34].

Thoracic malignancies

DWI can be used for distinguishing malignant from benign and inflammatory lung lesions and helps in differentiation of small cell cancers (SCLC) from non-small cell cancers (NSCLC)[35,36]. In a recent meta-analysis by Shen *et al*[35] reported that malignant pulmonary lesions have significantly lower ADC values than benign lesions [1.21 (95%CI: 1.19-1.22) mm^2/s *vs* 1.76 (95%CI: 1.72-1.80) mm^2/s]; and there is a significant difference between ADC values of small cell lung cancer and non-small cell lung cancer although differentiation of various histological subtypes were not possible[35,37]. Nomori *et al*[38] showed that signal intensity and heterogeneity of DWI reflect the histologic heterogeneity and biological aggressiveness in NSCLC. DWI also has a high specificity in the lymph node staging of NSCLC[39].

Breast cancer

Using *b* values up-to 400 s/mm^2, Sinha *et al*[40] reported that malignant breast lesions have significantly lower than the ADC values than benign diseases (1.36 ± 0.36 x 10^{-3} *vs* 2.01 ± 0.46 x 10^{-3}). It is now a routine part of multi-parametric MR evaluation of breast masses (Figure 3). Quantitative DTI measurements have been used as an adjunct to dynamic contrast enhanced (DCE)-MRI. Wang *et al*[41] have reported that compared to DCE-MRI used alone this strategy significantly improves the diagnostic performance of MRI for differential diagnosis between ductal carcinoma *in situ* (DCIS) and invasive breast cancer[42]. The sensitivity of the DTI parameters to detect breast cancer was found to be high, particularly in dense breasts.

Hepatobiliary pancreatic cancers

DWI is helpful in focal liver lesion detection and characterization and can be used as an alternative to Gadolinium enhanced MRI in patients with renal dysfunction (Figures 4-7)[25]. Clinical applications of DW MRI include treatment response monitoring and prognostication in patients receiving systemic and focal ablative therapies for hepatic and pancreatic malignancies[43-46]. Hardie *et al*[47] compared the utility of DWI in detection of liver metastases. They reported that DWI has 66.3% sensitivity compared to 73.5% for CE-MRI and hence it can serve as a useful alternative for this purpose. DW MR imaging has been investigated in diffuse hepatic parenchymal disease such as non-alcoholic fatty liver disease and hepatic fibrosis. However its clinical applicability is questionable as it suffers from multiple confounders making quantifying liver fibrosis through ADC difficult[48]. In a recent meta-analysis, Hong *et al*[48] reported that DWI has a sensitivity and specificity of 0.83 (95%CI: 0.79-0.87) and 0.77 (95%CI: 0.70-0.83) for differentiation of malignant from benign pancreatic lesions. In another meta-analysis, Niu *et al*[49] reported pooled sensitivity of 0.86 (95%CI: 0.80-0.91) and the pooled specificity of 0.82 (95%CI: 0.72-0.89) for differentiation of pancreatic carcinoma from mass-forming chronic pancreatitis. For most abdominal applications *b*-values of 0, 400 and 800 are standard except for prostate imaging where use of values up-to b1600 is considered more suitable.

Bowel disorders

DWI is useful for detection of colorectal cancer, nodal and hepatic metastases and prediction of response after radio-chemotherapy for locally advanced rectal

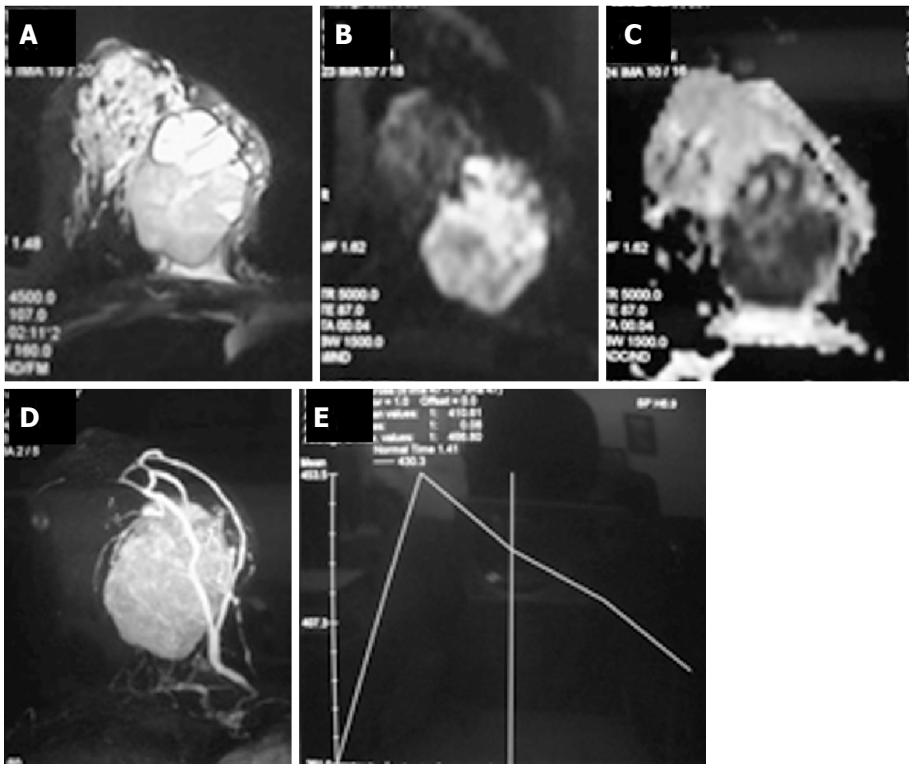

Figure 3 Carcinoma breast. Axial T2W fat saturated image (A) is showing a heterogeneously hyperintense mass lesion in right breast. Mass is showing hyperintense signal on b800 image (B), with low signal on apparent diffusion coefficient map (C); dynamic post-contrast MIP image (D) is showing contrast enhancement within the mass with type 3 enhancement curve (E).

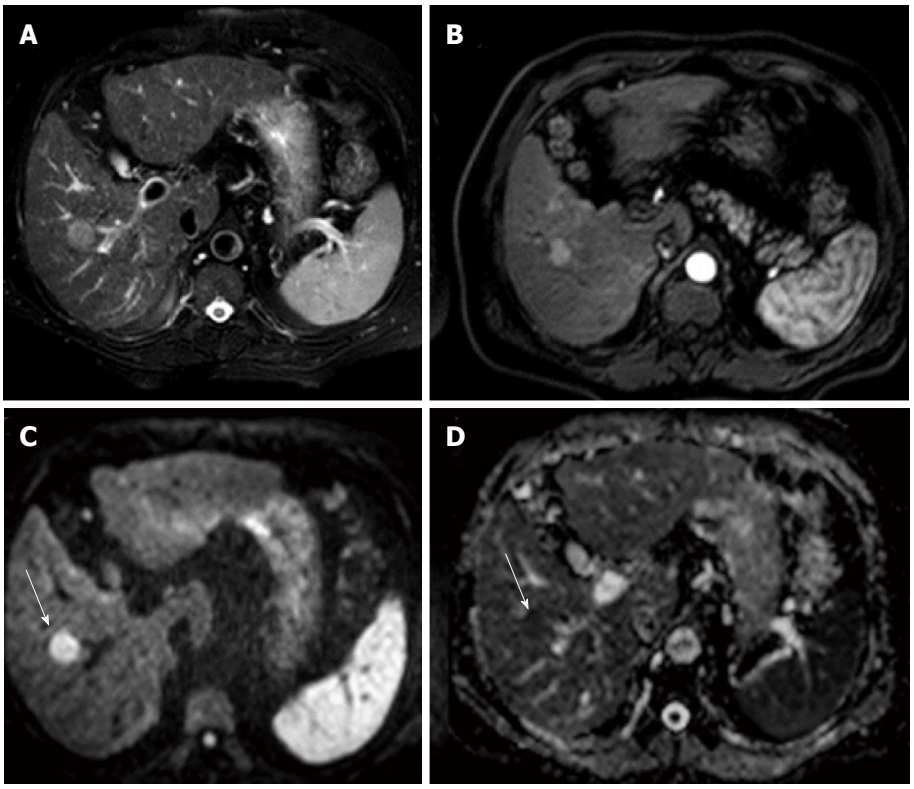

Figure 4 Hepatocellular carcinoma in cirrhotic liver. Axial T2W image is showing a hyperintense lesion in segment 5 of liver (A); lesion is enhancing in arterial phase (B); and it shows hyperintense signal on b800 image (C) and hypointense on apparent diffusion coefficient map (D).

cancer[50-52]. DWI detects therapy-induced modifications in lesion vascularity during anti-angiogenic therapy before significant changes in size are evident[53,54]. DWIBS has been reported a useful tool in detection of

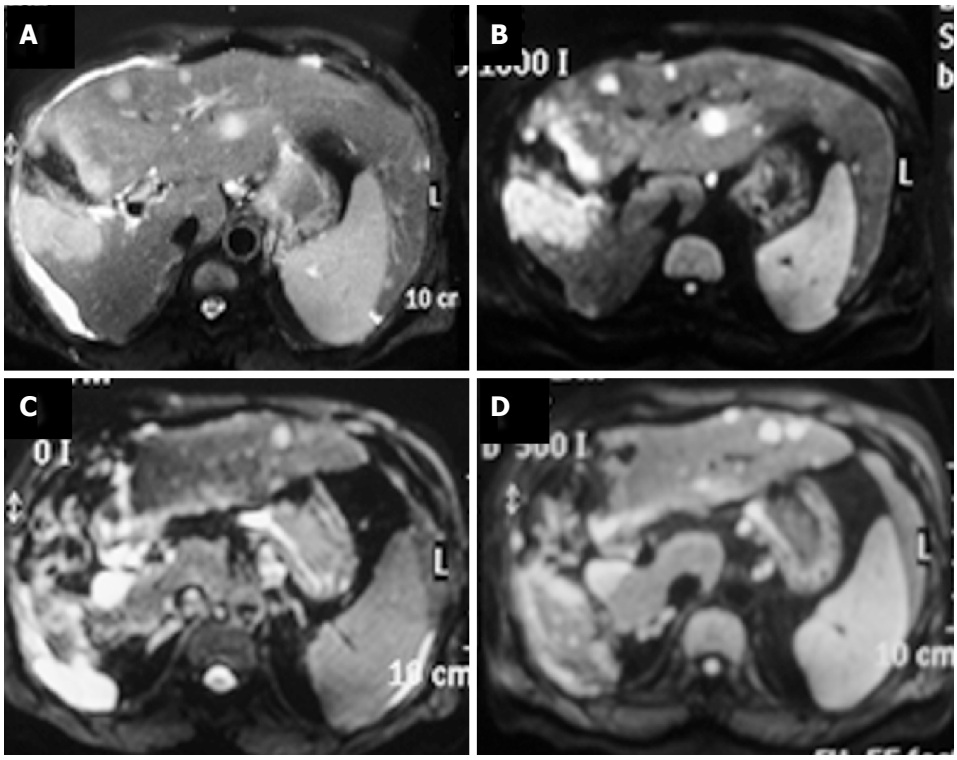

Figure 5 Liver metastases. Patient with gall bladder carcinoma is showing a large T2 hyperintense mass in gall bladder fossa (A) showing restricted diffusion on b1000 image (B); there are multiple metastatic lesions in liver in segments 2, 3 and 4. These lesions are also showing restricted diffusion. Another important point is the fact that a b500 image (D) is showing more lesion compared to a corresponding b0 image (C).

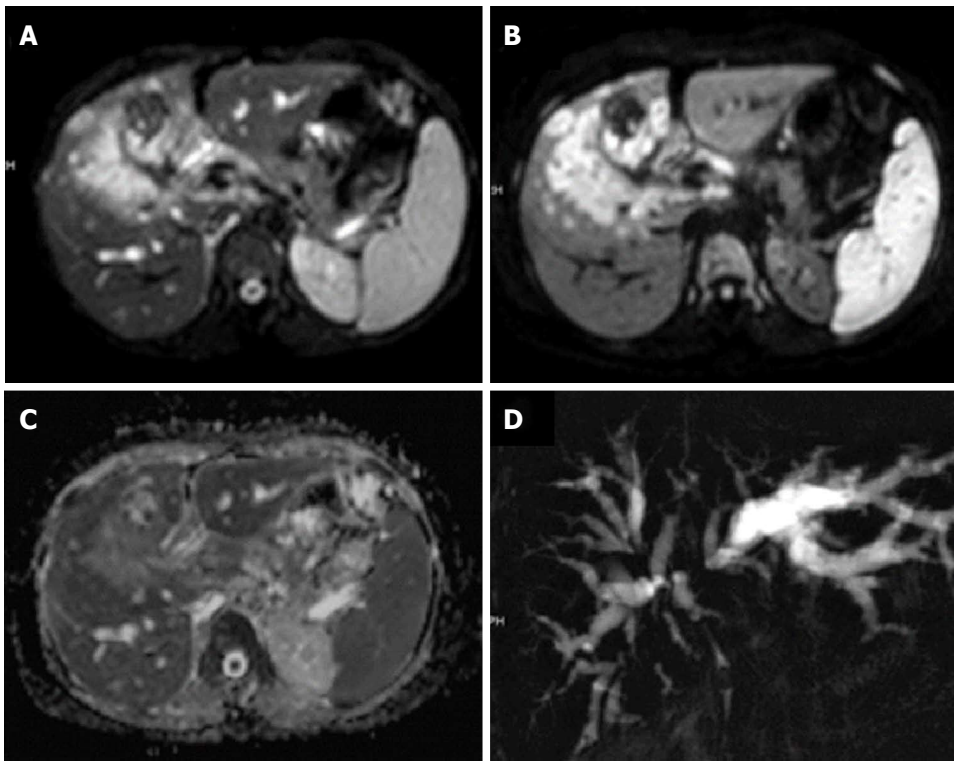

Figure 6 Carcinoma gall bladder. Axial T2W image showing a large heterogeneously hyperintense mass in gall bladder fossa of liver. It is showing hyperintense signal on b700 image (B) and are showing peripheral hyperintense signal on apparent diffusion coefficient map (C); coronal projectional MRCP image is showing biliary obstruction with involvement of primary and right secondary biliary confluence.

nodal metastasis of colorectal cancer[55]. In addition to its utility in abdominal malignancies, DWI has also been found useful in inflammatory bowel disease. Qi *et al*[56] reported that DWI combined with MR enterography

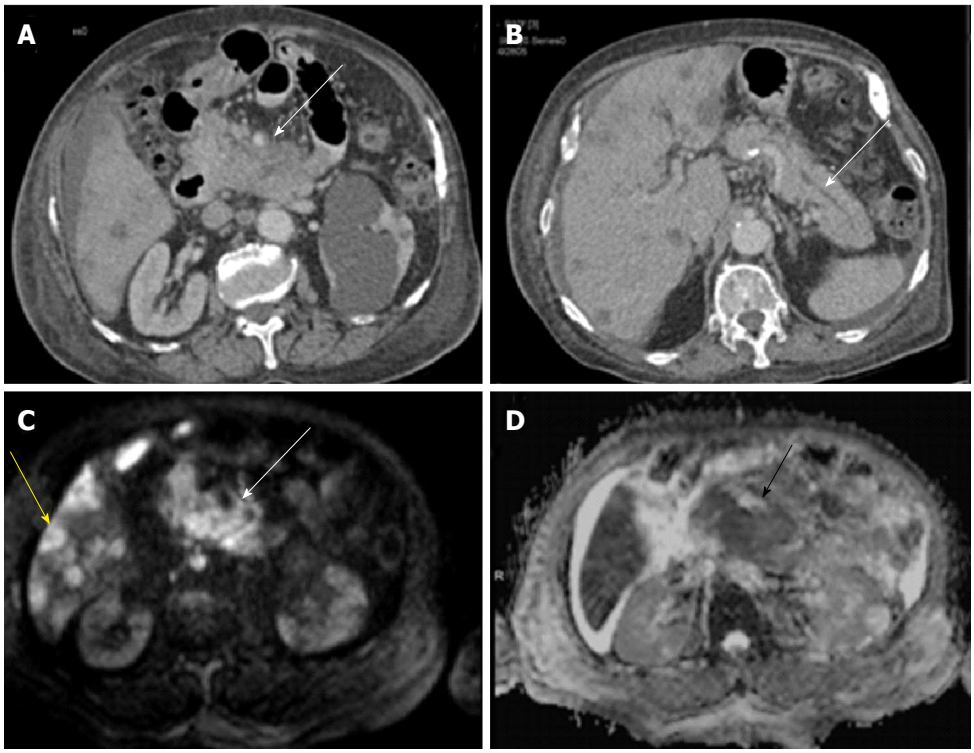

Figure 7 Pancreatic adenocarcinoma. Axial CECT images showing a hypo-enhancing mass in the neck and head region of pancreas (A) with a dilated pancreatic duct (B); multiple hypodense lesions can be noted within the liver parenchyma. Mass in the neck and head region of pancreas is showing hyperintense signal on b800 image and so are the focal liver lesions (C); corresponding apparent diffusion coefficient map shows hypointense signal within the mass (D).

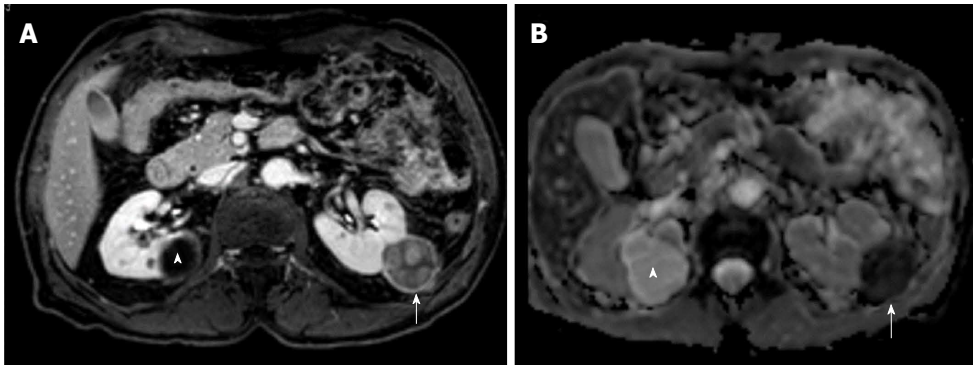

Figure 8 Renal cell carcinoma *vs* simple cyst. Axial contrast-enhanced magnetic resonance image shows non-enhancing bosniak category I cyst in right kidney (arrowhead) and Bosniak category IV cyst (enhancing mural nodules) in left kidney (arrow). Former shows free diffusion with high ADC while latter depicts restricted diffusion with low ADCs. Latter was found to be clear cell renal cell carcinoma. ADC: Apparent diffusion coefficient.

(MRE) has higher diagnostic accuracy (92%) than MRE alone (79%) for disease activity. It has also been found to be useful in detection and characterization of extraintestinal manifestations and complications[57]. Use of DWI with MR enterography improves mesenteric and small bowel tumor detection compared to unenhanced MR-enterography[58].

Genito-urinary applications

DWI can easily distinguish benign renal cysts from solid neoplasms (Figures 8 and 9)[59]. There have been attempts to distinguish various histological subtypes, but due to overlap in the ADC values such predictions have been found to be difficult[59-61]. In patients with transitional cell cancer, histological grade is the most important factor determining biological aggressiveness. ADC values correlate very well with histopathological grades of TCC, and hence predict the biological behaviour of bladder cancer and tumour recurrence (Figures 10 and 11)[59]. DWI helps to detect carcinoma in the transition zone and increases the diagnostic confidence in detection of peripheral zone cancer (Figure 12). DWIBS is useful in detection of skeletal metastasis (Figure 13)[59].

DWI improves the diagnosis of cervical and endometrial tumors[62]. DW MR imaging is especially useful for accurate determination of the depth of myometrial invasion in patients with endometrial cancer[63]. It has

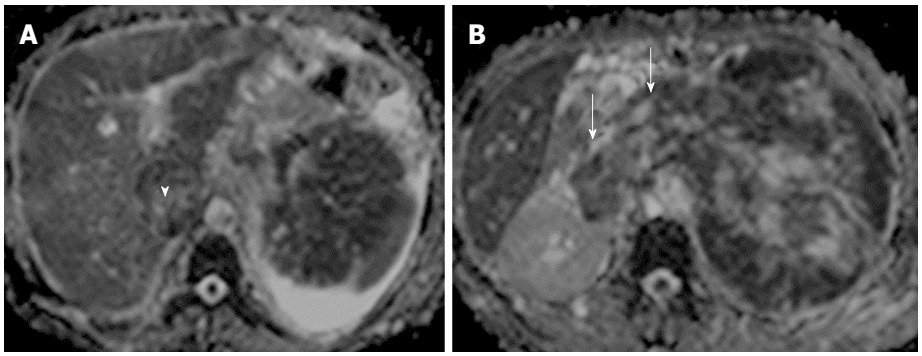

Figure 9 Renal cell carcinoma with malignant inferior vena cava thrombus. Apparent diffusion coefficient maps (A and B) of a patient with large left renal mass with contiguous extension into renal vein (arrows) and inferior vena cava (arrowhead) (malignant thrombosis). Both the renal mass and intravascular thrombus had similar apparent diffusion coefficient values.

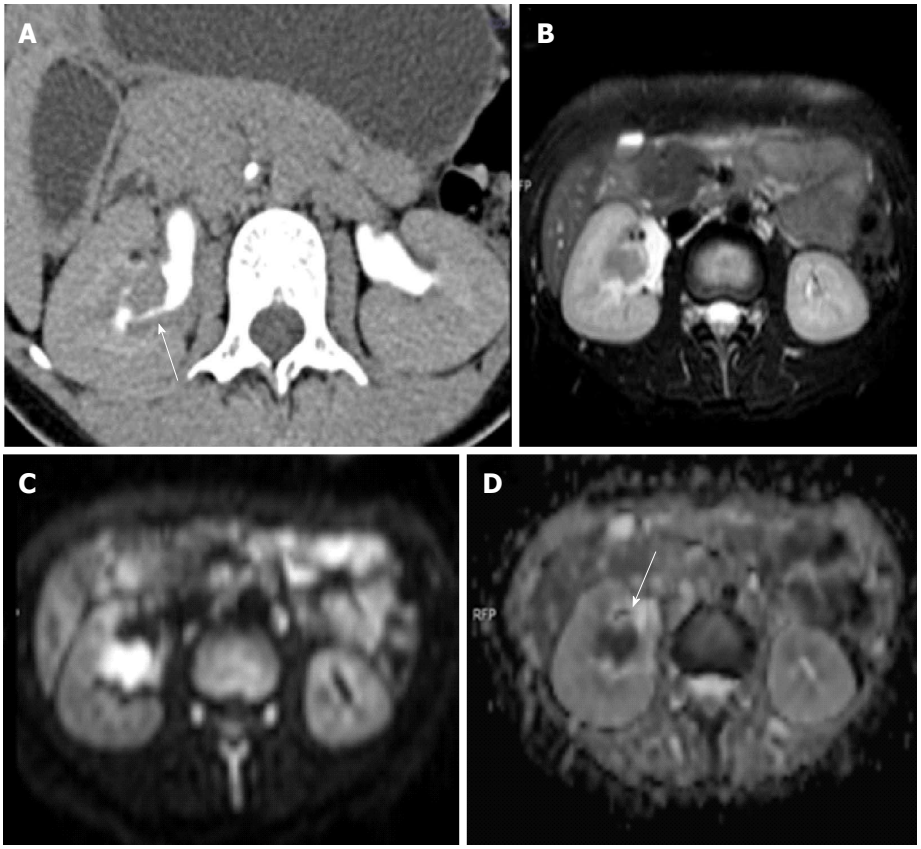

Figure 10 Transitional cell cancer. Computed tomography urography image (A) shows a filling defect within the mid-pole calyx and infundibular region. Axial T2W image (B) showing a corresponding hypointense lesion showing restricted diffusion on diffusion weighted imaging (C, D).

also been suggested to be a potential response biomarker in cervical cancer[64]. DWI is highly sensitive for detection of peritoneal dissemination in gynecological malignancy and plays an important role in the management of gynecological malignancies especially ovarian cancer (Figure 11)[65]. ADC changes have also been shown to be useful in prediction of uterine leiomyoma volume response after uterine artery embolization[66], preoperative differentiation between uterine leiomyoma and leiomyosarcoma[67].

Peripheral nerve imaging

Advancements in DTI technology have expanded its application to peripheral nervous system (Figure 14). DTI adds value to conventional MR Neurography as it is capable of axonal and myelin compartment differentiation. DTI parameters "axial diffusivity" and "fractional anisotropy" are considered as markers of axon integrity and myelin sheath integrity respectively. DTI has been used to quantitatively evaluate spinal nerve entrapment with foraminal stenosis. The entrapped roots and distal spinal nerve show increased diffusivity and significantly lower FA values than the normal nerves[68,69]. DTI has also been studied in animal models for monitoring peripheral nerve degeneration and regeneration[70]. The experience of DTI in nerve imaging is

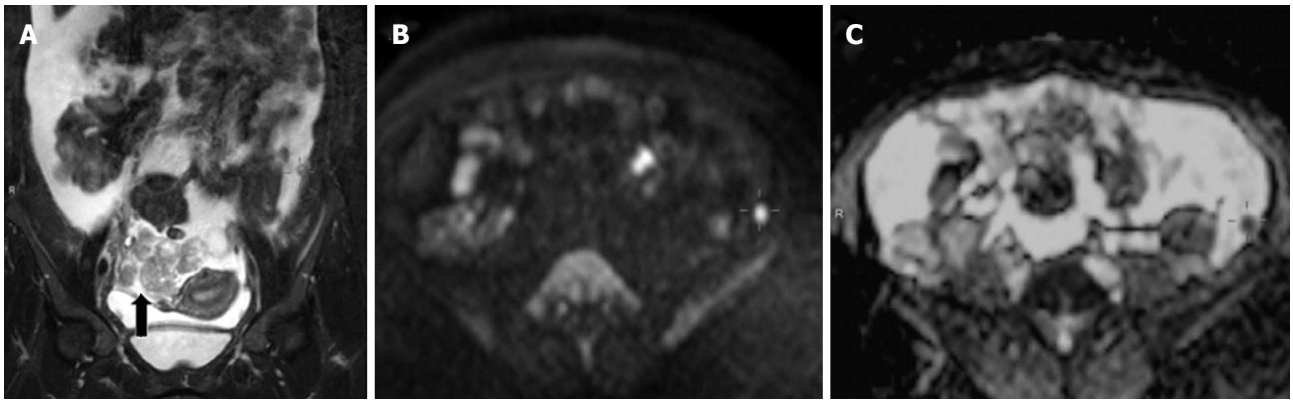

Figure 11 Carcinoma ovary. Coronal T2W image shows right adnexal mass with gross ascitis (A); B800 image (B) showing a focal hyperintense peritoneal nodule in left iliac fossa region with corresponding dark signal on apparent diffusion coefficient map (C).

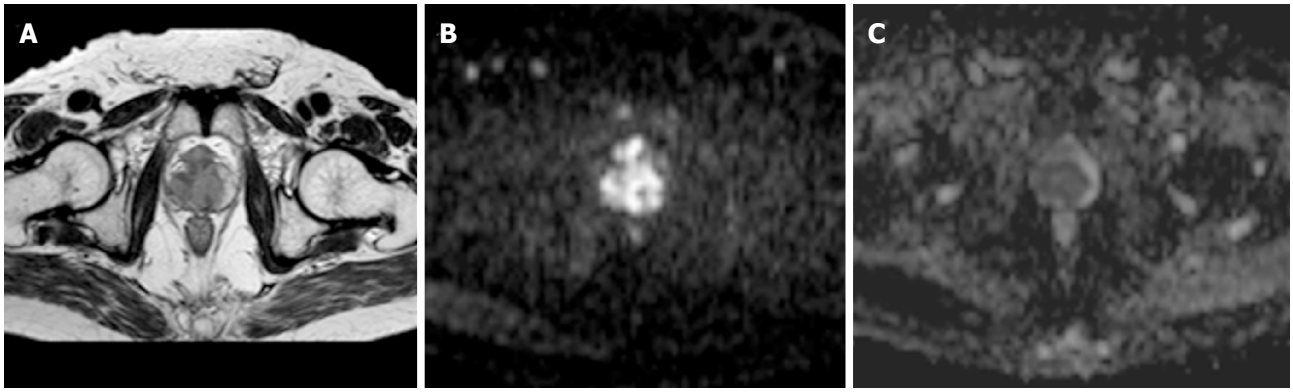

Figure 12 Carcinoma prostate. Axial T2W image (A) showing central T2 corresponding hypointensity on apparent diffusion coefficient map (C) and high signal on b1000 image (B) suggesting a central gland prostate cancer.

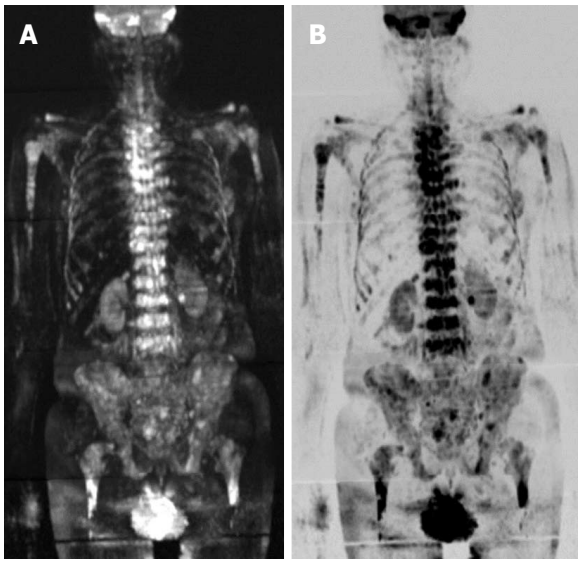

Figure 13 Carcinoma prostate metastases. DWIBS images showing multiple metastatic lesions within the vertebral bodies, pelvic bones, B/L proximal femur and humerus.

limited and it is yet to achieve its full potential[71].

Musculoskeletal applications

DWI improves diagnostic accuracy of MR imaging in the differentiation of acute osteoporotic from malignant compression fractures (Figure 15)[72]. Structural integrity of the spinal cord can be assessed by DTI. Quantitative analysis of anisotropy and diffusivity detects subtle abnormalities that can be easily missed on conventional imaging. DTI has been found to be useful tool in various conditions involving spinal cord. Such conditions include spinal cord injury, multiple sclerosis, amyotrophic lateral sclerosis, myelitis, and spinal cord tumors[73].

LIMITATIONS

The algorithms used in DWI acquisition make several assumptions, *e.g.*, perfect field homogeneity, infinitely fast gradient changes, and perfectly shaped RF pulses, *etc*. However, with the available technology, the gradient coils can generate gradient magnitudes and switch rate of the order of 40 mTm^{-1} and 200 $Tm^{-1}\cdot s^{-1}$ respectively. Such discrepancies limit DWI accuracy and result in lower image quality and image artifacts[74]. Major limitations of DWI are experienced in body imaging and are largely because of it being an EPI sequence[59,60]. DWI is susceptible to various artifacts, *e.g.,* T2 shine through, T2 black out, ghosting, blurring and distortions. Tissues with very long relaxation times might tend to retain signal on high *b* value images. This is known as "T2

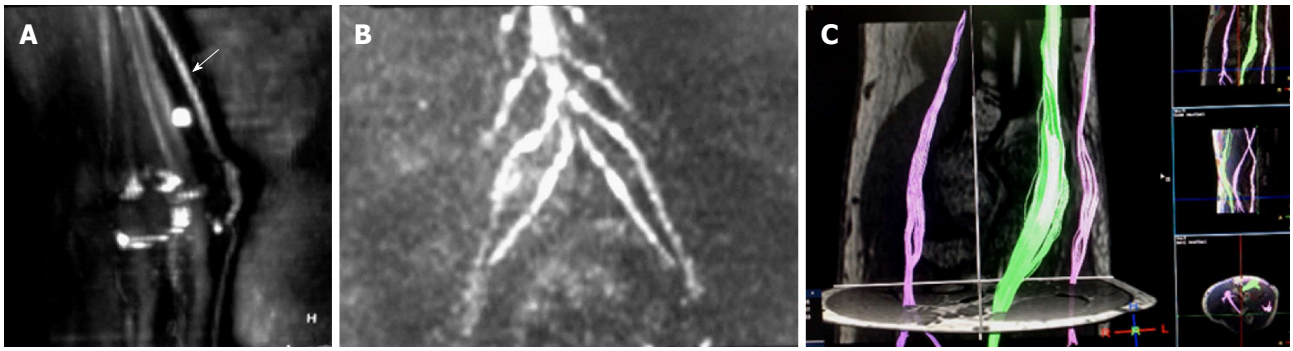

Figure 14 Diffusion tensor imaging images. It shows ulnar nerve (A) and sacral plexus (B); (C) is showing diffusion tensor imaging of nerve fibers of nerves around elbow.

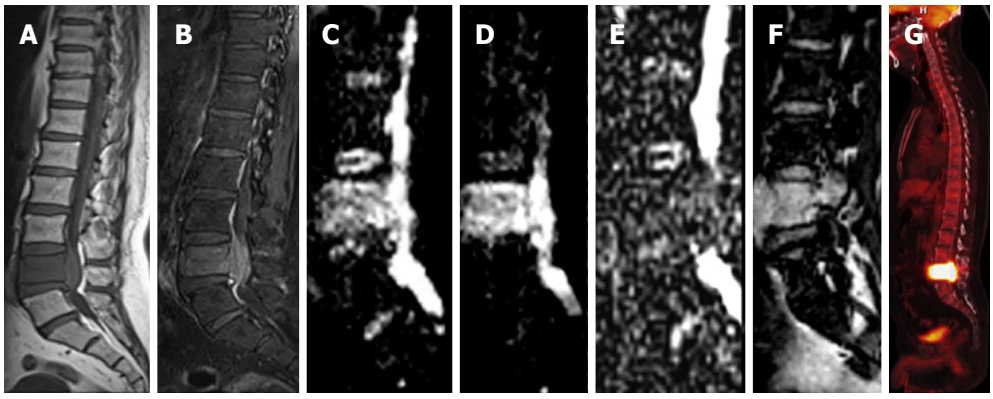

Figure 15 Vertebral metastasis. Sagittal T1W image (A) is showing diffuse T2 hypointese signal within the L5 vertebral body with corresponding hyperintese signal and associated prevertebral and extradural soft tissue on STIR image (B). Diffusion weighted imaging images (C, D) are showing hyperintense signal with low signal on apparent diffusion coefficient map (E). There is contrast enhancement within the involved vertebra (F) and intense uptake on positron emission tomography image (G).

shine through" effect. Corresponding bright signal on ADC map by such lesions helps to differentiate it from restricted diffusion, which appears dark on ADC maps. T2 blackout effect is the term used for low signal on ADC map due to lack of enough water protons and not due to restricted diffusion. Low signal on T2 weighted fat saturated images is the diagnostic sign for such an effect.

Image quality provided by single shot EPI is limited and has a low spatial resolution and a poor SNR. 3T MRI has an inherent high SNR, but presents several limitations as well. Susceptibility artifacts are more pronounced at 3T and uniform fat suppression is also a challenge with 3 Tesla magnets[75]. Parallel imaging technique improves SNR by allowing a decrease in TE[76].

Another bothersome limitation of DWI is the questionable reproducibility of ADC values. ADC values can vary even with the use of same MR system. Such variability has been attributed to the inherent low SNR, artifacts and distortions related to SS EPI sequence. Rapid on/off transition of diffusion gradients during EPI sequence causes eddy-current related distortions resulting in image degradation and systemic errors in ADC calculations[77].

ADDRESSING CURRENT CHALLENGES AND FUTURE DIRECTIONS

Most of the challenges encountered during DWI acquisitions can be minimized by optimizing the DW-MR protocol. Researchers have been focusing on further optimization of DWI sequences and have been making new advancements to enhance the utility of DWI. Non-EPI sequences (turbo-FLASH, HASTE, SSFP) or dual-source parallel RF excitation DWI are novel strategies to overcome the disadvantages of 3T systems[78,79]. Periodically rotated overlapping parallel lines with enhanced reconstruction technique based on the fast spin echo (FSE) sequence has been used for DWI acquisitions to nullify the geometric distortion of EPI[80]. It is of advantage in temporal bone and spinal cord imaging[81]. "TRacking Only Navigator echo" (TRON) is a new acquisition technique for DWI to address the motion related distortions. It allows continuous real-time slice tracking and position correction without use of any kind of gating[82]. Refocused spin echo preparation (bipolar EPI sequence) is an emerging approach to minimize distortions related to the eddy currents[83]. Fast advanced

spin-echo sequence DWI has been reported to be more sensitive and/or accurate than those obtained with EPI-DWI for N-stage assessments of NSCLC patients[84]. Intravoxel incoherent motion with bi-exponential diffusion model is a method of harnessing perfusion information from diffusion acquisitions[27]. Routine DW imaging assumes that water in biological environment follows Gaussian laws (normal distribution), which is an oversimplification. Actually water molecules in such environments have non-gaussian properties that can be quantified by diffusion kurtosis imaging (DKI). DKI provides a measure of tissue heterogeneity and indicate the complexity of the microstructural environment. It provides complementary information to that acquired with traditional diffusion imaging and may lead to broadening of DWI applications[85].

Recent work in the field of diffusion MRI has focused on its application to study the function of brain. Until recently positron emission tomography (PET) and functional BOLD MRI have been used for measurement of brain activity. Le Bihan *et al*[86] have shown that water diffusion properties are modulated by the brain activity. The changes on diffusion functional MRI are faster than the changes with BOLD functional MRI, which measure the reactive increase in blood flow[87]. The introduction of diffusion functional MRI has opened a new paradigm. It has got huge potential for resolving complex mysteries of neurophysiology.

CONCLUSION

DWI has become an indispensable imaging tool. It has well established roles in the fields of stroke imaging, white matter diseases and oncology. While conventional imaging provided only anatomical information, DWI has opened a new paradigm with information about molecular activity and cellular function. Recent advances in this field have touched new horizons with the arrival of functional diffusion MRI. Researchers believe that DWI has still not achieved to its full potential and it is expected that in future DWI may be able to solve the most complex puzzles of brain functioning.

REFERENCES

1 **Geva T**. Magnetic resonance imaging: historical perspective. *J Cardiovasc Magn Reson* 2006; **8**: 573-580 [PMID: 16869310]
2 **Le Bihan D**. Diffusion MRI: what water tells us about the brain. *EMBO Mol Med* 2014; **6**: 569-573 [PMID: 24705876 DOI: 10.1002/emmm.201404055]
3 **Turner R**, Le Bihan D, Maier J, Vavrek R, Hedges LK, Pekar J. Echo-planar imaging of intravoxel incoherent motion. *Radiology* 1990; **177**: 407-414 [PMID: 2217777 DOI: 10.1148/radiology.177.2.2217777]
4 **Moseley ME**, Cohen Y, Mintorovitch J, Chileuitt L, Shimizu H, Kucharczyk J, Wendland MF, Weinstein PR. Early detection of regional cerebral ischemia in cats: comparison of diffusion- and T2-weighted MRI and spectroscopy. *Magn Reson Med* 1990; **14**: 330-346 [PMID: 2345513]
5 **Warach S**, Chien D, Li W, Ronthal M, Edelman RR. Fast magnetic resonance diffusion-weighted imaging of acute human stroke. *Neurology* 1992; **42**: 1717-1723 [PMID: 1513459]
6 **Douek P**, Turner R, Pekar J, Patronas N, Le Bihan D. MR color mapping of myelin fiber orientation. *J Comput Assist Tomogr* 1991; **15**: 923-929 [PMID: 1939769]
7 **Basser PJ**, Mattiello J, LeBihan D. MR diffusion tensor spectroscopy and imaging. *Biophys J* 1994; **66**: 259-267 [PMID: 8130344 DOI: 10.1016/S0006-3495(94)80775-1]
8 **Naraghi AM**, Awdeh H, Wadhwa V, Andreisek G, Chhabra A. Diffusion tensor imaging of peripheral nerves. *Semin Musculoskelet Radiol* 2015; **19**: 191-200 [PMID: 25764243 DOI: 10.1055/s-0035-1546824]
9 **Chalela JA**, Kidwell CS, Nentwich LM, Luby M, Butman JA, Demchuk AM, Hill MD, Patronas N, Latour L, Warach S. Magnetic resonance imaging and computed tomography in emergency assessment of patients with suspected acute stroke: a prospective comparison. *Lancet* 2007; **369**: 293-298 [PMID: 17258669 DOI: 10.1016/S0140-6736(07)60151-2]
10 **Le Bihan D**, Johansen-Berg H. Diffusion MRI at 25: exploring brain tissue structure and function. *Neuroimage* 2012; **61**: 324-341 [PMID: 22120012 DOI: 10.1016/j.neuroimage.2011.11.006]
11 **Lee WJ**, Choi SH, Park CK, Yi KS, Kim TM, Lee SH, Kim JH, Sohn CH, Park SH, Kim IH. Diffusion-weighted MR imaging for the differentiation of true progression from pseudoprogression following concomitant radiotherapy with temozolomide in patients with newly diagnosed high-grade gliomas. *Acad Radiol* 2012; **19**: 1353-1361 [PMID: 22884399 DOI: 10.1016/j.acra.2012.06.011]
12 **Mabray MC**, Barajas RF, Cha S. Modern brain tumor imaging. *Brain Tumor Res Treat* 2015; **3**: 8-23 [PMID: 25977902 DOI: 10.14791/btrt.2015.3.1.8]
13 **Chabriat H**, Pappata S, Poupon C, Clark CA, Vahedi K, Poupon F, Mangin JF, Pachot-Clouard M, Jobert A, Le Bihan D, Bousser MG. Clinical severity in CADASIL related to ultrastructural damage in white matter: in vivo study with diffusion tensor MRI. *Stroke* 1999; **30**: 2637-2643 [PMID: 10582990]
14 **Eichler FS**, Itoh R, Barker PB, Mori S, Garrett ES, van Zijl PC, Moser HW, Raymond GV, Melhem ER. Proton MR spectroscopic and diffusion tensor brain MR imaging in X-linked adrenoleukodystrophy: initial experience. *Radiology* 2002; **225**: 245-252 [PMID: 12355012 DOI: 10.1148/radiol.2251011040]
15 **Hanyu H**, Sakurai H, Iwamoto T, Takasaki M, Shindo H, Abe K. Diffusion-weighted MR imaging of the hippocampus and temporal white matter in Alzheimer's disease. *J Neurol Sci* 1998; **156**: 195-200 [PMID: 9588857]
16 **Werring DJ**, Clark CA, Barker GJ, Thompson AJ, Miller DH. Diffusion tensor imaging of lesions and normal-appearing white matter in multiple sclerosis. *Neurology* 1999; **52**: 1626-1632 [PMID: 10331689]
17 **Horsfield MA**, Larsson HB, Jones DK, Gass A. Diffusion magnetic resonance imaging in multiple sclerosis. *J Neurol Neurosurg Psychiatry* 1998; **64** Suppl 1: S80-S84 [PMID: 9647291]
18 **Filippi CG**, Ulug AM, Ryan E, Ferrando SJ, van Gorp W. Diffusion tensor imaging of patients with HIV and normal-appearing white matter on MR images of the brain. *AJNR Am J Neuroradiol* 2001; **22**: 277-283 [PMID: 11156769]
19 **Moseley M**. Diffusion tensor imaging and aging - a review. *NMR Biomed* 2002; **15**: 553-560 [PMID: 12489101 DOI: 10.1002/nbm.785]
20 **Pfefferbaum A**, Sullivan EV, Hedehus M, Lim KO, Adalsteinsson E, Moseley M. Age-related decline in brain white matter anisotropy measured with spatially corrected echo-planar diffusion tensor imaging. *Magn Reson Med* 2000; **44**: 259-268 [PMID: 10918325]
21 **Dubois J**, Hertz-Pannier L, Dehaene-Lambertz G, Cointepas Y, Le Bihan D. Assessment of the early organization and maturation of infants' cerebral white matter fiber bundles: a feasibility study using quantitative diffusion tensor imaging and tractography. *Neuroimage* 2006; **30**: 1121-1132 [PMID: 16413790 DOI: 10.1016/j.neuroimage.2005.11.022]
22 **Takahashi M**, Ono J, Harada K, Maeda M, Hackney DB. Diffusional anisotropy in cranial nerves with maturation: quantitative evaluation with diffusion MR imaging in rats. *Radiology* 2000; **216**:

881-885 [PMID: 10966726 DOI: 10.1148/radiology.216.3.r00se41881]
23 **Engelbrecht V**, Scherer A, Rassek M, Witsack HJ, Mödder U. Diffusion-weighted MR imaging in the brain in children: findings in the normal brain and in the brain with white matter diseases. *Radiology* 2002; **222**: 410-418 [PMID: 11818607 DOI: 10.1148/radiol.2222010492]
24 **Charles-Edwards EM**, deSouza NM. Diffusion-weighted magnetic resonance imaging and its application to cancer. *Cancer Imaging* 2006; **6**: 135-143 [PMID: 17015238 DOI: 10.1102/1470-7330.2006.0021]
25 **Chan JH**, Tsui EY, Luk SH, Fung AS, Yuen MK, Szeto ML, Cheung YK, Wong KP. Diffusion-weighted MR imaging of the liver: distinguishing hepatic abscess from cystic or necrotic tumor. *Abdom Imaging* 2001; **26**: 161-165 [PMID: 11178693]
26 **Takahara T**, Imai Y, Yamashita T, Yasuda S, Nasu S, Van Cauteren M. Diffusion weighted whole body imaging with background body signal suppression (DWIBS): technical improvement using free breathing, STIR and high resolution 3D display. *Radiat Med* 2004; **22**: 275-282 [PMID: 15468951]
27 **Koh DM**, Collins DJ, Orton MR. Intravoxel incoherent motion in body diffusion-weighted MRI: reality and challenges. *AJR Am J Roentgenol* 2011; **196**: 1351-1361 [PMID: 21606299 DOI: 10.2214/AJR.10.5515]
28 **Schouten CS**, de Graaf P, Alberts FM, Hoekstra OS, Comans EF, Bloemena E, Witte BI, Sanchez E, Leemans CR, Castelijns JA, de Bree R. Response evaluation after chemoradiotherapy for advanced nodal disease in head and neck cancer using diffusion-weighted MRI and 18F-FDG-PET-CT. *Oral Oncol* 2015; **51**: 541-547 [PMID: 25725587 DOI: 10.1016/j.oraloncology.2015.01.017]
29 **Varoquaux A**, Rager O, Dulguerov P, Burkhardt K, Ailianou A, Becker M. Diffusion-weighted and PET/MR Imaging after Radiation Therapy for Malignant Head and Neck Tumors. *Radiographics* 2015; **35**: 1502-1527 [PMID: 26252192 DOI: 10.1148/rg.2015140029]
30 **Wang J**, Takashima S, Takayama F, Kawakami S, Saito A, Matsushita T, Momose M, Ishiyama T. Head and neck lesions: characterization with diffusion-weighted echo-planar MR imaging. *Radiology* 2001; **220**: 621-630 [PMID: 11526259 DOI: 10.1148/radiol.2202010063]
31 **Kato H**, Kanematsu M, Kato Z, Teramoto T, Mizuta K, Aoki M, Makita H, Kato K. Necrotic cervical nodes: usefulness of diffusion-weighted MR imaging in the differentiation of suppurative lymphadenitis from malignancy. *Eur J Radiol* 2013; **82**: e28-e35 [PMID: 22954412 DOI: 10.1016/j.ejrad.2012.08.014]
32 **Zhang Y**, Chen J, Shen J, Zhong J, Ye R, Liang B. Apparent diffusion coefficient values of necrotic and solid portion of lymph nodes: differential diagnostic value in cervical lymphadenopathy. *Clin Radiol* 2013; **68**: 224-231 [PMID: 22316593 DOI: 10.1016/j.crad.2011.04.002]
33 **Razek AA**. Diffusion-weighted magnetic resonance imaging of head and neck. *J Comput Assist Tomogr* 2010; **34**: 808-815 [PMID: 21084893 DOI: 10.1097/RCT.0b013e3181f01796]
34 **Şerifoğlu İ**, Oz İİ, Damar M, Tokgöz Ö, Yazgan Ö, Erdem Z. Diffusion-weighted imaging in the head and neck region: usefulness of apparent diffusion coefficient values for characterization of lesions. *Diagn Interv Radiol* 2015; **21**: 208-214 [PMID: 25910284 DOI: 10.5152/dir.2014.14279]
35 **Shen G**, Jia Z, Deng H. Apparent diffusion coefficient values of diffusion-weighted imaging for distinguishing focal pulmonary lesions and characterizing the subtype of lung cancer: a meta-analysis. *Eur Radiol* 2016; **26**: 556-566 [PMID: 26003791 DOI: 10.1007/s00330-015-3840-y]
36 **Deng Y**, Li X, Lei Y, Liang C, Liu Z. Use of diffusion-weighted magnetic resonance imaging to distinguish between lung cancer and focal inflammatory lesions: a comparison of intravoxel incoherent motion derived parameters and apparent diffusion coefficient. *Acta Radiol* 2015 May 13; Epub ahead of print [PMID: 25972370 DOI: 10.1177/0284185115586091]
37 **Liu LP**, Zhang XX, Cui LB, Li J, Yang JL, Yang HN, Zhang Y, Zhou Y, Tang X, Qi S, Fang Y, Zhang J, Yin H. Preliminary comparison of diffusion-weighted MRI and PET/CT in predicting histological type and malignancy of lung cancer. *Clin Respir J* 2015 Apr 27; Epub ahead of print [PMID: 25918835 DOI: 10.1111/crj.12316]
38 **Nomori H**, Cong Y, Abe M, Sugimura H, Kato Y. Diffusion-weighted magnetic resonance imaging in preoperative assessment of non-small cell lung cancer. *J Thorac Cardiovasc Surg* 2015; **149**: 991-996 [PMID: 25686657 DOI: 10.1016/j.jtcvs.2015.01.019]
39 **Zhang Y**, Qin Q, Li B, Wang J, Zhang K. Magnetic resonance imaging for N staging in non-small cell lung cancer: A systematic review and meta-analysis. *Thorac Cancer* 2015; **6**: 123-132 [PMID: 26273348 DOI: 10.1111/1759-7714.12203]
40 **Sinha S**, Lucas-Quesada FA, Sinha U, DeBruhl N, Bassett LW. In vivo diffusion-weighted MRI of the breast: potential for lesion characterization. *J Magn Reson Imaging* 2002; **15**: 693-704 [PMID: 12112520 DOI: 10.1002/jmri.10116]
41 **Wang Y**, Zhang X, Cao K, Li Y, Li X, Qi L, Tang L, Wang Z, Gao S. Diffusion-tensor imaging as an adjunct to dynamic contrast-enhanced MRI for improved accuracy of differential diagnosis between breast ductal carcinoma in situ and invasive breast carcinoma. *Chin J Cancer Res* 2015; **27**: 209-217 [PMID: 25937784 DOI: 10.3978/j.issn.1000-9604.2015.03.04]
42 **Nissan N**, Furman-Haran E, Feinberg-Shapiro M, Grobgeld D, Eyal E, Zehavi T, Degani H. Tracking the mammary architectural features and detecting breast cancer with magnetic resonance diffusion tensor imaging. *J Vis Exp* 2014; **(94)** [PMID: 25549209 DOI: 10.3791/52048]
43 **De Robertis R**, Tinazzi Martini P, Demozzi E, Puntel G, Ortolani S, Cingarlini S, Ruzzenente A, Guglielmi A, Tortora G, Bassi C, Pederzoli P, D'Onofrio M. Prognostication and response assessment in liver and pancreatic tumors: The new imaging. *World J Gastroenterol* 2015; **21**: 6794-6808 [PMID: 26078555 DOI: 10.3748/wjg.v21.i22.6794]
44 **Cuneo KC**, Chenevert TL, Ben-Josef E, Feng MU, Greenson JK, Hussain HK, Simeone DM, Schipper MJ, Anderson MA, Zalupski MM, Al-Hawary M, Galban CJ, Rehemtulla A, Feng FY, Lawrence TS, Ross BD. A pilot study of diffusion-weighted MRI in patients undergoing neoadjuvant chemoradiation for pancreatic cancer. *Transl Oncol* 2014; **7**: 644-649 [PMID: 25389460 DOI: 10.1016/j.tranon.2014.07.005]
45 **Kurosawa J**, Tawada K, Mikata R, Ishihara T, Tsuyuguchi T, Saito M, Shimofusa R, Yoshitomi H, Ohtsuka M, Miyazaki M, Yokosuka O. Prognostic relevance of apparent diffusion coefficient obtained by diffusion-weighted MRI in pancreatic cancer. *J Magn Reson Imaging* 2015; **42**: 1532-1537 [PMID: 25946483 DOI: 10.1002/jmri.24939]
46 **Mannelli L**, Bhargava P, Osman SF, Raz E, Moshiri M, Laffi G, Wilson GJ, Maki JH. Diffusion-weighted imaging of the liver: a comprehensive review. *Curr Probl Diagn Radiol* 2013; **42**: 77-83 [PMID: 23683849 DOI: 10.1067/j.cpradiol.2012.07.001]
47 **Hardie AD**, Naik M, Hecht EM, Chandarana H, Mannelli L, Babb JS, Taouli B. Diagnosis of liver metastases: value of diffusion-weighted MRI compared with gadolinium-enhanced MRI. *Eur Radiol* 2010; **20**: 1431-1441 [PMID: 20148251 DOI: 10.1007/s00330-009-1695-9]
48 **Hong BZ**, Li XF, Lin JQ. Differential diagnosis of pancreatic cancer by single-shot echo-planar imaging diffusion-weighted imaging. *World J Gastroenterol* 2015; **21**: 6374-6380 [PMID: 26034373 DOI: 10.3748/wjg.v21.i20.6374]
49 **Niu X**, Das SK, Bhetuwal A, Xiao Y, Sun F, Zeng L, Wang W, Yang H, Yang H. Value of diffusion-weighted imaging in distinguishing pancreatic carcinoma from mass-forming chronic pancreatitis: a meta-analysis. *Chin Med J* (Engl) 2014; **127**: 3477-3482 [PMID: 25269917]
50 **Ichikawa T**, Erturk SM, Motosugi U, Sou H, Iino H, Araki T, Fujii H. High-B-value diffusion-weighted MRI in colorectal cancer. *AJR Am J Roentgenol* 2006; **187**: 181-184 [PMID: 16794174 DOI: 10.2214/AJR.05.1005]
51 **Joye I**, Deroose CM, Vandecaveye V, Haustermans K. The role of diffusion-weighted MRI and (18)F-FDG PET/CT in the prediction

of pathologic complete response after radiochemotherapy for rectal cancer: a systematic review. *Radiother Oncol* 2014; **113**: 158-165 [PMID: 25483833 DOI: 10.1016/j.radonc.2014.11.026]
52 **Meng X**, Huang Z, Wang R, Yu J. Prediction of response to preoperative chemoradiotherapy in patients with locally advanced rectal cancer. *Biosci Trends* 2014; **8**: 11-23 [PMID: 24647108]
53 **Anzidei M**, Napoli A, Zaccagna F, Cartocci G, Saba L, Menichini G, Cavallo Marincola B, Marotta E, Di Mare L, Catalano C, Passariello R. Liver metastases from colorectal cancer treated with conventional and antiangiogenetic chemotherapy: evaluation with liver computed tomography perfusion and magnetic resonance diffusion-weighted imaging. *J Comput Assist Tomogr* 2011; **35**: 690-696 [PMID: 22082538 DOI: 10.1097/RCT.0b013e318230d905]
54 **Heijmen L**, Ter Voert EE, Nagtegaal ID, Span P, Bussink J, Punt CJ, de Wilt JH, Sweep FC, Heerschap A, van Laarhoven HW. Diffusion-weighted MR imaging in liver metastases of colorectal cancer: reproducibility and biological validation. *Eur Radiol* 2013; **23**: 748-756 [PMID: 23001604 DOI: 10.1007/s00330-012-2654-4]
55 **Shuto K**, Saito H, Ohira G, Miyauchi H, Matsubara H. Diffusion weighted whole body imaging with background body signal suppression (DWIBS) in nodal metastasis of colorectal cancer. *Nihon Rinsho* 2011; **69** Suppl 3: 315-319 [PMID: 22213976]
56 **Qi F**, Jun S, Qi QY, Chen PJ, Chuan GX, Jiong Z, Rong XJ. Utility of the diffusion-weighted imaging for activity evaluation in Crohn's disease patients underwent magnetic resonance enterography. *BMC Gastroenterol* 2015; **15**: 12 [PMID: 25653007 DOI: 10.1186/s12876-015-0235-0]
57 **Morani AC**, Smith EA, Ganeshan D, Dillman JR. Diffusion-weighted MRI in pediatric inflammatory bowel disease. *AJR Am J Roentgenol* 2015; **204**: 1269-1277 [PMID: 26001238 DOI: 10.2214/AJR.14.13359]
58 **Amzallag-Bellenger E**, Soyer P, Barbe C, Nguyen TL, Amara N, Hoeffel C. Diffusion-weighted imaging for the detection of mesenteric small bowel tumours with Magnetic Resonance--enterography. *Eur Radiol* 2014; **24**: 2916-2926 [PMID: 25113647 DOI: 10.1007/s00330-014-3303-x]
59 **Baliyan V**, Das CJ, Sharma S, Gupta AK. Diffusion-weighted imaging in urinary tract lesions. *Clin Radiol* 2014; **69**: 773-782 [PMID: 24581968 DOI: 10.1016/j.crad.2014.01.011]
60 **Koh DM**, Collins DJ. Diffusion-weighted MRI in the body: applications and challenges in oncology. *AJR Am J Roentgenol* 2007; **188**: 1622-1635 [PMID: 17515386 DOI: 10.2214/AJR.06.1403]
61 **Goyal A**, Sharma R, Bhalla AS, Gamanagatti S, Seth A, Iyer VK, Das P. Diffusion-weighted MRI in renal cell carcinoma: a surrogate marker for predicting nuclear grade and histological subtype. *Acta Radiol* 2012; **53**: 349-358 [PMID: 22496427 DOI: 10.1258/ar.2011.110415]
62 **Levy A**, Medjhoul A, Caramella C, Zareski E, Berges O, Chargari C, Boulet B, Bidault F, Dromain C, Balleyguier C. Interest of diffusion-weighted echo-planar MR imaging and apparent diffusion coefficient mapping in gynecological malignancies: a review. *J Magn Reson Imaging* 2011; **33**: 1020-1027 [PMID: 21509857 DOI: 10.1002/jmri.22546]
63 **Manoharan D**, Das CJ, Aggarwal A, Gupta AK. Diffusion weighted imaging in gynecological malignancies - present and future. *World J Radiol* 2016; **8**: 288-297 [PMID: 27027614 DOI: 10.4329/wjr.v8.i3.288]
64 **Makino H**, Kato H, Furui T, Morishige K, Kanematsu M. Predictive value of diffusion-weighted magnetic resonance imaging during chemoradiotherapy for uterine cervical cancer. *J Obstet Gynaecol Res* 2014; **40**: 1098-1104 [PMID: 24320754 DOI: 10.1111/jog.12276]
65 **Fujii S**, Matsusue E, Kanasaki Y, Kanamori Y, Nakanishi J, Sugihara S, Kigawa J, Terakawa N, Ogawa T. Detection of peritoneal dissemination in gynecological malignancy: evaluation by diffusion-weighted MR imaging. *Eur Radiol* 2008; **18**: 18-23 [PMID: 17701040 DOI: 10.1007/s00330-007-0732-9]
66 **Cao MQ**, Suo ST, Zhang XB, Zhong YC, Zhuang ZG, Cheng JJ, Chi JC, Xu JR. Entropy of T2-weighted imaging combined with apparent diffusion coefficient in prediction of uterine leiomyoma volume response after uterine artery embolization. *Acad Radiol* 2014; **21**: 437-444 [PMID: 24594413 DOI: 10.1016/j.acra.2013.12.007]
67 **Sato K**, Yuasa N, Fujita M, Fukushima Y. Clinical application of diffusion-weighted imaging for preoperative differentiation between uterine leiomyoma and leiomyosarcoma. *Am J Obstet Gynecol* 2014; **210**: 368.e1-368.e8 [PMID: 24368137 DOI: 10.1016/j.ajog.2013.12.028]
68 **Eguchi Y**, Ohtori S, Yamashita M, Yamauchi K, Suzuki M, Orita S, Kamoda H, Arai G, Ishikawa T, Miyagi M, Ochiai N, Kishida S, Masuda Y, Ochi S, Kikawa T, Takaso M, Aoki Y, Toyone T, Suzuki T, Takahashi K. Clinical applications of diffusion magnetic resonance imaging of the lumbar foraminal nerve root entrapment. *Eur Spine J* 2010; **19**: 1874-1882 [PMID: 20632042 DOI: 10.1007/s00586-010-1520-9]
69 **Chen YY**, Lin XF, Zhang F, Zhang X, Hu HJ, Wang DY, Lu LJ, Shen J. Diffusion tensor imaging of symptomatic nerve roots in patients with cervical disc herniation. *Acad Radiol* 2014; **21**: 338-344 [PMID: 24361075 DOI: 10.1016/j.acra.2013.11.005]
70 **Takagi T**, Nakamura M, Yamada M, Hikishima K, Momoshima S, Fujiyoshi K, Shibata S, Okano HJ, Toyama Y, Okano H. Visualization of peripheral nerve degeneration and regeneration: monitoring with diffusion tensor tractography. *Neuroimage* 2009; **44**: 884-892 [PMID: 18948210 DOI: 10.1016/j.neuroimage.2008.09.022]
71 **Heckel A**, Weiler M, Xia A, Ruetters M, Pham M, Bendszus M, Heiland S, Baeumer P. Peripheral Nerve Diffusion Tensor Imaging: Assessment of Axon and Myelin Sheath Integrity. *PLoS One* 2015; **10**: e0130833 [PMID: 26114630 DOI: 10.1371/journal.pone.0130833]
72 **Sung JK**, Jee WH, Jung JY, Choi M, Lee SY, Kim YH, Ha KY, Park CK. Differentiation of acute osteoporotic and malignant compression fractures of the spine: use of additive qualitative and quantitative axial diffusion-weighted MR imaging to conventional MR imaging at 3.0 T. *Radiology* 2014; **271**: 488-498 [PMID: 24484060 DOI: 10.1148/radiol.13130399]
73 **Bosma R**, Stroman PW. Diffusion tensor imaging in the human spinal cord: development, limitations, and clinical applications. *Crit Rev Biomed Eng* 2012; **40**: 1-20 [PMID: 22428796]
74 **Chilla GS**, Tan CH, Xu C, Poh CL. Diffusion weighted magnetic resonance imaging and its recent trend-a survey. *Quant Imaging Med Surg* 2015; **5**: 407-422 [PMID: 26029644 DOI: 10.3978/j.issn.2223-4292.2015.03.01]
75 **Rosenkrantz AB**, Oei M, Babb JS, Niver BE, Taouli B. Diffusion-weighted imaging of the abdomen at 3.0 Tesla: image quality and apparent diffusion coefficient reproducibility compared with 1.5 Tesla. *J Magn Reson Imaging* 2011; **33**: 128-135 [PMID: 21182130 DOI: 10.1002/jmri.22395]
76 **Bammer R**, Keeling SL, Augustin M, Pruessmann KP, Wolf R, Stollberger R, Hartung HP, Fazekas F. Improved diffusion-weighted single-shot echo-planar imaging (EPI) in stroke using sensitivity encoding (SENSE). *Magn Reson Med* 2001; **46**: 548-554 [PMID: 11550248]
77 **Sasaki M**, Yamada K, Watanabe Y, Matsui M, Ida M, Fujiwara S, Shibata E. Variability in absolute apparent diffusion coefficient values across different platforms may be substantial: a multivendor, multi-institutional comparison study. *Radiology* 2008; **249**: 624-630 [PMID: 18936317 DOI: 10.1148/radiol.2492071681]
78 **Dietrich O**, Biffar A, Baur-Melnyk A, Reiser MF. Technical aspects of MR diffusion imaging of the body. *Eur J Radiol* 2010; **76**: 314-322 [PMID: 20299172 DOI: 10.1016/j.ejrad.2010.02.018]
79 **Willinek WA**, Gieseke J, Kukuk GM, Nelles M, König R, Morakkabati-Spitz N, Träber F, Thomas D, Kuhl CK, Schild HH. Dual-source parallel radiofrequency excitation body MR imaging compared with standard MR imaging at 3.0 T: initial clinical experience. *Radiology* 2010; **256**: 966-975 [PMID: 20720078 DOI: 10.1148/radiol.10092127]
80 **Deng J**, Omary RA, Larson AC. Multishot diffusion-weighted SPLICE PROPELLER MRI of the abdomen. *Magn Reson Med* 2008; **59**: 947-953 [PMID: 18429036 DOI: 10.1002/mrm.21525]
81 **Karandikar A**, Loke SC, Goh J, Yeo SB, Tan TY. Evaluation of cholesteatoma: our experience with DW Propeller imaging. *Acta Radiol* 2015; **56**: 1108-1112 [PMID: 25260417 DOI: 10.1177/0284

185114549568]
82 **Takahara T**, Kwee TC, Van Leeuwen MS, Ogino T, Horie T, Van Cauteren M, Herigault G, Imai Y, Mali WP, Luijten PR. Diffusion-weighted magnetic resonance imaging of the liver using tracking only navigator echo: feasibility study. *Invest Radiol* 2010; **45**: 57-63 [PMID: 20057318 DOI: 10.1097/RLI.0b013e3181cc25ed]
83 **Kyriazi S**, Blackledge M, Collins DJ, Desouza NM. Optimising diffusion-weighted imaging in the abdomen and pelvis: comparison of image quality between monopolar and bipolar single-shot spin-echo echo-planar sequences. *Eur Radiol* 2010; **20**: 2422-2431 [PMID: 20711734 DOI: 10.1007/s00330-010-1826-3]
84 **Ohno Y**, Koyama H, Yoshikawa T, Takenaka D, Kassai Y, Yui M, Matsumoto S, Sugimura K. Diffusion-weighted MR imaging using FASE sequence for 3T MR system: Preliminary comparison of capability for N-stage assessment by means of diffusion-weighted MR imaging using EPI sequence, STIR FASE imaging and FDG PET/CT for non-small cell lung cancer patients. *Eur J Radiol* 2015; **84**: 2321-2331 [PMID: 26231045 DOI: 10.1016/j.ejrad.2015.07.019]
85 **Steven AJ**, Zhuo J, Melhem ER. Diffusion kurtosis imaging: an emerging technique for evaluating the microstructural environment of the brain. *AJR Am J Roentgenol* 2014; **202**: W26-W33 [PMID: 24370162 DOI: 10.2214/AJR.13.11365]
86 **Le Bihan D**, Urayama S, Aso T, Hanakawa T, Fukuyama H. Direct and fast detection of neuronal activation in the human brain with diffusion MRI. *Proc Natl Acad Sci USA* 2006; **103**: 8263-8268 [PMID: 16702549 DOI: 10.1073/pnas.0600644103]
87 **Tsurugizawa T**, Ciobanu L, Le Bihan D. Water diffusion in brain cortex closely tracks underlying neuronal activity. *Proc Natl Acad Sci USA* 2013; **110**: 11636-11641 [PMID: 23801756 DOI: 10.1073/pnas.1303178110]

P- Reviewer: Kilickesmez O, Lassandro F, Shen J, Theodorou K, Tirumani S **S- Editor**: Qiu S **L- Editor**: A **E- Editor**: Wu HL

World Journal of Radiology

Submit a Manuscript: http://www.wjgnet.com/esps/
Help Desk: http://www.wjgnet.com/esps/helpdesk.aspx
DOI: 10.4329/wjr.v8.i9.799

World J Radiol 2016 September 28; 8(9): 799-808
ISSN 1949-8470 (online)

MINIREVIEWS

Evaluation of DNA synthesis with carbon-11-labeled 4′-thiothymidine

Jun Toyohara

Jun Toyohara, Research Team for Neuroimaging, Tokyo Metropolitan Institute of Gerontology, Tokyo 173-0015, Japan

Author contributions: Toyohara J generated the figures and wrote the manuscript.

Supported by A Grant-in-Aid for Scientific Research from the Japan Society for the Promotion of Science, No. (B) 25293271.

Conflict-of-interest statement: The author declares that he has no competing interests.

Manuscript source: Invited manuscript

Correspondence to: Jun Toyohara, PhD, Theme Leader, Research Team for Neuroimaging, Tokyo Metropolitan Institute of Gerontology, 35-2 Sakae-cho, Itabashi-ku, Tokyo 173-0015, Japan. toyohara@pet.tmig.or.jp
Telephone: +81-3-39643210
Fax: +81-3-39641148

Received: February 25, 2016
Peer-review started: February 27, 2016
First decision: May 13, 2016
Revised: June 12, 2016
Accepted: July 29, 2016
Article in press: August 1, 2016
Published online: September 28, 2016

Abstract

In the cancer research field, the preferred method for evaluating the proliferative activity of cancer cells *in vivo* is to measure DNA synthesis rates. The cellular proliferation rate is one of the most important cancer characteristics, and represents the gold standard of pathological diagnosis. Positron emission tomography (PET) has been used to evaluate *in vivo* DNA synthetic activity through visualization of enhanced nucleoside metabolism. However, methods for the quantitative measurement of DNA synthesis rates have not been fully clarified. Several groups have been engaged in research on 4′-[methyl-^{11}C]-thiothymidine (^{11}C-4DST) in an effort to develop a PET tracer that allows quantitative measurement of *in vivo* DNA synthesis rates. This mini-review summarizes the results of recent studies of the *in vivo* measurement of cancer DNA synthesis rates using ^{11}C-4DST.

Key words: 4′-[methyl-^{11}C]-thiothymidine; DNA synthesis; Cell proliferation; Tumor; Positron emission tomography

Core tip: There is a continuous demand to measure *in situ* DNA synthesis rates in living human cancer. The thymidine derivative 4′-[methyl-^{11}C] thiothymidine (^{11}C-4DST) has the potential to visualize *in vivo* DNA synthesis rates with positron emission tomography (PET). To confirm whether ^{11}C-4DST is a valid DNA synthesis marker, clinical and basic research is being conducted at several PET centers in Japan, European Union, and the United States. This mini-review summarizes the progress of recent studies involving the *in vivo* imaging of cancer DNA synthesis using ^{11}C-4DST PET.

Toyohara J. Evaluation of DNA synthesis with carbon-11-labeled 4′-thiothymidine. *World J Radiol* 2016; 8(9): 799-808 Available from: URL: http://www.wjgnet.com/1949-8470/full/v8/i9/799.htm DOI: http://dx.doi.org/10.4329/wjr.v8.i9.799

INTRODUCTION

Rationale for DNA synthesis imaging

The basic principle of DNA synthesis measurement using positron emission tomography (PET) and the rationale for tracer development for DNA synthesis imaging were extensively reviewed by Bading *et al*[1], and Toyohara *et al*[2], respectively.

Briefly, thymidine is the only nucleoside that is exclusively incorporated into DNA. Therefore, DNA incorporation using [methyl-^{3}H]-thymidine is used as the gold standard for a cell proliferation marker. The challenge in visualizing *in vivo* DNA synthesis with ^{11}C-thymidine has been pursued since 1972[3]. Extensive developments in the 1990s and early 2000s realized the estimation of thymidine flux from blood to DNA in somatic and brain tumors[4-7]. From these studies, it became clear that the routine use of ^{11}C-thymidine has several limitations, including issues related to the use of radiolabeled catabolites, the short half-life of ^{11}C, and relatively difficult synthesis. While ^{11}C-thymidine is effectively incorporated into DNA, it is also rapidly catabolized by thymidine phosphorylase, which complicates image analysis. Thymidine is a substrate for mitochondrial thymidine kinase 2 as well as cytosolic thymidine kinase 1, which leads to the absence of cell proliferation related uptake in tissues with high mitochondria content, such as the heart. Therefore, the ideal tracer for DNA synthesis imaging requires resistance to catabolism by thymidine phosphorylase, selective phosphorylation by thymidine kinase 1, and ready incorporation into DNA (Figure 1).

4'-[methyl-^{11}C] thiothymidine

4′-[methyl-^{11}C] thiothymidine (^{11}C-4DST) is a derivative of thymidine in which the 4′-oxygen is replaced with sulfur and the 5-methyl group is radiolabeled with ^{11}C by the C-C cross-coupling reaction (Figure 2)[8,9]. The first synthesis conditions reported involved using 5-tributylstannyl-4′-thio-2′-deoxyuridine (precursor)/tris (dibenzylideneacetone) dipalladium (0) [$Pd_2(dba)_3$]/tri(*o*-tryl) phosphine [P(*o*-$CH_3C_6H_4)_3$] (1.5:1:3.9 in molar ratio) at 130 ℃ for 5 min in *N*,*N*-dimethylformamide (DMF), which gave the desired products at only 30% decay-corrected yields based on [^{11}C]CH_3I[9]. Subsequently, slight modifications of the conditions, using precursor/$Pd_2(dba)_3$/P(*o*-$CH_3C_6H_4)_3$/CuCl/K_2CO_3 (1.5:1:3.9:4:3.6) at 80 ℃, resulted in greatly improved decay-corrected yields (70%) based on [^{11}C]CH_3I[10]. Other reported conditions using precursor/$Pd_2(dba)_3$/P(*o*-$CH_3C_6H_4)_3$/CuCl/K_2CO_3 (25:1:32:2:5) at 80 ℃ also gave improved decay-corrected yields (42%-60%) using the two-pot method, and 65% by the one-pot method based on ^{11}C-CH_3I[11,12].

Preclinical evaluation indicated that the stability of ^{11}C-4DST within the body is higher than that of thymidine, and unlike 3′-deoxy-3′-[^{18}F]fluorothymidine (^{18}F-FLT), it is taken up into DNA as a substrate for DNA synthesis. Therefore, Toyohara *et al*[8,9] postulated that ^{11}C-4DST might be used as a valid *in vivo* DNA synthesis marker. ^{11}C-4DST was developed at the National Institute of Radiological Sciences (NIRS; Chiba, Japan) and has been approved for clinical use by the committee for medical use of cyclotron-produced radiopharmaceuticals of NIRS, as well as the medical use of cyclotron-produced radiopharmaceuticals and ethics committees of Tokyo Metropolitan Institute of Gerontology (TMIG; Tokyo, Japan). The first-in-human study was performed at TMIG in March 2010. ^{11}C-4DST was also described as ^{11}C-S-dThd[8,9], however, the names have since been unified to ^{11}C-4DST with the commencement of its clinical use[10].

INITIAL CLINICAL TRIAL

An initial clinical trial of ^{11}C-4DST, which was equivalent to a phase 1 trial, was performed according to guidelines approved in January 2008 by the institutional committee of TMIG for first-in-human use of novel radiopharmaceuticals. Briefly, five brain tumor patients volunteered to participate in a study of the side effects associated with administration of ^{11}C-4DST, which were assessed by clinical symptoms, physical findings, and blood tests. Concurrently, ^{11}C-4DST dynamic PET measurements were performed to assess the efficacy with which the desired function (DNA synthesis) can be measured. In addition, radiation dosimetry was estimated through whole-body PET measurement in three healthy volunteers.

The results of the initial clinical trial revealed no adverse events accompanying administration of ^{11}C-4-DST, and the effective dose was calculated as 4.2 μSv/MBq. Whole-body PET indicated ^{11}C-4DST accumulations in bone marrow and spleen, where DNA synthesis is active in the adult. These observations suggest that ^{11}C-4DST uptake reflects the dynamics of DNA synthesis activity (Figure 3). In addition, physiological accumulation of radioactivity was observed in the liver, kidney, and salivary glands, which are components of the metabolic excretion pathway. The levels of ^{11}C-4DST accumulation in the mediastinum, cerebral parenchyma, lungs, cardiac muscles, and skeletal muscles were very low.

The distribution of ^{11}C-4DST within the human body was different from that in rodents, and a high level of ^{11}C-4DST accumulation was observed in the human liver. This may have been due to species differences in ^{11}C-4DST metabolism; the metabolism of ^{11}C-4DST in humans is faster than that in rodents and produces hydrophilic metabolites. Treatment of the main component of the hydrophilic metabolites with β-glucuronidase results in the formation of ^{11}C-4DST. Therefore, the high level of ^{11}C-4DST accumulation in the human liver is due to conjugation of ^{11}C-4DST.

^{11}C-4DST is a nucleoside derivative and therefore does not readily pass through the blood-brain barrier. Thus, accumulation of radioactivity in normal brain is low. However, the majority of brain tumor lesions could be imaged, and the accumulation of ^{11}C-4DST in brain

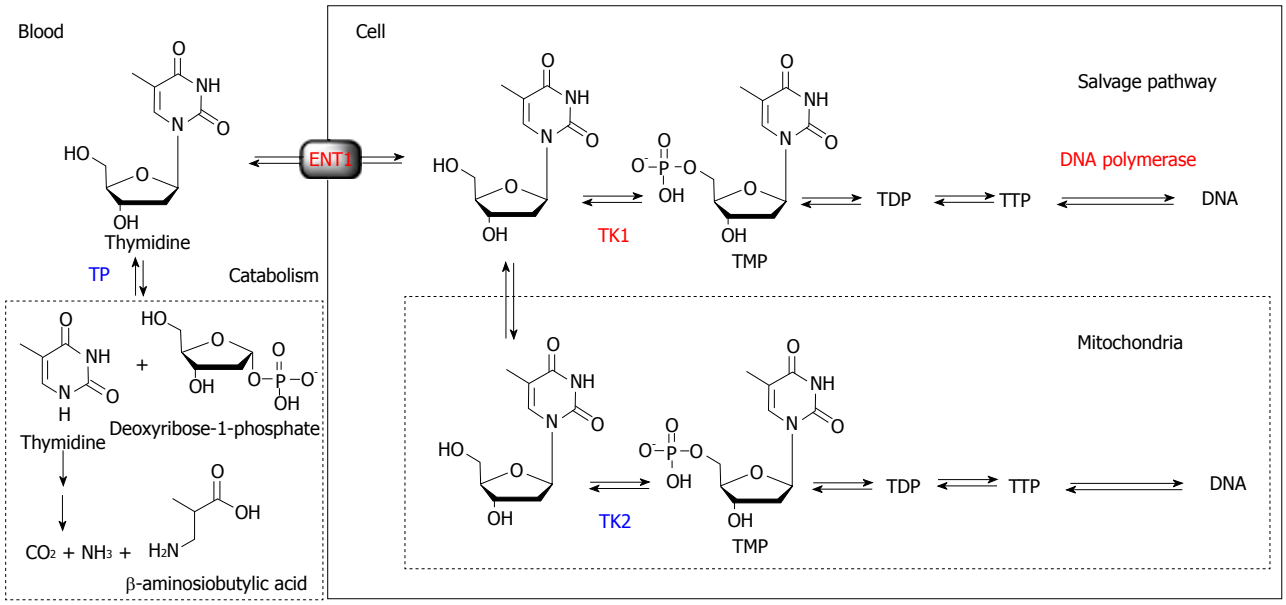

Figure 1 Rationale for designing an ideal DNA synthesis tracer for cell proliferation imaging. The ideal tracer must block catabolism by thymidine phosphorylase, while retaining anabolism by the salvage pathway. ENT1: Equilibrative nucleoside transporter 1; TDP: Thymidine di-phosphate; TMP: Thymidine monophosphate; TTP: Thymidine tri-phosphate; TK1: Thymidine kinase 1; TK2: Thymidine kinase 2; TP: Thymidine phosphorylase.

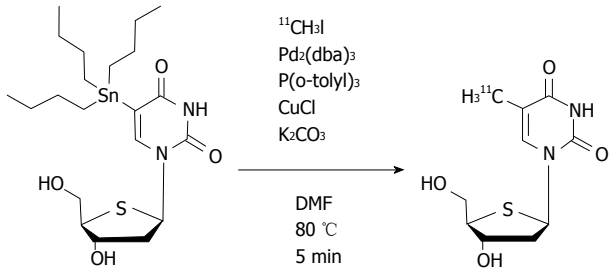

Figure 2 Radiosynthesis of 4'-[methyl-^{11}C]-thiothymidine. The imaging agent ^{11}C-4DST was synthesized by methylation of 5-tributylstannyl-4'-thio-2'-deoxyuridine *via* a palladium-mediated Stille cross-coupling reaction with ^{11}C-methyl iodide. ^{11}C-4DST: 4'-[methyl-^{11}C]-thiothymidine; DMF: N,N-Dimethylformamide; $P(o\text{-}tolyl)_3$: Tri(o-tryl)phosphine; $Pd_2(dba)_3$: Tris(dibenzylide neacetone)dipalladium(0).

tumor lesions varied depending on the treatment conditions. In some cases, the accumulation of ^{11}C-4DST was clearly different from ^{11}C-methionine (^{11}C-MET) images acquired at the same time. The images in Figure 4A shows a case that was resistant to the anticancer agent temozolomide, while the Figure 4B shows a case that was responsive to temozolomide. As can be seen in this figure, ^{11}C-4DST sensitively captures the responsiveness of the tumor cells toward radiotherapy or chemotherapy.

KINETIC ANALYSIS

Time-activity curves (TACs) of ^{11}C-4DST accumulation in brain tumors indicated irreversible kinetics, suggesting that ^{11}C-4DST might be metabolically trapped. In addition, Patlak graph analysis showed a linear plot, which supports the above suggestion[8,9]. The results of the preliminary kinetic analysis indicated that ^{11}C-4DST was irreversibly taken up into the DNA because ^{11}C-4DST fits the two-tissue three-compartment model, and k_4 is negligibly small. The value of k_3 (k_4 = 0) obtained by the analysis showed a strong correlation with K_i (k_4 = 0), which reflects the rate of ^{11}C-4DST incorporation flux (Pearson's r = 0.925, P = 0.001), and no correlation was observed with K_1 (k_4 = 0), which reflects intracellular transport. In addition, the standardized uptake value (SUV) showed the best correlation with K_i (Patlak) and also showed good correlations with K_i (k_4 = 0) and k_3 (k_4 = 0) (Pearson's r = 0.942, P = 0.0005; r = 0.857, P = 0.0065, respectively). The above results suggest that images of DNA synthesis might be obtained through non-quantitative analysis using SUV images.

In addition, we performed a basic validation study of ^{11}C-4DST accumulation kinetics into the DNA. The time course of the DNA uptake ratio in proliferating tissues in rats was illustrated by a Michaelis-Menten-type hyperbolic curve, and 50% of the radioactivity was taken into DNA at 5 and 8 min after administration in the duodenum and spleen, with maximum uptake ratios of 99% and 94%, respectively. The TACs of these tissues as a whole were almost identical to the TACs of DNA incorporated radioactivity (DNA fraction) and were different from the soluble non-DNA fraction (unchanged form + phosphorylated form) (Figure 5). On the other hand, in the AH109A rat liver cancer transplantation model, significant variation in DNA uptake rates between sampling sites was due to heterogeneity in the tumor tissues, with some regions exhibiting 60% DNA uptake at 1 min after administration (where cell proliferation is active). The above results indicate that the process of DNA uptake is the rate-limiting step in ^{11}C-4DST accumulation.

Furthermore, Plotnik *et al*[13] evaluated the kinetics of ^{3}H-4DST transport and metabolism in the human

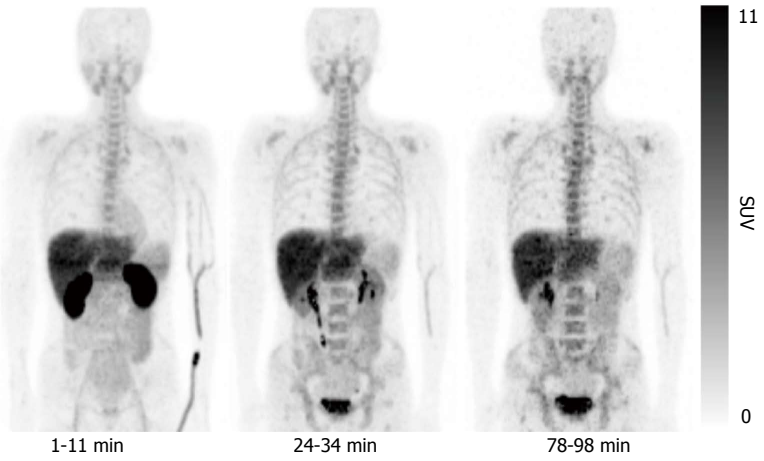

Figure 3 Representative whole-body decay-corrected maximum intensity-projection images of 4'-[methyl-^{11}C]-thiothymidine positron emission tomography images. ^{11}C-4DST showed high uptake in the excretory organs, such as the kidneys, liver, and urinary bladder. Moderate uptake was observed in the proliferative organs, such as bone marrow, spleen, and small intestine. The lowest uptake was observed in the non-proliferating tissues, such as muscle and lungs. This research was originally published in JNM[10]. ^{11}C-4DST: 4'-[methyl-^{11}C]-thiothymidine; SUV: Standardized uptake value.

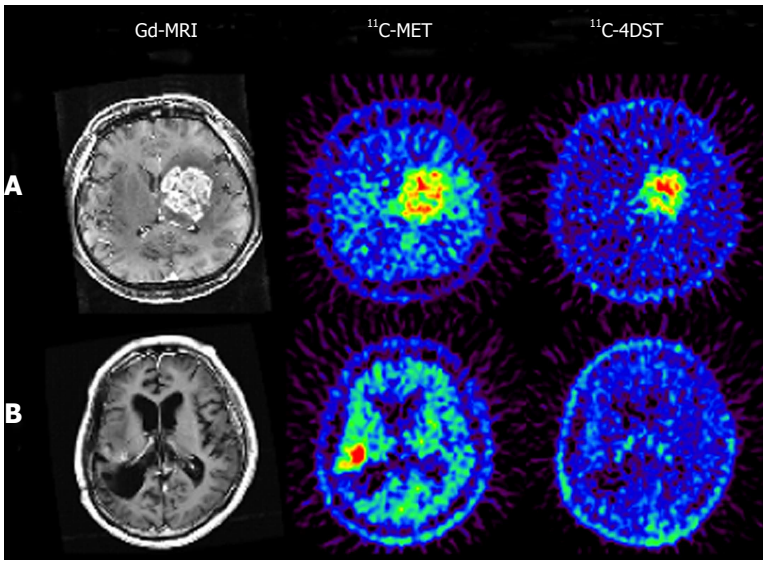

Figure 4 Brain tumor imaging in temozolomide-resistant (A) and -responsive (B) patients. DNA synthesis images provide completely different information from those obtained with an amino acid transport agent. In the case of recurrent anaplastic oligodendroglioma (A), both ^{11}C-MET and ^{11}C-4DST showed high uptake in the gadolinium-enhanced region of the MRI. However, the distribution pattern of each tracer in the tumor region was not identical. The tumor in this patient showed progressive enlargement despite continuous treatment with the DNA alkylating agent temozolomide. In the case of recurrent anaplastic astrocytoma (B), the patient received one course of treatment with temozolomide 3 d before PET examinations, and it was found that the ^{11}C-4DST uptake was negligible in the gadolinium-enhanced region where high uptake of ^{11}C-MET was observed. The enhanced tumor mass in this patient remained unchanged over 6 mo after commencement of temozolomide treatment. These observations suggest that DNA synthesis in the tumor was suspended by temozolomide treatment. Reprinted from Nariai *et al*[14], with the permission of Springer. ^{11}C-4DST: 4'-[methyl-^{11}C]-thiothymidine; ^{11}C-MET: ^{11}C-Methionine; Gd-MRI: Gadolinium-enhanced magnetic resonance image; PET: Positron emission tomography.

adenocarcinoma cell line A549 under exponential-growth conditions. ^{3}H-4DST behaved qualitatively similar to endogenous thymidine in terms of equilibrative nucleoside transporter dependent cellular transport, shapes of cellular uptake curves, and relative DNA incorporation levels. As 4DST closely mimics thymidine metabolism, ^{11}C-4DST should provide a robust measurement of DNA synthesis. However, overall ^{3}H-4DST metabolism was significantly lower than that of thymidine, which may reflect its lower affinity toward thymidine kinase 1. This slower metabolism might limit its usefulness because of the relatively short half-life of the ^{11}C label, especially in the case of slow-growing tumors like prostate cancer.

CLINICAL STUDY IN VARIOUS TUMOR TYPES

Although the presence of metabolites in blood was not desirable in terms of quantitative measurement, the results of the ^{11}C-4DST early clinical trials indicated that its usability exceeded the drawbacks. In addition, as

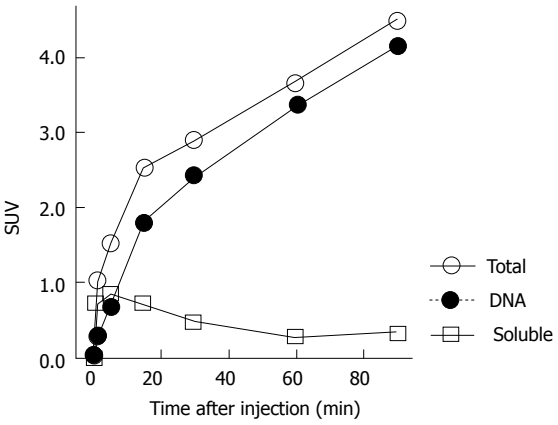

Figure 5 Time courses of 4'-[methyl-^{11}C]-thiothymidine activity in the mouse duodenum. The data is presented as the SUVmean in the indicated fractions (n = 3-5). Rapid DNA separation was performed using the DNAzol reagent[30]. The increase in total tissue radioactivity paralleled that of DNA incorporated radioactivity. The soluble fraction (4DST itself, phosphorylated 4DST, and other metabolites) was low and stable at 30 min after tracer injection. The contribution of the DNA incorporation process overshadows both the phosphorylation and dephosphorylation rates at later phases of the PET scan. PET: Positron emission tomography; SUV: Standardized uptake value.

high usability of ^{11}C-4DST was expected from the basic data obtained in animal experiments[8,9], collaborative research was initiated with the National Center for Global Health and Medicine (NCGM; Tokyo, Japan) and Kagawa University (Kagawa, Japan). In this collaborative research, technology transfer of radiosynthesis was first performed and then an application was submitted to the ethics committee. The clinical trial was started at approximately the same time as the early clinical trial performed at TMIG. A study to fundamentally support the clinical data is also being conducted in collaboration with the University of Groningen Medical Center (UMCG; Groningen, The Netherlands) and the University of Washington (Seattle, WA).

BRAIN TUMORS

Initial clinical studies of ^{11}C-4DST in brain tumors were performed at TMIG[14]. Fourteen patients with brain tumors (11 malignant gliomas, 2 metastatic tumors, 1 craniopharyngioma, and 1 malignant lymphoma) were included and the uptake of ^{11}C-4DST and ^{11}C-MET into gadolinium-enhanced lesions on T1 weighted magnetic resonance image (MRI) was evaluated. In this study, Nariai *et al*[14] observed a unique characteristic of ^{11}C-4DST in one case. They observed a marked decrease of ^{11}C-4DST uptake into metastatic lung cancer 5 d after gamma knife therapy. Although ring form enhancement with cystic formation did not disappear completely, tumor growth ceased with this treatment and the patient has maintained favorable activity of daily living 1 year after treatment (Figure 6). In another case, ^{11}C-4DST could differentiate oligodendroglioma from malignant transformation (Figure 7). However, ^{11}C-MET showed increased uptake, which indicates malignant transformation. An increased microvessel surface of

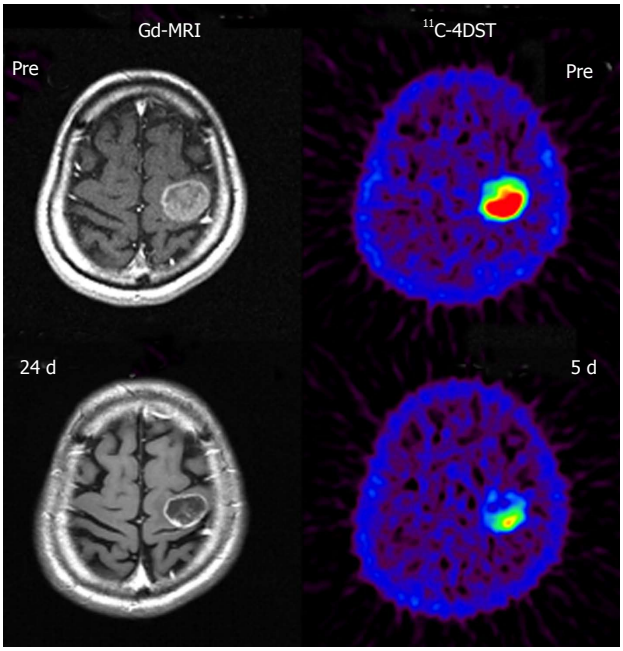

Figure 6 Early evaluation of the effectiveness of radiosurgery with 4'-[methyl-^{11}C]-thiothymidine positron emission tomography. A marked decrease in ^{11}C-4DST uptake into metastatic lung cancer was observed 5 d after gamma knife radiosurgery. Although ring form enhancement with cystic formation did not disappear completely, tumor growth was halted by this treatment and the patient has maintained favorable activity of daily living 1 year after treatment. These observations indicated that the effectiveness of gamma knife therapy was correctly monitored by ^{11}C-4DST only 5 d after treatment. Reprinted from Nariai *et al*[14], with the permission of Springer. ^{11}C-4DST: 4'-[methyl-^{11}C]-thiothymidine; Gd-MRI: Gadolinium-enhanced magnetic resonance image.

oligodendroglioma causes the increased uptake of ^{11}C-MET despite low proliferation of the tumor cells. This case study suggests that ^{11}C-4DST accumulates in growing tumors but not in tumors stabilized by treatment. ^{11}C-4DST uptake into tumors was not influenced by increased transport from blood to tissue, as observed for ^{11}C-MET.

Further in-depth research of ^{11}C-4DST in brain tumors was conducted at Kagawa University. Toyota *et al*[15] directly compared ^{11}C-4DST and ^{18}F-FLT in the same subjects. Twenty patients with primary (n = 9) and recurrent (n = 11) gliomas underwent ^{11}C-4DST and ^{18}F-FLT PET/CT scans. In the normal brain, ^{11}C-4DST uptake was significantly higher than ^{18}F-FLT (SUVmean; 0.34 ± 0.06 *vs* 0.19 ± 0.04, P < 0.001 by paired t-test). Individual ^{11}C-4DST SUVmax in the tumor was very similar to ^{18}F-FLT. Therefore, the average tumor-to-normal tissue uptake (T/N) ratio of ^{18}F-FLT in the tumor was significantly higher than that of ^{11}C-4DST (10.55 ± 5.45 *vs* 5.96 ± 3.86, P < 0.001 by paired t test), resulting in better tumor visualization with ^{18}F-FLT. Both of these tracers did not show significant differences in T/N ratio among different glioma grades. Linear regression analysis showed a significant correlation between proliferative activity indicated by the Ki-67 labeling index and the T/N ratios of ^{11}C-4DST (r = 0.50, P < 0.05) and ^{18}F-FLT (r = 0.55,

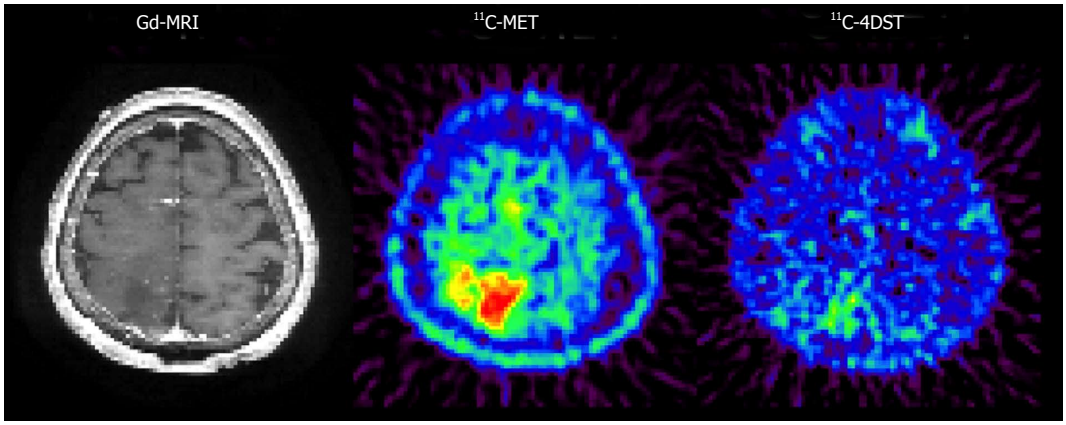

Figure 7 4'-[methyl-^{11}C]-thiothymidine uptake in oligodendroglioma. A patient was diagnosed with grade 2 astrocytoma during the initial operation. At the 1-year follow-up, an enhanced lesion appeared on MRI and ^{11}C-MET uptake increased around the initially resected lesion. These findings suggested that the malignant transformation of astrocytoma occurred. However, ^{11}C-4DST uptake into the tumor was not different from basal brain levels. The pathological diagnosis at the second operation was grade 2 oligodendrocytoma with a newly appearing oligodendroglioma component, but without malignant transformation. Reprinted from Nariai *et al*[14], with the permission of Springer. ^{11}C-4DST: 4'-[methyl-^{11}C]-thiothymidine; ^{11}C-MET: ^{11}C-Methionine; Gd-MRI: Gadolinium-enhanced magnetic resonance image.

$P < 0.05$). A highly significant correlation was observed between the individual T/N ratios of ^{11}C-4DST and ^{18}F-FLT ($r = 0.79$, $P = 0.0001$). These results indicate that the uptake pattern and uptake values of ^{11}C-4DST in gliomas are similar to those of ^{18}F-FLT. Two exceptions were observed, one non-enhanced primary diffuse astrocytoma and one recurrent glioblastoma with an oligodendroglioma component, in which only ^{18}F-FLT could detect the tumor well, with ^{11}C-4DST showing no and faint uptake in the tumor, respectively.

In a follow-up study, Tanaka *et al*[16] retrospectively evaluated ^{11}C-4DST uptake in 23 patients with newly diagnosed gliomas, and correlated the results with the Ki-67 index and tumor grade in comparison with ^{11}C-MET[16]. ^{11}C-4DST PET/CT showed a slightly lower detection rate for gliomas than ^{11}C-MET (87% *vs* 96%); however, the difference was not statistically significant. The tracer uptake for normal brain tissue of ^{11}C-4DST was significantly lower than that of ^{11}C-MET (0.48 ± 0.19 *vs* 1.52 ± 0.36, $P < 0.001$). The tracer uptake of ^{11}C-4DST in the tumor was also significantly lower than that of ^{11}C-MET (2.14 ± 1.58 *vs* 5.39 ± 2.22, $P < 0.001$). Therefore, no significant difference in T/N ratio or metabolic tumor volume (MTV: volume with a threshold of 40% of SUVmax) was observed between ^{11}C-4DST and ^{11}C-MET. A weak correlation was observed between ^{11}C-4DST and Ki-67 index for SUVmax ($r = 0.46$, $P < 0.03$), for T/N ratio ($r = 0.43$, $P < 0.05$), and for MTV ($r = 0.68$, $P < 0.001$) and between ^{11}C-MET MTV and Ki-67 index ($r = 0.43$, $P < 0.04$). Among them, the correlation coefficient between ^{11}C-4DST MTV and Ki-67 index was the highest. There was a significant difference in SUVmax of ^{11}C-4DST between grades Ⅱ and Ⅳ ($P < 0.03$) and in MTV between grades Ⅱ and Ⅳ ($P < 0.0009$) and grades Ⅲ and Ⅳ ($P < 0.02$).

HEAD AND NECK CANCER

Ito *et al*[17] prospectively compared the diagnostic value of ^{11}C-4DST PET/CT and ^{18}F-FDG PET/CT in patients with head and neck squamous cell carcinoma (HNSCC)[17]. Thirty-eight patients with advanced HNSCC underwent ^{11}C-4DST PET/CT and ^{18}F-FDG PET/CT before treatment. All patients were followed for 13.5 ± 7.5 mo to monitor recurrence. The total lesion glycolysis (TLG) for ^{18}F-FDG and total lesion proliferation (TLP) for ^{11}C-4DST were used as outcome measures of the combination of functional information and volumetric data to predict patient prognosis[18-21]. Nine of the 38 patients with post-treatment recurrence were identified. Receiver operating characteristic curves for $TLG_{3.0}$ (sensitivity: 89%; specificity: 72%) and $TLP_{2.5}$ (sensitivity: 89%; specificity: 55%) showed the highest prognostic ability for recurrence. There was no significant correlation between the Ki-67 index and whether ^{18}F-FDG SUVmax ($P = 0.81$) or ^{11}C-4DST SUVmax ($P = 0.49$) was observed in the primary tumor. One possible reason for this finding may be that the Ki-67 index was obtained mainly from biopsy specimens, not from resected specimens.

LUNG CANCER

At NCGM, the first study focused mainly on lung cancer cases[22]. The subjects were 18 primary lung cancer patients (19 lesions) who underwent segmental resection and lymph node dissection. ^{18}F-FDG PET/CT and ^{11}C-4DST PET/CT were performed in these patients during the same period and SUVmax was measured at the lesioned region in each patient. The results and histopathological evaluation (*e.g.*, Ki-67 index) were compared. The observed histological types included 16 adenocarcinomas (including bronchioloalveolar carcinoma), 2 squamous cell carcinomas, and 1 large cell carcinoma, and the average tumor size was 27.2 mm. The average levels of SUVmax in the primary tumors were 2.9 ± 1.0 and 6.2 ± 4.5 for ^{11}C-4DST and ^{18}F-FDG, respectively; SUVmax of ^{11}C-4DST was

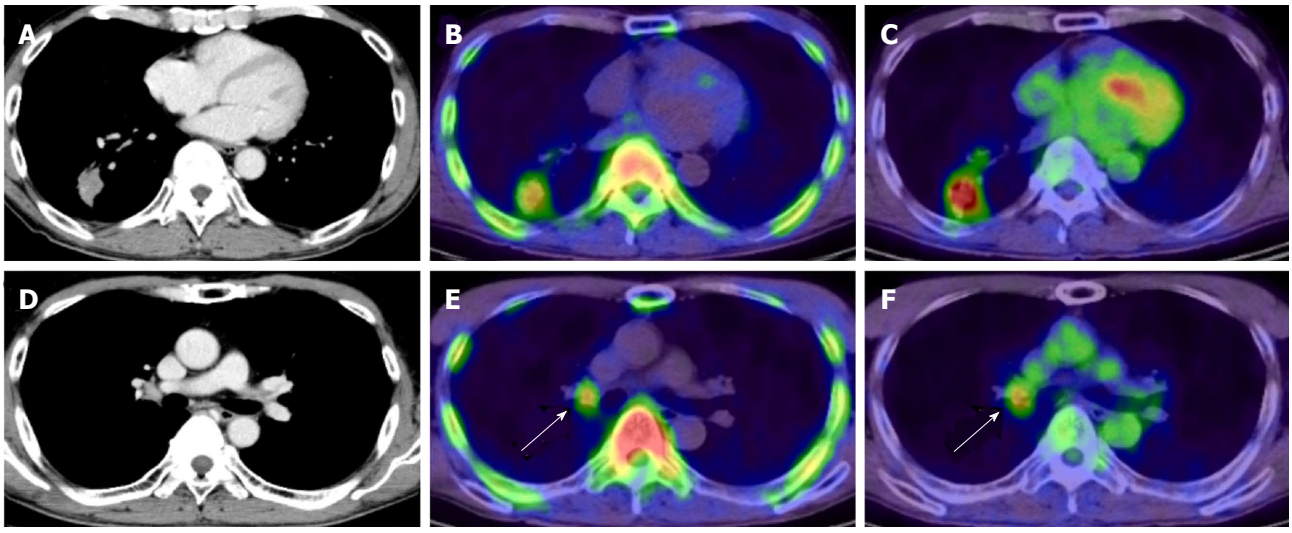

Figure 8 4'-[methyl-^{11}C]-thiothymidine images in non-small cell lung cancer. Axial images of CT (A), ^{11}C-4DST PET (B), and ^{18}F-FDG PET (C) in a 58-year-old man with lung adenocarcinoma in the right lower lobe. Radioactivity of ^{11}C-4DST in the ascending aorta (representing blood pool) is lower than that of ^{18}F-FDG. Both ^{11}C-4DST and ^{18}F-FDG clearly visualize lung lesions. Right hilar lymph node metastasis is confirmed on CT (D), and uptake of both ^{11}C-4DST PET (E) and ^{18}F-FDG PET (F) identifies the lesion (arrow). However, ^{11}C-4DST images are clearer than ^{18}F-FDG images because of low physiologic ^{11}C-4DST in the mediastinum (blood pool). This research was originally published in JNM[22]. ^{11}C-4DST: 4'-[methyl-^{11}C]-thiothymidine; PET: Positron emission tomography; ^{18}F-FDG: 2-Deoxy-2-[^{18}F]fluoro-D-glucose; CT: Computed tomography.

approximately half that of ^{18}F-FDG. Figure 8 shows representative images of ^{11}C-4DST in patients with lung adenocarcinoma. ^{11}C-4DST clearly visualized hilar lymph node metastasis because of low physiologic accumulation in the mediastinum blood pool. The correlation coefficients between SUVmax and Ki-67 index were 0.81 and 0.71 for ^{11}C-4DST and ^{18}F-FDG, respectively, and that of ^{11}C-4DST was significantly higher. ^{11}C-4DST appears to be effective as a PET tracer in primary lung cancer indicating DNA synthetic activity (cell proliferation activity).

The diagnostic ability of ^{11}C-4DST for detecting regional lymph node metastasis of non-small cell lung cancer (NSCLC) was prospectively evaluated by the same group (NCGM)[23]. A total of 31 patients with NSCLC underwent ^{11}C-4DST PET/CT and ^{18}F-FDG PET/CT. Patients were followed for up to 2 years to assess disease-free survival. A total of 123 nodal groups were defined for 27 patients, with proven malignancy in 17 nodal groups of 9 patients. The sensitivity on a per-node basis was significantly higher with ^{11}C-4DST than with ^{18}F-FDG (82.5% *vs* 29.4%, $P < 0.002$). In contrast, the specificity on a per-node basis was significantly lower with ^{11}C-4DST than with ^{18}F-FDG (71.7% *vs* 85.8%, $P < 0.02$). The disease-free survival rate with positive ^{11}C-4DST uptake in nodal lesions was 0.35, which was considerably lower than the rate of 0.83 with negative findings ($P = 0.04$). Interestingly, nodal staging by ^{11}C-4DST was the most influential prognostic factor ($P = 0.05$) among the factors tested. The high sensitivity of ^{11}C-4DST for nodal metastasis indicates that it may be efficient in detecting lymph node micrometastasis.

MULTIPLE MYELOMA

In whole-body imaging diagnosis of multiple myeloma (MM), it was demonstrated that myeloma has various characteristics that become prominent at different stages, including energy metabolism (^{18}F-FDG), production of M protein (^{11}C-MET), and cell proliferation (^{11}C-4DST). We hope to be able to accurately determine the periods where follow-up observation is sufficient and aggressive chemotherapy is necessary, to optimize treatment in such cases. Okasaki *et al*[24] prospectively evaluated the possibility of ^{11}C-MET and ^{11}C-4DST whole-body PET/CT when searching for bone marrow involvement in patients with MM, in comparison with those for ^{18}F-FDG PET/CT and aspiration cytology[24]. A total of 64 patients with MM or monoclonal gammopathy of undetermined significance (MUGS) underwent three whole-body PET/CT scans with ^{18}F-FDG, ^{11}C-MET, and ^{11}C-4DST within a period of 1 wk. The tracer accumulation was evaluated as positive, equivocal, or negative for 55 lytic lesions visualized using CT in 24 patients. To verify tracer uptake by lesions, 36 patients underwent bone aspiration cytology within 1 wk of the three PET/CT scans. The SUVmax of ^{11}C-4DST in lytic lesions were highest among the three tracers. ^{11}C-4DST and ^{11}C-MET provided clearer findings than ^{18}F-FDG for lytic lesions. A typical MM patient with multiple active lesions is shown in Figure 9. ^{11}C-MET and ^{11}C-4DST detected positive lesions, whereas ^{18}F-FDG detected an equivocal lesion. ^{18}F-FDG was rarely able to detect skull lesions because of the high physiological accumulation in the brain, whereas ^{11}C-MET and ^{11}C-4DST were capable of clearly detecting skull lesions because of their low accumulation in the brain. Furthermore, ^{11}C-4DST and ^{11}C-MET had higher diagnostic accuracies than that of ^{18}F-FDG, when compared with iliac crest biopsy. However, no significant difference was observed between the ^{11}C-MET and ^{11}C-4DST findings.

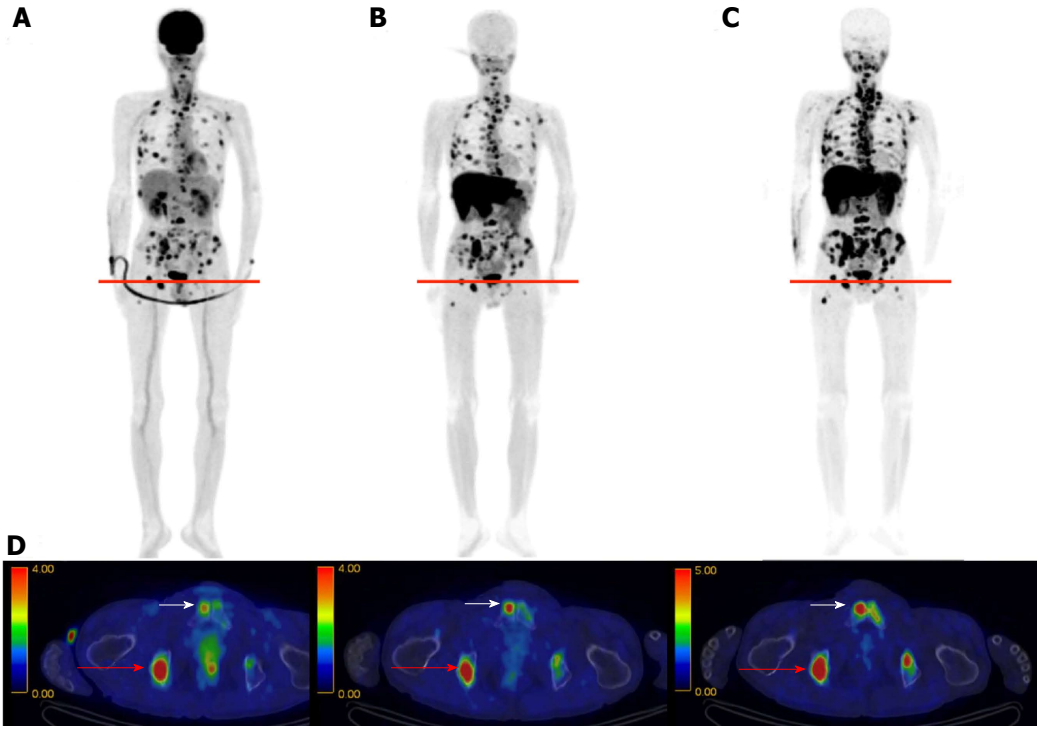

Figure 9 4'-[methyl-^{11}C]-thiothymidine images in multiple myeloma. ^{18}F-FDG (A), ^{11}C-MET (B), and ^{11}C-4DST (C) PET images obtained in a 63-year-old man with multiple myeloma. Numerous active lesions are visible in the three maximum intensity projection images. The fusion images are for the cross-section at the level indicated by the red lines (D). The lesion in the right ischium (red arrow) was positive in all three PET scans. However, the lesion in the right pubis (white arrow) was only positive on the ^{11}C-MET and ^{11}C-4DST PET scans and was equivocal on the ^{18}F-FDG PET scan. Reprinted from Okasaki *et al*[24], with the permission of Springer. ^{11}C-4DST: 4'-[methyl-^{11}C]-thiothymidine; ^{11}C-MET: ^{11}C-Methionine; ^{18}F-FDG: 2-Deoxy-2-[^{18}F]fluoro-D-glucose; PET: Positron emission tomography.

RENAL CELL CANCER

Minamimoto *et al*[25] evaluated the potential of ^{11}C-4DST PET/CT for imaging cellular proliferation in advanced clear cell renal cell cancer (RCC), compared with ^{18}F-FDG PET/CT[25]. Five patients with a single RCC lesion were examined. The typical tumor accumulation pattern of ^{18}F-FDG was diffuse or with a thick uptake layer, in contrast to outer surface-dominant uptake with ^{11}C-4DST (Figure 10). The SUVmax of ^{11}C-4DST (7.3 ± 12.2) was slightly higher than that of ^{18}F-FDG (6.0 ± 12.8). The correlation between SUVmax and Ki-67 index was higher with ^{11}C-4DST (r = 0.61) than with ^{18}F-FDG (r = 0.43). Tumor uptake of both tracers was correlated with the Fuhrman nuclear grading system. Interestingly, the ^{11}C-4DST uptake increased as the degree of pathological phosphorylation of mammalian target of rapamycin (pmTOR) increased. This might indicate that ^{11}C-4DST has potential for use in evaluating the therapeutic effect of mTOR inhibitors in patients with RCC.

4DST IN BASIC RESEARCH

In cancer, differential diagnosis of benign *vs* malignant lesions is important. Toyohara *et al*[26] investigated whether 4DST is useful for differentially diagnosing tumors and inflammation in animal models[26]. C6 glioma cells were transplanted into the right shoulder of Wistar rats, and turpentine was injected into the left hind leg 9 d later to create a tumor and acute inflammation model. Dynamic ^{11}C-4DST PET scan was performed one day after turpentine injection. The biodistribution of ^{11}C-4DST was determined and compared with those of ^{18}F-FLT, ^{18}F-FDG, ^{11}C-choline, ^{11}C-MET, and two sigma receptor ligands 1-4-2'-^{18}F-fluoroethoxy-3-methoxyphenethyl-4-3-4-fluorophenyl-propyl-piperazine (^{18}F-FE-SA5845) and 1-3,4-^{11}C-dimethoxyphenylethyl-4-3-phenylpropyl-piperazine (^{11}C-SA4503). The results showed that ^{11}C-4DST had the highest tumor uptake among the tracers examined (SUV = 4.9), and the tumor muscle ratio was 13, which is equivalent to that of ^{18}F-FDG. ^{11}C-4DST showed an extremely high tumor inflammation ratio of 49, which was comparable to that of ^{18}F-FE-SA5845, and was more than 10-fold higher than that of ^{18}F-FDG. ^{11}C-4DST showed a persistent increase in accumulation in the tumor and bone marrow. On the other hand, it was not retained in inflammatory tissues, and returned to the same level as in muscles 40 min after injection. As indicated here, ^{11}C-4DST is a useful PET tracer with high sensitivity and specificity, with completely different dynamics in tumors and inflammatory tissue. The above results strongly suggest that ^{11}C-4DST will be effective in clinical settings.

In a follow-up study, Toyohara *et al*[27] evaluated longitudinal changes in ^{11}C-4DST uptake in turpentine-induced acute, subacute, and chronic phases of inflammatory tissues[27]. They found that ^{11}C-4DST uptake in inflammatory tissue was transiently increased during the subacute phase and subsequently decreased to normal levels. The transient increase in ^{11}C-4DST

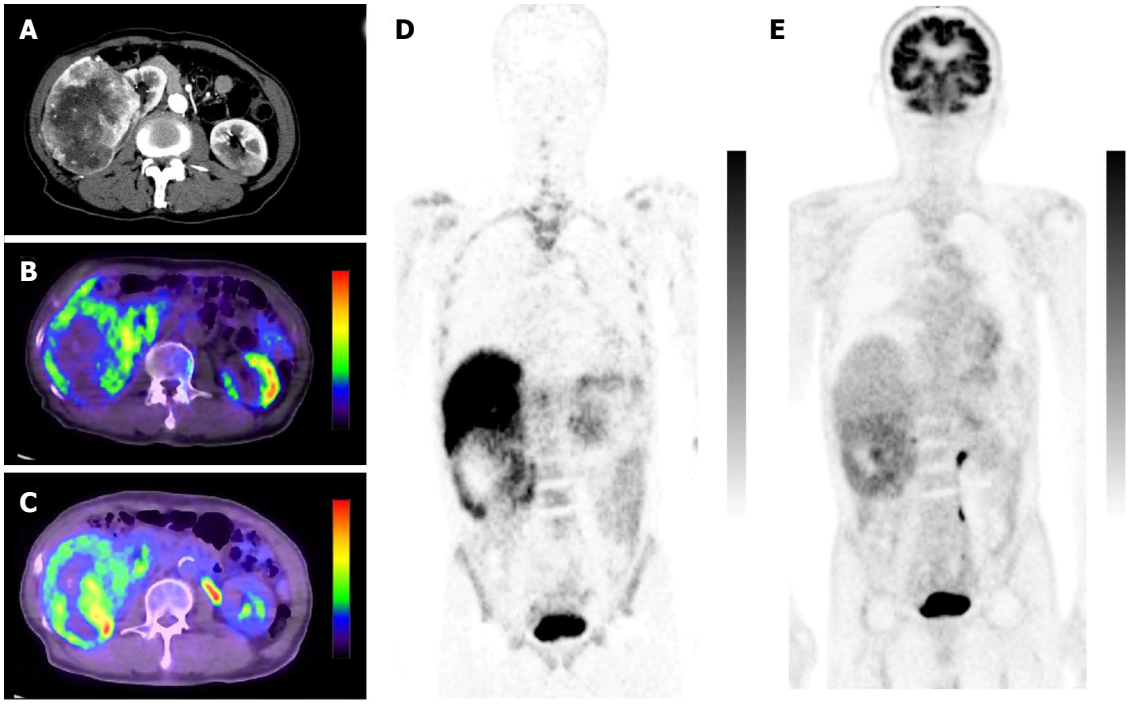

Figure 10 4'-[methyl-^{11}C]-thiothymidine images in clear cell renal carcinoma. A 78-year-old male with a clear cell renal carcinoma (RCC) in the right kidney. Contrast-enhanced abdominal CT (A), fused ^{11}C-4DST PET/CT (axial image) (B), fused ^{18}F-FDG PET/CT (axial image) (C), coronal ^{11}C-4DST PET (D), and coronal ^{18}F-FDG PET (E) images are shown. The uptake of ^{11}C-4DST was predominantly near the outer surface of the RCC tumor; the uptake of ^{18}F-FDG was more diffuse. Reprinted from Minamimoto *et al*[25], with the permission of Springer. ^{11}C-4DST: 4'-[methyl-^{11}C]-thiothymidine; ^{18}F-FDG: 2-Deoxy-2-[^{18}F]fluoro-D-glucose; PET: Positron emission tomography; CT: Computed tomography.

uptake paralleled changes in the Ki-67 labeling index in inflammatory tissues. These data indicate that avoiding the subacute phase is required for proper evaluation of tumor responses using ^{11}C-4DST PET.

Tsuji *et al*[28] established a clinically relevant mouse model of mesothelioma[28] and applied ^{11}C-4DST as a tool to differentiate histological subtypes. In their mouse model, ^{11}C-4DST was suitable for imaging the epithelioid subtype, while ^{18}F-FDG was more suitable for the sarcomatoid subtype.

Hasegawa *et al*[29] evaluated radiation induced carcinogenesis and its suppression by ^{11}C-4DST PET in a radiation-induced thymic lymphoma model[29]. They found initial higher ^{11}C-4DST uptake in irradiated thymus at 1 wk after fractionated whole-body X-ray irradiation. The increased ^{11}C-4DST uptake in the thymus was completely abolished by bone marrow transplantation. This study demonstrates the feasibility of cellular proliferation imaging with ^{11}C-4DST for the noninvasive monitoring of tumorigenic processes in animal models of radiation-induced cancer.

CONCLUSION

^{11}C-4DST is a newly developed PET tracer that can be used to image DNA synthesis, and its application in clinical settings is being studied at several facilities. In the future, ^{11}C-4DST will be applied to more types of cancer, which will further establish the significance of ^{11}C-4DST PET diagnoses through the accumulation of data on the physiological accumulation in lesions.

ACKNOWLEDGMENTS

The author thanks Mr. Kunpei Hayashi for the production of ^{11}C-4DST. Figures 4, 6 and 7 were reprinted from Nariai *et al*[14], with the permission of Springer. Figures 3 and 8 were reprinted from Toyohara *et al*[10] and Minamimoto *et al*[22], respectively, with the permission of the Society of Nuclear Medicine and Molecular Imaging, Inc. Figures 9 and 10 were reprinted from Okasaki *et al*[24] and Minamimoto *et al*[25], respectively, with the permission of Springer.

REFERENCES

1 **Bading JR**, Shields AF. Imaging of cell proliferation: status and prospects. *J Nucl Med* 2008; **49** Suppl 2: 64S-80S [PMID: 18523066 DOI: 10.2967/jnumed.107.046391]

2 **Toyohara J**, Fujibayashi Y. Trends in nucleoside tracers for PET imaging of cell proliferation. *Nucl Med Biol* 2003; **30**: 681-685 [PMID: 14499325 DOI: 10.1016/S0969-8051(03)00084-2]

3 **Christman D**, Crawford EJ, Friedkin M, Wolf AP. Detection of DNA synthesis in intact organisms with positron-emitting (methyl-11 C)thymidine. *Proc Natl Acad Sci USA* 1972; **69**: 988-992 [PMID: 4554538 DOI: 10.1073/pnas.69.4.988]

4 **Mankoff DA**, Shields AF, Graham MM, Link JM, Eary JF, Krohn KA. Kinetic analysis of 2-[carbon-11]thymidine PET imaging studies: compartmental model and mathematical analysis. *J Nucl Med* 1998; **39**: 1043-1055 [PMID: 9627342]

5 **Mankoff DA**, Shields AF, Link JM, Graham MM, Muzi M, Peterson LM, Eary JF, Krohn KA. Kinetic analysis of 2-[11C]thymidine PET imaging studies: validation studies. *J Nucl Med* 1999; **40**: 614-624

[PMID: 10210220]
6 **Wells JM**, Mankoff DA, Eary JF, Spence AM, Muzi M, O'Sullivan F, Vernon CB, Link JM, Krohn KA. Kinetic analysis of 2-[11C]thymidine PET imaging studies of malignant brain tumors: preliminary patient results. *Mol Imaging* 2002; **1**: 145-150 [PMID: 12920852 DOI: 10.1162/153535002760235445]
7 **Wells JM**, Mankoff DA, Muzi M, O'Sullivan F, Eary JF, Spence AM, Krohn KA. Kinetic analysis of 2-[11C]thymidine PET imaging studies of malignant brain tumors: compartmental model investigation and mathematical analysis. *Mol Imaging* 2002; **1**: 151-159 [PMID: 12920853 DOI: 10.1162/153535002760235454]
8 **Toyohara J**, Kumata K, Fukushi K, Irie T, Suzuki K. Evaluation of 4'-[methyl-14C]thiothymidine for in vivo DNA synthesis imaging. *J Nucl Med* 2006; **47**: 1717-1722 [PMID: 17015909]
9 **Toyohara J**, Okada M, Toramatsu C, Suzuki K, Irie T. Feasibility studies of 4'-[methyl-(11)C]thiothymidine as a tumor proliferation imaging agent in mice. *Nucl Med Biol* 2008; **35**: 67-74 [PMID: 18158945 DOI: 10.1016/j.nucmedbio.2007.10.001]
10 **Toyohara J**, Nariai T, Sakata M, Oda K, Ishii K, Kawabe T, Irie T, Saga T, Kubota K, Ishiwata K. Whole-body distribution and brain tumor imaging with (11)C-4DST: a pilot study. *J Nucl Med* 2011; **52**: 1322-1328 [PMID: 21764794 DOI: 10.2967/jnumed.111.088435]
11 **Koyama H**, Siqin Z, Sumi K, Hatta Y, Nagata H, Doi H, Suzuki M. Highly efficient syntheses of [methyl-11C]thymidine and its analogue 4'-[methyl-11C]thiothymidine as nucleoside PET probes for cancer cell proliferation by Pd(0)-mediated rapid C-[11C]methylation. *Org Biomol Chem* 2011; **9**: 4287-4294 [PMID: 21503302 DOI: 10.1039/c0ob01249a]
12 **Zhang Z**, Doi H, Koyama H, Watanabe Y, Suzuki M. Efficient syntheses of [^{11}C]zidovudine and its analogs by convenient one-pot palladium(0)-copper(I) co-mediated rapid C-[^{11}C]methylation. *J Labelled Comp Radiopharm* 2014; **57**: 540-549 [PMID: 24992010 DOI: 10.1002/jlcr.3213]
13 **Plotnik DA**, Wu S, Linn GR, Yip FC, Comandante NL, Krohn KA, Toyohara J, Schwartz JL. In vitro analysis of transport and metabolism of 4'-thiothymidine in human tumor cells. *Nucl Med Biol* 2015; **42**: 470-474 [PMID: 25659855 DOI: 10.1016/j.nucmedbio.2014.12.005]
14 **Nariai T**, Inaji M, Sakata M, Toyohara J. Use of 11C-4DST-PET for imaging human brain tumors. In: Hayat MA. Tumors of the Central Nervous System, Volume 11. Netherlands: Springer, 2014: 41-48 [DOI: 10.1007/978-94-007-7037-9_3]
15 **Toyota Y**, Miyake K, Kawai N, Hatakeyama T, Yamamoto Y, Toyohara J, Nishiyama Y, Tamiya T. Comparison of 4'-[methyl-(11)C]thiothymidine ((11)C-4DST) and 3'-deoxy-3'-[(18)F]fluorothymidine ((18)F-FLT) PET/CT in human brain glioma imaging. *EJNMMI Res* 2015; **5**: 7 [PMID: 25853013 DOI: 10.1186/s13550-015-0085-3]
16 **Tanaka K**, Yamamoto Y, Maeda Y, Yamamoto H, Kudomi N, Kawai N, Toyohara J, Nishiyama Y. Correlation of 4'-[methyl-(11)C]-thiothymidine uptake with Ki-67 immunohistochemistry and tumor grade in patients with newly diagnosed gliomas in comparison with (11)C-methionine uptake. *Ann Nucl Med* 2016; **30**: 89-96 [PMID: 26511019 DOI: 10.1007/s12149-015-1035-x]
17 **Ito K**, Yokoyama J, Miyata Y, Toyohara J, Okasaki M, Minamimoto R, Morooka M, Ishiwata K, Kubota K. Volumetric comparison of positron emission tomography/computed tomography using 4'-[methyl-^{11}C]-thiothymidine with 2-deoxy-2-^{18}F-fluoro-D-glucose in patients with advanced head and neck squamous cell carcinoma. *Nucl Med Commun* 2015; **36**: 219-225 [PMID: 25369751 DOI: 10.1097/MNM.0000000000000241]
18 **Koyasu S**, Nakamoto Y, Kikuchi M, Suzuki K, Hayashida K, Itoh K, Togashi K. Prognostic value of pretreatment 18F-FDG PET/CT parameters including visual evaluation in patients with head and neck squamous cell carcinoma. *AJR Am J Roentgenol* 2014; **202**: 851-858 [PMID: 24660716 DOI: 10.2214/AJR.13.11013]
19 **Lim R**, Eaton A, Lee NY, Setton J, Ohri N, Rao S, Wong R, Fury M, Schöder H. 18F-FDG PET/CT metabolic tumor volume and total lesion glycolysis predict outcome in oropharyngeal squamous cell carcinoma. *J Nucl Med* 2012; **53**: 1506-1513 [PMID: 22895812 DOI: 10.2967/jnumed.111.101402]
20 **Dibble EH**, Alvarez AC, Truong MT, Mercier G, Cook EF, Subramaniam RM. 18F-FDG metabolic tumor volume and total glycolytic activity of oral cavity and oropharyngeal squamous cell cancer: adding value to clinical staging. *J Nucl Med* 2012; **53**: 709-715 [PMID: 22492732 DOI: 10.2967/jnumed.111.099531]
21 **Moon SH**, Choi JY, Lee HJ, Son YI, Baek CH, Ahn YC, Park K, Lee KH, Kim BT. Prognostic value of 18F-FDG PET/CT in patients with squamous cell carcinoma of the tonsil: comparisons of volume-based metabolic parameters. *Head Neck* 2013; **35**: 15-22 [PMID: 22307893 DOI: 10.1002/hed.22904]
22 **Minamimoto R**, Toyohara J, Seike A, Ito H, Endo H, Morooka M, Nakajima K, Mitsumoto T, Ito K, Okasaki M, Ishiwata K, Kubota K. 4'-[Methyl-11C]-thiothymidine PET/CT for proliferation imaging in non-small cell lung cancer. *J Nucl Med* 2012; **53**: 199-206 [PMID: 22190643 DOI: 10.2967/jnumed.111.095539]
23 **Minamimoto R**, Toyohara J, Ito H, Seike A, Miyata Y, Morooka M, Okasaki M, Nakajima K, Ito K, Ishiwata K, Kubota K. A pilot study of 4'-[methyl-11C]-thiothymidine PET/CT for detection of regional lymph node metastasis in non-small cell lung cancer. *EJNMMI Res* 2014; **4**: 10 [PMID: 24593883 DOI: 10.1186/2191-219X-4-10]
24 **Okasaki M**, Kubota K, Minamimoto R, Miyata Y, Morooka M, Ito K, Ishiwata K, Toyohara J, Inoue T, Hirai R, Hagiwara S, Miwa A. Comparison of (11)C-4'-thiothymidine, (11)C-methionine, and (18)F-FDG PET/CT for the detection of active lesions of multiple myeloma. *Ann Nucl Med* 2015; **29**: 224-232 [PMID: 25421383 DOI: 10.1007/s12149-014-0931-9]
25 **Minamimoto R**, Nakaigawa N, Nagashima Y, Toyohara J, Ueno D, Namura K, Nakajima K, Yao M, Kubota K. Comparison of 11C-4DST and 18F-FDG PET/CT imaging for advanced renal cell carcinoma: preliminary study. *Abdom Radiol* (NY) 2016; **41**: 521-530 [PMID: 27039323 DOI: 10.1007/s00261-015-0601-y]
26 **Toyohara J**, Elsinga PH, Ishiwata K, Sijbesma JW, Dierckx RA, van Waarde A. Evaluation of 4'-[methyl-11C]thiothymidine in a rodent tumor and inflammation model. *J Nucl Med* 2012; **53**: 488-494 [PMID: 22315439 DOI: 10.2967/jnumed.111.098426]
27 **Toyohara J**, Sakata M, Oda K, Ishii K, Ishiwata K. Longitudinal observation of [11C]4DST uptake in turpentine-induced inflammatory tissue. *Nucl Med Biol* 2013; **40**: 240-244 [PMID: 23141551 DOI: 10.1016/j.nucmedbio.2012.10.008]
28 **Tsuji AB**, Sogawa C, Sugyo A, Sudo H, Toyohara J, Koizumi M, Abe M, Hino O, Harada YN, Furukawa T, Suzuki K, Saga T. Comparison of conventional and novel PET tracers for imaging mesothelioma in nude mice with subcutaneous and intrapleural xenografts. *Nucl Med Biol* 2009; **36**: 379-388 [PMID: 19423005 DOI: 10.1016/j.nucmedbio.2009.01.018]
29 **Hasegawa S**, Morokoshi Y, Tsuji AB, Kokubo T, Aoki I, Furukawa T, Zhang MR, Saga T. Quantifying initial cellular events of mouse radiation lymphomagenesis and its tumor prevention in vivo by positron emission tomography and magnetic resonance imaging. *Mol Oncol* 2015; **9**: 740-748 [PMID: 25510653 DOI: 10.1016/j.molonc.2014.11.009]
30 **Lu L**, Bergström M, Fasth KJ, Langström B. Synthesis of [76Br]bromofluorodeoxyuridine and its validation with regard to uptake, DNA incorporation, and excretion modulation in rats. *J Nucl Med* 2000; **41**: 1746-1752 [PMID: 11038007]

P- Reviewer: Chow J, Gao BL **S- Editor**: Qiu S
L- Editor: Wang TQ **E- Editor**: Wu HL

World Journal of Radiology

Submit a Manuscript: http://www.wjgnet.com/esps/
Help Desk: http://www.wjgnet.com/esps/helpdesk.aspx
DOI: 10.4329/wjr.v8.i9.809

World J Radiol 2016 September 28; 8(9): 809-815
ISSN 1949-8470 (online)

ORIGINAL ARTICLE

Prospective Study

Effects of oral contrast on dose in abdominopelvic computed tomography with pure iterative reconstruction

Kevin P Murphy, Liam J Healy, Lee Crush, Maria Twomey, Fiachra Moloney, Sylvia Sexton, Owen J O'Connor, Michael M Maher

Kevin P Murphy, Liam J Healy, Lee Crush, Maria Twomey, Fiachra Moloney, Sylvia Sexton, Owen J O'Connor, Michael M Maher, Department of Radiology, Cork University Hospital, A0001 Cork, Ireland

Author contributions: Murphy KP was the primary author and drafted the manuscript; Healy LJ, Crush L and Twomey M collected the data; Sexton S performed the studies and collected data; Moloney F, O'Connor OJ and Maher MM performed image analysis and edited the manuscript.

Institutional review board statement: The study received institutional board approval from the Cork Clinical Research Ethics Committee, Lancaster Hall, 6 Little Hanover Street, Cork, Ireland.

Informed consent statement: Informed consent was not deemed necessary for this study. Clinical and radiological data was collected prospectively in an anonymised fashion and no patient underwent additional procedures or investigations as a result of inclusion in the study. No potential risks to patients were identified. The clinical research ethics committee granted approval for the study without a requirement of consent from each patient.

Conflict-of-interest statement: All authors declare no conflicts of interest.

Data sharing statement: Technical appendix, statistical code, and dataset available from the corresponding author at fiachramoloney@hotmail.com.

Manuscript source: Invited manuscript

Correspondence to: Fiachra Moloney, FFR, RCSI, Department of Radiology, Cork University Hospital, 1 Bishopstown Road, Wilton, A0001 Cork, Munster, Ireland. fiachramoloney@hotmail.com
Telephone: +353-21-4922000
Fax: +353-21-4922002

Received: April 13, 2016
Peer-review started: April 15, 2016
First decision: May 19, 2016
Revised: June 23, 2016
Accepted: August 11, 2016
Article in press: August 15, 2016
Published online: September 28, 2016

Abstract

AIM

To assess the effect of neutral (NC) and positive (PC) oral contrast use on patient dose in low-dose abdominal computed tomography (CT).

METHODS

Low-dose clinically indicated CTs were performed on 79 Crohn's patients (35 = PC, 1 L 2% gastrografin; 44 = NC, 1.5 L polyethylene glycol). Scanner settings for both acquisitions were identical apart from 25 s difference in intravenous contrast timing. Body mass index (BMI), scan-ranges, dose-length product and size-specific dose estimated were recorded. Data was reconstructed with pure model-based iterative reconstruction. Image quality was objectively and subjectively analysed. Data analysis was performed with Statistical Package for Social Scientists.

RESULTS

Higher doses were seen in neutral contrast CTs (107.60 ± 78.7 mGy.cm, 2.47 ± 1.21 mGy *vs* 85.65 ± 58.2 mGy.cm, 2.18 ± 0.96 mGy). The difference

was significant in 2 of 4 BMI groups and in those that had both NC and PC investigations. Image-quality assessment yielded 6952 datapoints. NC image quality was significantly superior ($P < 0.001$) (objective noise, objective signal to noise ratio, subjective spatial resolution, subjective contrast resolution, diagnostic acceptability) at all levels. NC bowel distension was significantly ($P < 0.001$) superior.

CONCLUSION

The use of polyethylene glycol as a neutral OC agent leads to higher radiation doses than standard positive contrast studies, in low dose abdominal CT imaging. This is possibly related to the osmotic effect of the agent resulting in larger intraluminal fluid volumes and resultant increased overall beam attenuation.

Key words: Radiation dose; Low dose computed tomography; Abdominal imaging; Oral contrast; Computed tomography

Core tip: The use of neutral oral contrast agent results in higher radiation doses than standard positive contrast studies when performed low dose abdominopelvic computed tomography imaging. This likely relates to the osmotic effect of the agent resulting in larger intraluminal fluid volumes and resultant increased overall beam attenuation.

Murphy KP, Healy LJ, Crush L, Twomey M, Moloney F, Sexton S, O'Connor OJ, Maher MM. Effects of oral contrast on dose in abdominopelvic computed tomography with pure iterative reconstruction. *World J Radiol* 2016; 8(9): 809-815 Available from: URL: http://www.wjgnet.com/1949-8470/full/v8/i9/809.htm DOI: http://dx.doi.org/10.4329/wjr.v8.i9.809

INTRODUCTION

The industry and profession-wide drive for computed tomography (CT) dose reduction has resulted in considerable progress towards substantial dose reduction for abdominopelvic CT. These developments have been achieved as a result of improved detectors, tailored protocols, automated exposure control (AEC) and more recently newer reconstruction techniques such as iterative reconstruction. All elements of the acquisition process are now under scrutiny as part of the overall dose reduction strategies. The use of intraluminal contrast agents in the setting of abdominal imaging is one such factor. Traditionally, positive oral contrast agents were favoured but there is a significant body of evidence that suggests that negative or no oral contrast have a similar efficacy both in the trauma[1-3] and non-trauma setting[4,5]. In addition, neutral contrast agents are superior for bowel wall assessment, particularly in the setting of CT enterography (CTE)[6-11] such that CTE or magnetic resonance enterography are recommended as first-line investigations in diagnosing Crohn's disease (CD) or in detecting Crohn's complications[12,13].

Positive oral contrast universally contains either a dilute iodine-containing compound, *e.g.,* 2% gastrografin or dilute barium. Negative oral contrast agents include water, polyethylene glycol (PEG), very dilute (0.1%) barium, methylcellulose, mannitol and milk. Water alone is not favoured as an oral contrast agent in the setting of CTE as bowel distension is suboptimal due to absorption. Most of the commonly utilised negative contrast agents contain a substance that retains or increases the intraluminal fluid volume thus improving bowel distension. A bulking agent such as PEG is amongst the most commonly employed. PEG ingestion entails consuming 1 to 1.5 L of a water-based solution over approximately 45 min preceding the scan. The intraluminal volume is further increased by osmosis due to the high effective osmolality of the consumed solution.

It is generally assumed that positive oral contrast agents lead to higher radiation doses than negative oral contrast agents, due to the increased radiation attenuation as a result of the increased density. In a prior study, Wang *et al*[14] demonstrated that the use of water resulted in decreased radiation doses when compared with utilization of positive oral contrast, in a phantom model. No published study has examined the effect that PEG oral contrast has on radiation dose when compared to positive contrast *in vivo* or *in vitro*.

To this end, we designed a study to examine the influence that positive oral contrast has on patient radiation dose on low dose abdominal imaging when compared with PEG neutral oral contrast.

MATERIALS AND METHODS

The institutional ethics research committee approved the study. Seventy-nine low-dose clinically indicated CTs were performed on patients with histologically diagnosed CD over a 3-year period. All patients were suspected of having an exacerbation of CD and CT was performed in order to assess the extent and severity of CD and to assess for fibrostenotic or extraluminal complications. Exclusion criteria included patients with CD who were less than sixteen years of age, pregnancy, patients with a contra-indication to intravenous contrast medium, patients presenting acutely *via* the emergency department and those without histological confirmation of CD. A positive oral contrast CT examination was performed on patients referred for CT in the first 18-mo of this study period and a negative contrast study was undertaken on patients referred for CT in the latter 18-mo of the study period. Written informed consent was obtained from all patients. Patients had their weight and height measured using a digital device (Seca electronic measuring station, Model 763, Seca Medical, Hamburg, Germany) and individual body mass indices (BMI) were recorded.

CT acquisition

All CT images were acquired using a 64-slice multi-detector General Electric Lightspeed VCT-XTe (GE Healthcare, GE Medical Systems, Milwaukee, WI). Written consent was obtained from all patients and each one consented to having two contrast-enhanced CT scans of the abdomen and pelvis contemporaneously. The initial CT scan was a low dose scan which imparted approximately 10%-20% of a standard CT dosage regimen and the second scan was a conventional dosage scan which imparted approximately 80%-90% of a standard dosage regimen. The low dose studies only, performed with positive and neutral oral contrast, represented the imaging studies which underwent analysis as part of the current study.

All low dose scans were acquired with the following parameters: Tube voltage 100 kV, noise index 70, Z-axis tube current modulation range 20-350 mA and rotation time 0.5 s. For the positive contrast studies, the scan was commenced on arrested inspiration 45 s after peak aortic enhancement of 100 hounsfield units (HU). In the case of the negative contrast studies, to ensure a more "enteric phase" of enhancement, the scan commenced 20 s after peak aortic enhancement of 100 HU was surpassed on arrested inspiration.

Type of contrast used

Each patient was given either positive or neutral oral contrast as follows: With regard to positive contrast use, 2% Gastrografin solution was given as 1 L over 1 h as per departmental protocol. In contradistinction, neutral contrast, PEG "Klean Prep", was ingested as a 1.5 L solution over 45 min. Along with this, each patient was given a single 100 mL bolus of intravenous contrast (Iohexol, Omnipaque 300, GE Healthcare, Mississauga, ON) at a flow rate of 2.5 mL/s.

CT image reconstruction and CT dosage calculation

Images acquired were acquired at 0.625 mm thickness and reconstructed with a slice thickness of 2 mm. Low dose images were reconstructed using pure model based iterative reconstruction (MBIR) (GE Healthcare) in addition to hybrid iterative reconstruction (Adaptive Statistical Iterative Reconstruction, (ASiR, GE Heathcare).

The imaging performance and assessment in CT patient dosimetry calculator (ImPACT version 0.99x, London, England) was used to calculate effective dosage (ED) in all studies. Size specific dose estimates (SSDE) were also calculated, by a single observer, by multiplying the $CTDI_{vol}$ by multiplication factors as per American Association of Physicists in Medicine[15].

Subjective and objective evaluation of CT image quality

The low dose MBIR images were objectively and subjectively analysed. Spherical regions of interest (ROI's) (10 mm diameter; 519 mm^3 volume) were used to calculate objective noise and signal to noise ratio at multiple levels. Mean attenuation in HU and standard deviation (SD) of the mean attenuation were recorded for all datasets. The standard deviation served as an objective measure of noise with mean attenuation divided by SD serving as a measure of signal to noise ratio (SNR)[16,17]. The regions used to assess subjective and objective image quality were the liver at the right hemi-diaphragm level (level 1), liver at the porta hepatis (level 2), right renal cortex at the renal hilum (level 3), psoas muscle at the iliac crest (level 4), and gluteus maximus at the level of the acetabular roof (level 5). Subjective parameters assessed were spatial resolution, contrast resolution, streak artefact, subjective noise and diagnostic acceptability utilizing a previously employed grading system[17-19] adopted from the European Guidelines on Quality Criteria for CT document[20]. Subjective parameter assessments were performed by 2 readers (KPM, MMM) in consensus. Image quality of the solid organs, large bowel, small bowel, peri-colonic fat as well as the peri-enteric fat was subjectively assessed to ascertain diagnostic acceptability. Other subjective evaluations were performed at the 5 levels used in the objective analyses. All subjective parameters apart from streak artefact were scored using a 1 to 10 ranking system where 1 indicated poor image quality, 5 was deemed as acceptable, and 10 indicated excellent imaging quality for the relevant factor. The presence of streak artefact was assessed using a 3-point key where 0 represented no streak artefact, 1 corresponds to the presence of streak artefact that is not affecting the image quality and 3 represents interference with image quality.

Finally, the level of bowel distension was scored on a 3-point scale whereby 0 indicates unacceptable distension, 1 implies distension that is acceptable and 2 specifies excellent and complete distension. The jejunum, ileum, terminal ileum, caecum, ascending colon, transverse colon, descending colon, sigmoid colon and rectum were individually scored.

Statistical analysis

All statistical tests were performed with the Statistical Package for Social Scientists (SPSS) version 20.0 (IBM, Armonk, NY). Wilcoxon signed rank test was used for statistical analysis to compare the qualitative parameters (diagnostic acceptability, image noise, streak artefact, spatial resolution and contrast resolution). Normally distributed quantitative indices were compared using a paired *t* test. A difference with a *P* value of < 0.05 was considered statistically significant. All data are presented as mean ± SD unless otherwise stated.

RESULTS

Patient BMI, radiation dose and scan range

Seventy nine scans were performed over a 3-year period. Thirty-five positive contrast (PC) studies were acquired on patients with a mean age of 37.8 ± 13.7 years (range = 16-74 years) and mean BMI of 24.7 ± 4.97 kg/m^2 (range = 17.4-38.8 kg/m^2). Forty-four

Table 1 Comparison of dose-length product and size-specific dose estimated measurements by body mass index range

Group	*n*	Parameter	PC	NC	*P* value
1	PC *n* = 7	DLP (mGy.cm)	40.08 ± 6.42	52.07 ± 12.09	0.355
	NC *n* = 18	SSDE (mGy)	1.46 ± 0.29	1.58 ± 0.30	0.021[1]
2	PC *n* = 15	DLP (mGy.cm)	64.57 ± 9.98	2.03 ± 0.26	0.002[1]
	NC *n* = 18	SSDE (mGy)	111.68 ± 34.38	2.56 ± 0.58	< 0.001[1]
3	PC *n* = 9	DLP (mGy.cm)	94.75 ± 33.54	145.75 ± 33.54	0.017[1]
	NC *n* = 3	SSDE (mGy)	2.79 ± 0.70	2.95 ± 0.57	0.719
4	PC *n* = 4	DLP (mGy.cm)	224.09 ± 57.69	269.94 ± 111.24	0.951
	NC *n* = 5	SSDE (mGy)	5.09 ± 0.82	5.04 ± 1.32	0.483

Significant differences are denoted by[1]. Group 1: BMI < 20 kg/m^2; group 2: BMI 20-25 kg/m^2; group 3: BMI 25-30 kg/m^2; group 4: BMI > 30 kg/m^2. DLP: Dose-length product; SSDE: Size-specific dose estimated; BMI: Body mass index; PC: Positive contrast; NC: Negative contrast.

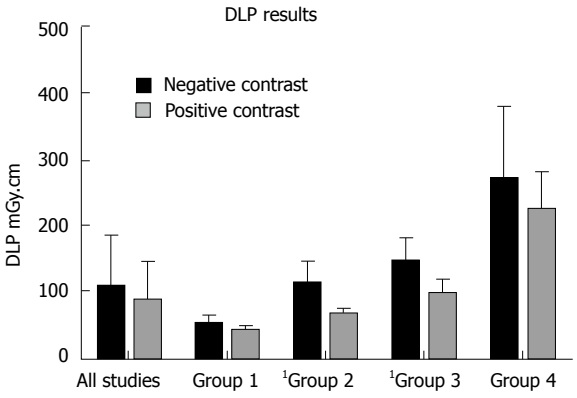

Figure 1 Comparison of dose-length product measurements for all studies in the neutral and positive cohorts and by body mass index range. Group 1: BMI < 20 kg/m^2; group 2: BMI 20-25 kg/m^2; group 3: BMI 25-30 kg/m^2; group 4: BMI > 30 kg/m^2. Significant differences are denoted by[1]. BMI: Body mass index.

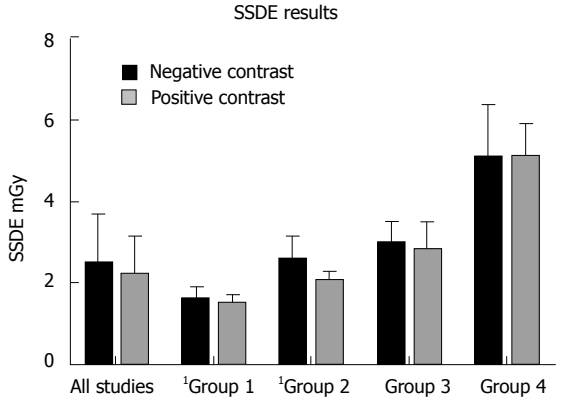

Figure 2 Comparison of size-specific dose estimated measurements for all studies in the neutral and positive cohorts and by body mass index range. Group 1: BMI < 20 kg/m^2; group 2: BMI 20-25 kg/m^2; group 3: BMI 25-30 kg/m^2; group 4: BMI > 30 kg/m^2. Significant differences are denoted by[1]. BMI: Body mass index.

patients underwent negative contrast (NC) studies. A mean age of 38.5 ± 12.98 years and a mean BMI of 22.17 ± 5.31 kg/m^2 (range 14.4-38.5 kg/m^2) were recorded in this cohort. Six patients underwent both positive and negative contrast studies over the 3-year period. The NC cohort had, on average, lower BMIs than the PC group, though this difference was not statistically significant (24.44 ± 5.05 kg/m^2 *vs* 22.17 ± 5.32 kg/m^2, *P* = 0.064).

The PC studies had the following mean radiation exposure parameters: Dose-length product (DLP) 85.65 ± 58.2 mGy.cm; ED 1.28 ± 0.87 mSv; SSDE 2.18 ± 0.96 mGy. Mean NC exposure parameters were: DLP 107.60 ± 78.7 mGy.cm; ED 1.61 ± 1.18 mSv; 2.47 ± 1.21 mGy. Averages for all exposure measures were greater for NC examinations but these differences were not statistically significant (DLP, *P* = 0.173; ED, *P* = 0.173; SSDE, *P* = 0.268) (Figures 1 and 2). No significant difference (*P* = 0.939) was observed between both groups in terms of scan range - positive: 429.78 ± 33.4 mm; negative: 430.41 ± 39.5 mm.

Radiation exposures (DLP and SSDE) by BMI range were compared between the cohorts - group 1: BMI < 20 kg/m^2; group 2: BMI 20-25 kg/m^2; group 3: BMI 25-30 kg/m^2; group 4: BMI > 30 kg/m^2. The results are depicted in Table 1 and Figures 1 and 2. DLPs were significantly higher for the NC studies in groups 2 and 3 and SSDEs were significantly higher for NC patients in groups 1 and 2. Other comparisons were not significant.

Of the 6 patients that had both PC and NC studies, all dose measurements were higher for all NC studies. Mean increases were as follows: DLP 21.11 mGy.cm (range 10.31-38.38 mGy.cm), ED 0.317 mSv (range 0.155-0.576 mSv) and SSDE 0.246 mGy (range 0.013-0.414 mGy). When mean dose indices were compared for these 6 patients, significant differences were seen for DLP (*P* = 0.005) and ED (*P* = 0.005) but SSDE was not significant (*P* = 0.175). The BMIs of these patients showed minimal change between study acquisitions - the BMI was lower for the NC studies in 4 cases (range 0.1-3.12 kg/m^2) and higher in 2 cases (range 1.2-5.7 kg/m^2). The effective abdominal diameter changed by < 2 cm in all cases.

Objective and subjective image quality analysis

Objective noise was measured at each of the 5 previously mentioned levels. The NC group had a significantly reduced objective noise when compared to the PC group at each of the 5 measured locations. Results as follows - liver at the hemi-diaphragm: 21.75 ± 3.27 HU *vs* 83.61 ± 13.47 HU; liver at the porta hepatis: 23.19 ± 3.07 HU *vs* 82.35 ± 8.15 HU; renal hilum:

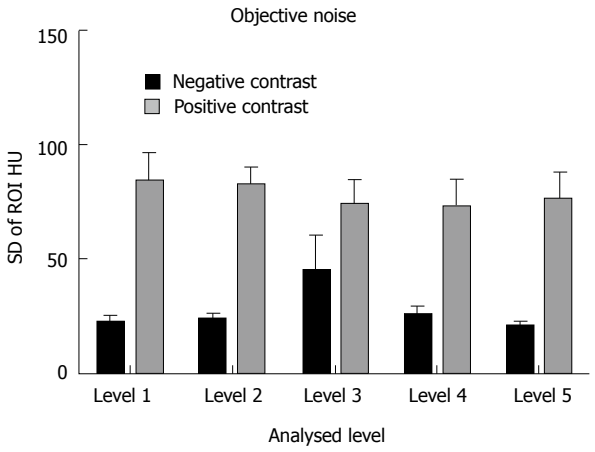

Figure 3 Comparison of objective noise measurements between the neutral and positive studies. Level 1: Liver at the right hemi-diaphragm level; level 2: Liver at the porta hepatis; level 3: Right renal cortex at the renal hilum; level 4: Psoas muscle at the iliac crest; level 5: Gluteus maximus at the level of the acetabular roof. All neutral measurements were significantly superior. ROI: Regions of interest.

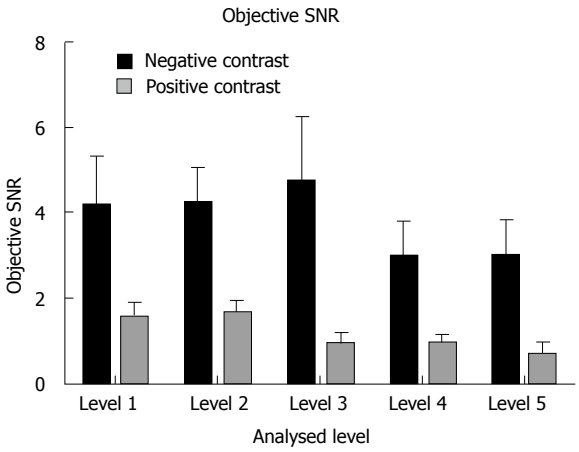

Figure 4 Comparison of objective signal to noise ratio measurements between the neutral and positive studies. Level 1: Liver at the right hemi-diaphragm level; level 2: Liver at the porta hepatis; level 3: Right renal cortex at the renal hilum; level 4: Psoas muscle at the iliac crest; level 5: Gluteus maximus at the level of the acetabular roof. All neutral measurements were significantly superior.

44.57 ± 16.09 HU *vs* 73.72 ± 11.11 HU; psoas muscle at the iliac crest: 25.36 ± 4.21 HU *vs* 72.68 ± 12.27 HU; gluteus maximus at acetabular roof: 20.05 ± 2.33 HU *vs* 76.30 ± 11.55 HU; ($P < 0.05$ for all values) (Figure 3).

The objective signal to noise ratio (SNR) at each of the 5 locations was significantly superior for the NC studies - liver at the hemi-diaphragm: 4.17 ± 1.22 HU *vs* 1.54 ± 0.35 HU; liver at the porta hepatis: 4.24 ± 0.84 HU *vs* 1.64 ± 0.32 HU; renal hilum: 4.71 ± 1.58 HU *vs* 0.93 ± 0.27 HU; psoas muscle at the iliac crest: 2.98 ± 0.85 HU *vs* 0.930 ± 0.22 HU; gluteus maximus at acetabular roof: 2.98 ± 0.85 HU *vs* 0.66 ± 0.27 HU; ($P < 0.05$ for all comparisons) (Figure 4).

Subjective image noise, contrast resolution, spatial resolution and diagnostic acceptability were superior for the NC studies when compared with the PC examinations ($P < 0.001$ for all comparisons). NC streak artefact was insignificantly superior ($P = 0.051$) to PC streak artefact. Results are depicted in Figure 5.

Bowel distension was significantly superior in the NC studies (median score 2, interquartile range 0) ($P < 0.001$) than the PC examinations (median score 1, IQR 1).

DISCUSSION

We found that negative PEG oral contrast examinations had significantly higher radiation doses than positive contrast studies, for most BMI subgroups and in those that had both NC and PC examinations, despite matched scan ranges. On the other hand, the resultant NC images reconstructed with MBIR were significantly superior to the PC MBIR images in terms of objective noise, objective signal to noise ratio, subjective noise, subjective contrast resolution, subjective spatial resolution and subjective diagnostic acceptability. NC subjective streak artefact was also insignificantly superior.

In terms of protocol parameter differences, settings for both the NC and PC studies were identical apart from the type of oral contrast and the intravenous (IV) contrast phase. The NC studies utilised an enteric phase IV contrast and the PC CT examinations utilised a more portovenous phase. It is worth noting firstly that the overall volume of IV contrast within the scan range is the same for both protocols hence this should not alter radiation dose. Secondly, when automated tube current modulation (ATCM) is employed, as was the case in these examinations, the selected mA gets chosen from the scanned projection radiograph before IV contrast is administered, hence the phase of IV contrast does not influence this aspect.

Hence, the type of oral contrast is the most important and perhaps only significant reason as to why the NC examinations had higher radiation doses than the PC scans.

Their results also indicated that bowel distension and hence intraluminal volume was greater with PEG oral contrast. It is likely that the overall attenuation influence of PEG oral contrast, when the total volume of fluid and per unit attenuation value are taken into account, particularly when used in combination with AEC/ATCM is in fact greater than positive oral contrast.

Future studies may involve the comparison of other negative contrast media and calculation of the overall intraluminal volume increase that results when PEG is consumed.

The greatest difference between each cohort with regard to radiation dose was observed in patients with a BMI of less than 25 kg/m^2. Therefore, choice of contrast agent is especially important in this cohort as it may have a greater impact on radiation dose than in overweight patients. The reason for this remains unclear but it is possible that patients with a high BMI

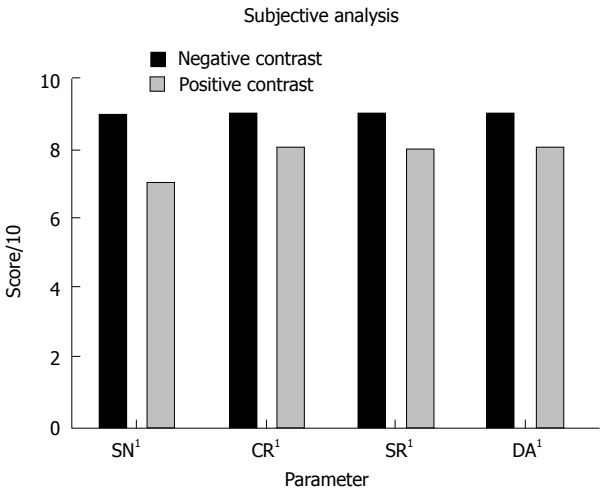

Figure 5 Comparison of median subjective image quality parameters for all neutral and positive studies. [1]All neutral measurements were significantly superior. SN: Subjective noise; CR: Contrast resolution; SR: Spatial resolution; DA: Diagnostic acceptability.

may behave differently with regard to other parameters such as ATCM performance. A further consideration in patients with a high BMI is that as intra-peritoneal inflammatory conditions often manifest as abnormalities of the adipose tissue adjacent to the inflamed organ, a larger quantity of adipose may a result in inflammatory changes being more readily apparent. This had led some authors to suggest the omission of oral contrast when scanning patients with a high BMI[21].

The results of the current study are important. As stated previously, major progress has been made in recent years in the area of radiation exposure reduction in abdomino-pelvic CT and the era of sub-millisievert abdomino-pelvic CT is fast approaching. This substantial progress has been achieved as a result of improved detectors, tailored protocols, AEC and more recently newer reconstruction techniques such as iterative reconstruction. Future reductions in radiation exposure will likely be smaller and will rely on finer protocol modifications. All elements of the acquisition process are now under scrutiny as part of the overall dose reduction strategy. The results of this study suggest that choice of oral contrast agent influences radiation exposure and should be added to a list of factors, which are worthy of further study.

In conclusion, our results suggest that PEG solution, when used as a negative oral contrast agent, results in significantly higher radiation doses in low dose abdominal CT imaging when compared with positive oral contrast, despite it being of lower density. This is likely attributable to the greater intraluminal volume and thus bowel distension achieved with PEG. This however, may have led to the significantly greater image quality recorded with the PEG studies. The choice of oral contrast agent should be tailored to the individual clinical scenario. In cases where bowel assessment is the key consideration, we suggest the use of a NC agent where in cases where bowel assessment may be a secondary consideration, a PC agent may be more appropriate so as to optimise overall radiation dose. Our study is novel and further examination of the relationship between oral contrast, radiation dose and diagnostic performance is warranted.

COMMENTS

Background

There has been considerable industry and profession-wide drive to reduce the radiation dose incurred by patients form diagnostic imaging with computed tomography. All elements of the acquisition process including technical parameters and reconstruction algorithm are now under scrutiny as part of an overall dose reduction strategy. The use of intraluminal contrast agents in the setting of abdominal imaging is another factor that warrants further assessment. Traditionally, positive oral contrast agents were favoured but there is a significant body of evidence that suggests that negative or no oral contrast have a similar efficacy. It is generally assumed that positive oral contrast agents lead to higher radiation doses than negative oral contrast agents, due to the increased radiation attenuation as a result of the increased density. Positive oral contrast universally contains either a dilute iodine-containing compound, *e.g.,* 2% gastrografin or dilute barium. Negative oral contrast agents include water, polyethylene glycol (PEG), very dilute (approximately 0.1%) barium, methylcellulose, mannitol and milk. The authors designed a study to examine the influence that positive oral contrast has on patient radiation dose on low dose abdominal imaging when compared with PEG neutral oral contrast.

Research frontiers

A single previous study demonstrated that the use of water resulted in decreased radiation doses when compared with utilization of positive oral contrast, in a phantom model. No published study has examined the effect that PEG oral contrast has on radiation dose when compared to positive contrast *in vivo* or *in vitro*.

Innovations and breakthroughs

The results suggest that PEG solution, when used as a negative oral contrast agent, results in significantly higher radiation doses in low dose abdominal computed tomography (CT) imaging when compared with positive oral contrast, despite it being of lower density.

Applications

All elements of the acquisition process are now under scrutiny as part of an overall dose reduction strategy in CT. The results of this study suggest that choice of oral contrast agent influences radiation exposure and should be added to a list of factors when considering how best to optimise patient radiation dose from CT.

Terminology

PEG is a negative oral contrast agent.

Peer-review

The paper is interesting and clinically relevant.

REFERENCES

1 **Allen TL**, Mueller MT, Bonk RT, Harker CP, Duffy OH, Stevens MH. Computed tomographic scanning without oral contrast solution for blunt bowel and mesenteric injuries in abdominal trauma. *J Trauma* 2004; **56**: 314-322 [PMID: 14960973 DOI: 10.1148/radiol.2492072055]

2 **Stafford RE**, McGonigal MD, Weigelt JA, Johnson TJ. Oral contrast solution and computed tomography for blunt abdominal trauma: a randomized study. *Arch Surg* 1999; **134**: 622-626; discussion 626-627 [PMID: 10367871 DOI: 10.1001/archsurg.134.6.622]

3 **Stuhlfaut JW**, Soto JA, Lucey BC, Ulrich A, Rathlev NK, Burke PA, Hirsch EF. Blunt abdominal trauma: performance of CT without oral contrast material. *Radiology* 2004; **233**: 689-694 [PMID: 15516605]

4 **Hill BC**, Johnson SC, Owens EK, Gerber JL, Senagore AJ. CT scan for suspected acute abdominal process: impact of combinations of IV, oral, and rectal contrast. *World J Surg* 2010; **34**: 699-703 [PMID: 20054539 DOI: 10.1007/s00268-009-0379-6]

5 **Lee SY**, Coughlin B, Wolfe JM, Polino J, Blank FS, Smithline HA. Prospective comparison of helical CT of the abdomen and pelvis without and with oral contrast in assessing acute abdominal pain in adult Emergency Department patients. *Emerg Radiol* 2006; **12**: 150-157 [PMID: 16738930 DOI: 10.1007/s10140-006-0474-z]

6 **Ilangovan R**, Burling D, George A, Gupta A, Marshall M, Taylor SA. CT enterography: review of technique and practical tips. *Br J Radiol* 2012; **85**: 876-886 [PMID: 22553291 DOI: 10.1259/bjr/27973476]

7 **Paulsen SR**, Huprich JE, Fletcher JG, Booya F, Young BM, Fidler JL, Johnson CD, Barlow JM, Earnest F. CT enterography as a diagnostic tool in evaluating small bowel disorders: review of clinical experience with over 700 cases. *Radiographics* 2006; **26**: 641-657; discussion 657-662 [PMID: 16702444 DOI: 10.1148/rg.263055162]

8 **Mazzeo S**, Caramella D, Battolla L, Melai L, Masolino P, Bertoni M, Giusti P, Cappelli C, Bartolozzi C. Crohn disease of the small bowel: spiral CT evaluation after oral hyperhydration with isotonic solution. *J Comput Assist Tomogr* 2001; **25**: 612-616 [PMID: 11473194]

9 **Aiyappan SK**, Kalra N, Sandhu MS, Kochhar R, Wig JD, Khandelwal N. Comparison of neutral and positive enteral contrast media for MDCT enteroclysis. *Eur J Radiol* 2012; **81**: 406-410 [PMID: 21239131 DOI: 10.1016/j.ejrad.2010.12.001]

10 **Hara AK**, Swartz PG. CT enterography of Crohn's disease. *Abdom Imaging* 2009; **34**: 289-295 [PMID: 18649092 DOI: 10.1007/s00261-015-0357-4]

11 **Minordi LM**, Vecchioli A, Mirk P, Bonomo L. CT enterography with polyethylene glycol solution vs CT enteroclysis in small bowel disease. *Br J Radiol* 2011; **84**: 112-119 [PMID: 20959377 DOI: 10.1259/bjr/71649888]

12 **Huprich JE**, Rosen MP, Fidler JL, Gay SB, Grant TH, Greene FL, Lalani T, Miller FH, Rockey DC, Sudakoff GS, Gunderman R, Coley BD. ACR Appropriateness Criteria on Crohn's disease. *J Am Coll Radiol* 2010; **7**: 94-102 [PMID: 20142082 DOI: 10.1016/j.jacr.2009.10.009]

13 **Van Assche G**, Dignass A, Panes J, Beaugerie L, Karagiannis J, Allez M, Ochsenkühn T, Orchard T, Rogler G, Louis E, Kupcinskas L, Mantzaris G, Travis S, Stange E. The second European evidence-based Consensus on the diagnosis and management of Crohn's disease: Definitions and diagnosis. *J Crohns Colitis* 2010; **4**: 7-27 [PMID: 21122488 DOI: 10.1136/gut.2005.081950a]

14 **Wang ZJ**, Chen KS, Gould R, Coakley FV, Fu Y, Yeh BM. Positive enteric contrast material for abdominal and pelvic CT with automatic exposure control: what is the effect on patient radiation exposure? *Eur J Radiol* 2011; **79**: e58-e62 [PMID: 21493028 DOI: 10.1016/j.ejrad.2011.03.059]

15 **Boone J**, Strauss K. Size-specific dose estimate (SSDI) in pediatric and adult body CT examinations. College Park: American Association of Physicists in Medicine, 2011

16 **Marin D**, Nelson RC, Schindera ST, Richard S, Youngblood RS, Yoshizumi TT, Samei E. Low-tube-voltage, high-tube-current multidetector abdominal CT: improved image quality and decreased radiation dose with adaptive statistical iterative reconstruction algorithm--initial clinical experience. *Radiology* 2010; **254**: 145-153 [PMID: 20032149 DOI: 10.1148/radiol.09090094]

17 **O'Neill SB**, Mc Laughlin PD, Crush L, O'Connor OJ, Mc Williams SR, Craig O, Mc Garrigle AM, O'Neill F, Bye J, Ryan MF, Shanahan F, Maher MM. A prospective feasibility study of sub-millisievert abdominopelvic CT using iterative reconstruction in Crohn's disease. *Eur Radiol* 2013; **23**: 2503-2512 [PMID: 23740025 DOI: 10.1007/s00330-013-2858-2]

18 **Siddiki HA**, Fidler JL, Fletcher JG, Burton SS, Huprich JE, Hough DM, Johnson CD, Bruining DH, Loftus EV, Sandborn WJ, Pardi DS, Mandrekar JN. Prospective comparison of state-of-the-art MR enterography and CT enterography in small-bowel Crohn's disease. *AJR Am J Roentgenol* 2009; **193**: 113-121 [PMID: 19542402 DOI: 10.2214/AJR.08.2027]

19 **Winklehner A**, Karlo C, Puippe G, Schmidt B, Flohr T, Goetti R, Pfammatter T, Frauenfelder T, Alkadhi H. Raw data-based iterative reconstruction in body CTA: evaluation of radiation dose saving potential. *Eur Radiol* 2011; **21**: 2521-2526 [PMID: 21822785 DOI: 10.1007/s00330-011-2227-y]

20 **Bongartz G**, Geleijns J, Golding S, Jurik A, Leonardi M, van Meerten E. European guidelines on quality criteria for computed tomography. European Commission, 1999

21 **Harrison ML**, Lizotte PE, Holmes TM, Kenney PJ, Buckner CB, Shah HR. Does high body mass index obviate the need for oral contrast in emergency department patients? *West J Emerg Med* 2013; **14**: 595-597 [PMID: 24381678 DOI: 10.5811/westjem.2013.5.12950]

P- Reviewer: Cerwenka HR, Li YZ, Shen J, Yu TH **S- Editor**: Qiu S
L- Editor: A **E- Editor**: Wu HL

Published by **Baishideng Publishing Group Inc**
8226 Regency Drive, Pleasanton, CA 94588, USA
Telephone: +1-925-223-8242
Fax: +1-925-223-8243
E-mail: bpgoffice@wjgnet.com
Help Desk: http://www.wjgnet.com/esps/helpdesk.aspx
http://www.wjgnet.com